5-1976

Albedo of the Earth's Surface -- A Comparison of Measurements Taken on the Ground and from Flying Platforms

Frank D. Eaton
Utah State University

ALBEDO OF THE EARTH'S SURFACE--A COMPARISON OF MEASUREMENTS TAKEN ON THE GROUND AND FROM FLYING PLATFORMS

by

Frank D. Eaton

A dissertation submitted in partial fulfillment
of the requirements for the degree

of

DOCTOR OF PHILOSOPHY

in

Soil Science and Biometeorology

(Biometeorology)

Approved:

UTAH STATE UNIVERSITY
Logan, Utah

1976

ACKNOWLEDGMENTS

I wish to express my sincere gratitude to Dr. Inge Dirmhirn for her counsel and guidance and for the priviledge of working on a stimulating problem.

Sincere appreciation is also extended to the committee members, Dr. D. Baker, Professor J. Fletcher, Dr. R. J. Hanks, and Dr. E. Hatch for their suggestions and criticisms and for serving as members of the advisory committee.

Thanks is extended to the Atmospheric Sciences Lab., White Sands Missile Range for supporting this research under Project #DAAD 07-73-C-0159. Special appreciation is also granted to the Goddard Space Flight Center for loan of the Nimbus MRIR and TIROS five-channel radiometer.

I give thanks also to Mrs. Ruth Cartee for typing and editing this thesis.

Frank D. Eaton

TABLE OF CONTENTS

TABLE OF CONTENTS (Continued)

LIST OF TABLES

LIST OF FIGURES

LIST OF FIGURES (Continued)

LIST OF FIGURES (Continued)

LIST OF FIGURES (Continued)

LIST OF FIGURES (Continued)

LIST OF FIGURES (Continued)

LIST OF FIGURES (Continued)

LIST OF FIGURES (Continued)

ABSTRACT

ALBEDO OF THE EARTH'S SURFACE--A COMPARISON OF

MEASUREMENTS TAKEN ON THE GROUND

AND FROM FLYING PLATFORMS

by

Frank D. Eaton, Doctor of Philosophy

Utah State University, 1976

Major Professor: Dr. Inge Dirmhirn
Department: Soil Science and Biometeorology

The main objectives of this study were to develop the indicatrices of reflected solar radiation from different natural surfaces and to show comparisons between values sensed in space of emergent radiation to ground values obtained from accounting for anisotropic reflection and estimating the effect of the intervening atmosphere. Thus, this study demonstrated that a prior knowledge of the angular distribution of reflected radiation allows determining the true hemispherical reflected radiation from a narrow field of view instrument such as found on a flying platform. Measurements for determining the indicatrices were made from a tower-mounted Nimbus MRIR and, in one case, with a hand-held TIROS five-channel radiometer.

Anisotropy of reflected radiation was found for all surfaces examined and increased with decreasing solar angle. Different surfaces showed different degrees and patterns of forward and backscatter. A clearly defined anti-solar point was found for plowed field, various agricultural crops and vegetated desert surfaces, while snow, the Alkali Flats, and Bonneville Salt Flats showed a broad pattern of

backscatter. As a consequence of surfaces exhibiting well-defined antisolar points the anisotropic correction factors relating normal reflectances to 2π reflected values were less than 100 percent for solar angles greater than approximately 60°. All surfaces examined showed anisotropic correction factors increasing with decreasing solar angles.

The albedo over the White Sands dune field decreased with decreasing solar angles due to large shadow patterns which are produced at low solar angles. The sand dunes values were derived from aircraft measurements.

Comparisons were made between estimated emergent radiation from the top of the earth's atmosphere accounting for anisotropy of the ground reflection pattern and estimates of atmospheric attenuation to values of reflected radiation obtained from the MSS subsystem of the ERTS program for the lava beds region and White Sands area in New Mexico. Also comparisons were shown between the estimated emergent radiation from the earth's surface for the same features and spectral bands to the values sensed in space. Under high albedo conditions as found in the White Sands area there was a decrease in emergent radiation to space while with low surface albedo, such as the lava beds region, the extra-terrestrial radiation increased from the ground values.

(184 pages)

INTRODUCTION

Satellite-mounted radiometers, providing comprehensive coverage over the entire earth in both space and time, have been used for many years to determine the albedo of terrestrial surfaces and the planetary heat balance. Surface albedo is of vital importance since it accounts for differential heating of the lower atmosphere while the heat budget is connected to general circulation, air mass modification, and regional climate. Net heating, represented as the difference between absorbed solar radiation and outgoing terrestrial radiation, is the basic energy source of the earth-atmosphere system.

Radiometers aboard space satellites measure the reflected radiation from the earth-atmosphere system. For the actual reflected radiation of various surface features, the influence of the atmosphere has to be taken into consideration. If additional values for the average reflected radiation close to the ground are known, the contributing effect of the atmosphere can be ascertained.

Estimates of the mean global albedo have been made using space satellite-obtained data. Analyses with both the first generation (TIROS-type) and second generation (Nimbus and ESSA) instruments showed a planetary albedo of 30 percent (Vonder Haar and Suomi, 1971). Raschke et al. (1973) found annual global averages of the albedo of 28.4 percent from measurements made from the meteorological Nimbus 3 satellite. These

albedo values are in disagreement with earlier computational studies by other authors.

London (1957) calculated the planetary albedo to be 35 percent but a re-evaluation of this earlier work (London and Sasamori, 1971) decreased the results to 33 percent. There is concern in the atmospheric science community to explain the discrepancies between these computed and measured albedo values.

Lettau and Lettau (1969) developed a budgetary-type method to estimate the albedo at the top of the earth's atmosphere. The results were not extended to estimate the planetary system but were presented over specific surfaces such as a desert, an open prarie, and an industrialized urban area. In the method, the functional relations expressing absorbing and scattering processes of shortwave radiation in the atmosphere were included as well as the absorption at the earth's surface.

Albedo is the ratio of the total reflected electromagnetic radiation to the total amount of incident radiation on a surface within a specified waveband such as the solar spectrum. Pyranometers have traditionally been used to measure shortwave albedo. They have an opening angle of 2π steradians and sense the total incident or reflected radiation if exposed upward or downward, respectively.

Since a pyranometer is a hemispherical sensor, the radiant flux density received by the instrument is

$$F = \int_{o}^{\frac{\pi}{2}} \int_{o}^{2\pi} I_{(\theta,\alpha,\zeta)} \cos\theta \sin\theta \, d\alpha d\theta \qquad [1]$$

where:

F = radiant flux density

θ = zenith angle of reflected intensity

α = solar azimuth angle

ζ = solar zenith angle

I = intensity (radiant flux density per unit solid angle) over the wavelength range of the solar spectrum.

If the reflecting surface is isotropic and homogeneous, $I_{(\theta,\alpha,\zeta)}$ is a constant and by integrating [1] we obtain:

$$F = I \int_{o}^{\frac{\pi}{2}} \int_{o}^{2\pi} d(\tfrac{1}{2} \sin^2 \theta)\, d\alpha d\theta = \pi I \qquad [2]$$

Satellite-mounted radiometers sense a narrow angle field of view in contrast to the 2π steradian field of view of a pyranometer. From equation [2], above, it can be seen that if the surface sensed is isotropic in its reflection pattern, reliable data can be obtained with space satellite sensors. However, if the surface viewed is non-Lambertian, albedo values derived from satellite data will be in error depending on the degree of anisotropy by assuming that the integrated directional reflectance is equal to πI. Space-obtained data of reflected radiation are particularly difficult to interpret because they are dependent on both the effect of the pattern of reflected radiation from the ground surface and the effect of the intervening atmosphere; both of which are dependent on the nadir angle of measurement.

Laboratory studies, examining the pattern of reflected radiation on a microscale, (Coulson, Bouricius, and Gray, 1965; Coulson, 1966) show a strong dependence of the intensity of the reflected radiation on angle of incidence of the radiation, azimuth, and elevation angles from which many natural surfaces were viewed. Hapke and Van Horn (1963) similarly studied over 200 surfaces of different materials and textures from powders to solid rocks. They concluded from their results of the optical scattering properties of the surfaces that the moon is covered with a layer of fine dust. Although these conclusions were reached before the Apollo program, the results were later verified.

There are some shortcomings of these studies if the results were to be applied to field conditions. The light sources used did not duplicate the solar spectrum or resemble the combination of both a direct solar beam and diffuse component since the laboratory apparatus illuminated the surfaces with a single angle of illumination. Also, the surfaces viewed were in general not natural as in the case of soil surfaces which were passed through mesh screens and evenly spread out on the sample tray.

The interaction of radiation and surface characteristics differs for water surfaces from the mineral surfaces previously discussed. Fresnel's law of reflection may be applied to a quiet water surface but a natural water surface containing waves or ripples needs different treatment. A rough water surface, approached theoretically from a standpoint of radiation considerations, involves the interaction of many changing slopes with both a direct beam and diffuse component of solar radiation.

Burt (1954) compared a semi-theoretical approach to observed albedo and included the solar elevation, cloud cover, and distribution of slopes on the sea in his model. Wind velocity and turbidity were also related to albedo over the sea. The results show a positive correlation between effective albedo and wind velocity for medium solar angles and a negative correlation between the same two variables for low solar angles.

Cox and Munk (1954) co-ordinated aerial photographs with wind measurements over the sea to develop statistics of the sea surface derived from sun glitter. The slope distributions of the sea surf ce were interpreted.

Since clouds occupy a large proportion of satellite imagery and have a high albedo, Ruff et al. (1967) studied the angular pattern of reflection of solar radiation by statistical analysis of TIROS IV data and found a non-isotropic pattern varying with solar zenith angle. Each individual cloud could not be studied but reflection patterns representative of several clouds were obtained. Very pronounced anisotropy was found in the backscatter with large zenith angles. Salomonson (1966) using an aircraft-mounted scanning radiometer showed similar results over stratus clouds at large solar zenith angles. A few flights over other surfaces also exhibited anisotropic reflection patterns. Bartman (1967) found anisotropic reflection from snow surfaces using a Nimbus MRIR on a balloon. Anisotropic reflection patterns were also found over cloud, water, and land surfaces with an MRIR mounted in a Convair 990 (Brennan, 1969; Brennan and Bandeen, 1970). Clouds and forests were found to have similar patterns of reflection while the ocean showed

strong sun glitter in the results. All of the indicatrices of reflected radiation mentioned above include the radiances originating from the intervening atmosphere as well as from the surface itself.

Since the intervening atmosphere contains many variables effecting radiative transfer such as temperature, pressure, humidity, clouds, carbon dioxide, aerosol number density, aerosol size and composition, ozone concentration, lapse rates, wind, and convective currents, the measurements taken from balloons and high flying aircraft will be expected to show different indicatrices than those from ground measurements. Actual measurements on the ground surface were made by Middleton and Mungall (1952) with a portable goniophotometer. Much specular reflection from snow surfaces at high angles of incidence was found. Christie (1953) discusses the problem of luminous directional reflectance from snow theoretically and shows the limitations of the apparatus used by Middleton and Mungall (1952). Dirmhirn and Eaton (1975) discuss some characteristics of the albedo of snow in regards to the proper interpretation of reflectance data taken under distinct nadir angles.

In this study indicatrices of reflected radiation were developed from measurements near the surface, thus eliminating the variables associated with the intervening atmosphere. Values of reflectance obtained from low flying aircraft were obtained in some instances to determine spatial variation of reflectance. Finally actual radiation values measured with space satellites were compared to ground values after estimating and accounting for the effects of the intervening atmosphere.

Objectives

The relationships between the actual heat loss by radiative processes within the solar spectrum (0.2 to 4.0 μm) and measurements taken with narrow angle instruments from flying platforms were developed by the following objectives:

1. To develop the geometrical characteristics of the reflected solar radiation (0.2 to 4.0 μm) from different surface features on the ground.
2. To obtain data from aircraft and space satellites regarding reflected solar radiation during comparable times with the ground data.
3. To estimate the effect of the atmospheric attenuation on the flying platform data considering scattering and absorption effects.
4. To combine the results of points 1, 2, and 3, i.e., angular distribution of reflected radiation, aircraft-obtained values and effects of the intervening atmosphere for determining the relationships between the actual reflected radiation of natural features and space-obtained values found with narrow angle instruments.

Description of the Study Areas

The study areas included the Bonneville Salt Flats, the White Sands dune field and Alkali Flats, a lava bed in southern New Mexico,

fields of various agricultural crops including a plowed field near Logan, Utah and two desert sites in Curlew Valley, Utah.

Ground measurements for the determination of albedo were taken for all of the study areas while indicatrices of reflected radiation were found for all surfaces except the lava bed and White Sands dune field which have too large topographical dimensions to permit the indicatrices to be developed from the ground.

Aircraft measurements were done primarily over the White Sands dune field with some flights over the Alkali Flats for calibration purposes.

The satellite measurements were analysed for the lava bed, White Sands dune field and Alkali Flats, all in southern New Mexico.

Bonneville Salt Flats

The Bonneville Salt Flats were measured in August 1973 and August 1974 at a site located at approximately 40°47' latitude and 113°30' longitude near Wendover, Utah. The site was on the edge of the Bonneville Race Track and was devoid of vegetation. The surfaces were completely covered with salt crystals and visual observation showed differences in the surface characteristics between the two years. In 1973, the surface was smoother than in 1974. The 1974 surface appeared to have had many fissures by which a salt solution exuded and crystallized forming small ridges on the surface.

The climatological station in Wendover, Utah reported an acculmulated precipitation of 6.61 inches for October 1, 1972 to July 31, 1973 and 2.19 inches for October 1, 1973 to July 31, 1974 (Utah Climatological Data bulletin, Vol. 74,75,76). It is assumed that the antecedent

precipitation produced the differences in the surface appearances for the two consecutive years.

White Sands dune field
and Alkali Flats

The White Sands dune field and Alkali Flats are located in the Tularosa Basin in soutnern New Mexico about 15 miles southwest of Alamogordo and 50 miles northeast of Las Cruces. The entire region occupies approximately 275 square miles of which the Alkali Flats covers 165 square miles. The sand dunes are comprised predominantly of gypsum ($CaSO_4 \cdot 2H_2O$) crystals with association of some sodium salts (McKee 1966). Aerial examination of the dunes region shows that the sand dunes lie in broad bands oriented at right angles to the southwest direction where Lake Lucero is located, the source of the gypsum.

Daily wind measurements at Holloman Air Force Base were analysed for both speed and frequency of direction for a 15-year period (McKee, 1966). It was found that most moderate (15-25 knots) and strong (above 25 knots) winds are largely from the southwest and occur most frequently during March and April. There was also found a short period characterized by strong north winds in late winter. Winds from other directions were generally too weak to be effective in dune development and migration. Skidmore and Woodruff (1968) discuss wind erosion forces and developed a method of analysis based on the capacity of wind to cause soil movement such as found in the sand dune field.

The dunes found in the White Sands dune field are classified into four types; dome-shaped, transverse, barchan or crescentic and parabolic. These are located in the above order from Lake Lucero (McKee, 1966). The

particular form of dune depends on the constancy of wind direction which becomes more variable going from Lake Lucero across the dune field due to interference of the wind caused by the dunes themselves. There is also a dissipation of energy as the winds blow across the dune field which produces a deposition of different particle sizes in different locations.

Most of the measurements in this study were taken at 32°52' latitude and 106°17' longitude which is located on the border of the Alkali Flats and barchan dunes, the predominant dune type. The site is on Holloman Air Force Base near the border to the White Sands Nationa Monument.

The area west of the sand dunes region is the Alkali Flats which is stable and has a smooth, flat topography. Examination of the surface showed it to be composed of a crust with areas of dark coloration, unlike the loose sand found in the sand dunes. Visual observation shows the surface to be encrusted with algae and lichens. The surface crust of the Alkali Flats appears to be stabilized by the microflora except in the vicinity of seed plants.

Fletcher and Martin (1948) studied the phenomena of the effects of algae and molds in the raincrust of desert soils and reported that the mold mycelium and algal filaments consolidate the sand particles, reduce erosion and influence infiltration. They also found the presence of the algae and molds made separation of the crust for study easier, the micro-flora altered soil structure at the surface and the soil fertility changed with microbial development. Considerably more nitrogen was found in the crust than in the soil below. Shields, Mitchell and Drouet

(1957) studied the alga- and lichen- stabilized surface crusts of the gypsum flats at the White Sands region and reported that *Palmogloea protuberans* associated with *Plectonema nostocorum* commonly forms a bright-green seam 2-5 mm below the surface and a black-green patchy surface growth which has been observed to become darker after rain. Lichens composed of *Heppia* and *Dermatocarpon* spp. form black warty hummocks on the surface up to several inches across.

Even though the Alkali Flats are heavily encrusted with algae and lichens, occasionally loose gypsum sand is blown in on top of the stabilized crust and collects in depressions. The total area covered by this loose sand is generally small, thus there is little change in the overall reflection characteristics with the fresh sand present, except in the immediate neighborhood of the dunes.

Plowed field

The soil surface examined was a plowed field on the Evans Experimental Farm in Nibley, Utah, latitude 41°40' and longitude 111°50'. The soil was mapped as a Nibley silty clay loam with 0-3 percent slopes and is a member of the fine, mixed, mesic family of Aquic Argiustolls. The soil surface had a uniform spatial appearance after plowing.

Snow surface

The snow measurements were made approximately 10 miles west of Logan, Utah, latitude 41°45' and longitude 112°10' on snow overlying dry farm land. The site was generally flat and showed no appreciable drifting. The snow pack was mature and the surface showed a glazed appearance.

Agricultural crops

Two alfalfa fields, both in Nibley, Utah, were used to determine the indicatrices. In both cases the fields were mature and ready for cutting. The approximate height of the crops was 2 feet and the foliage formed a uniform, dense canopy.

Sugar beets were measured in 1973 and 1974 on two different fields near Smithfield, Utah, latitude 41°50' and longitude 111°50'. The approximate height of the plants was 2 feet with the foliage covering most of the soil between the rows. The plants were thinned with an electronic thinner and were very uniform in spacing and size.

Corn was also measured on two fields near Smithfield, Utah. The corn was approximately 5 feet tall for the 1973 measurements and 3 feet tall for the 1974 measurements. Bare soil was particularly noticeable during the second year of data collection due to the developmental stage of the crop.

Desert surfaces

The Curlew Valley desert located near Snowville, Utah, latitude 42°00' and longitude 113°00' was examined in this study. The site chosen for the measurements was composed of big sagebrush (*Artemisia tridentata*) with the height of the individual bushes being approximately 2 feet. A mean spacing for the individual plants was about 3 feet.

Another site, about one-fourth mile from the sagebrush site, was a conversion from sagebrush to crested wheatgrass (*Agropyron cristatum*). The vegetation was dormant at the time of measurement. The individual

plants were spaced about 1 foot apart with a mean height slightly greater than 1 foot.

A third desert surface studied was the recent lava flow near Carrizozo, New Mexico. The measurements were made at 33°17' latitude and 106°15' longitude. The lava rock is fractured but relatively unweathered. However, the accumulated soil in depressions of the lava bed region is capable of supporting around 130 different seed plants (Shields, Mitchell, and Drouet, 1957).

Procedure

Measurement of indicatrices design and instrumentation

The indicatrices of reflected radiation were determined for various surfaces; Bonneville Salt Flats, White Sands Alkali Flats, bare soil, snow, fields of alfalfa, sugar beets and corn, and desert surfaces of sagebrush and crested wheatgrass.

Figure 1 illustrates the relationship as seen in Equation [1]:

$$F = \int_0^{\frac{\pi}{2}} \int_0^{2\pi} I_{(\theta,\alpha,\zeta)} \cos\theta \sin\theta \, d\alpha d\theta. \qquad [1]$$

The z-axis is normal to the surface while the x-axis represents the direction toward the sun. The nadir angle is shown as θ while α is the solar azimuth angle.

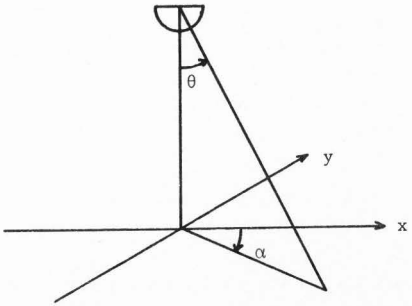

Figure 1. Geometry of the hemispherical sensor of a pyranometer.

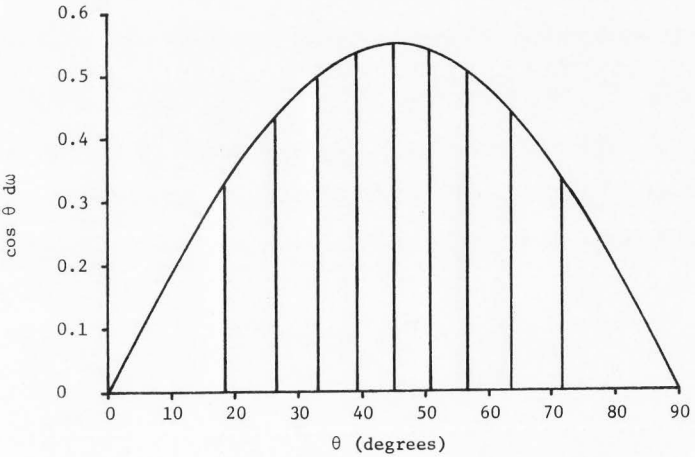

Figure 2. Relationship of cos θ dω to nadir angle (θ)

For the measurements, a form of Equation [1] was used as:

$$F = \sum_{\theta} \sum_{\alpha} \{I_{(\theta,\alpha,\zeta)} \cos\theta \sin\theta \, \Delta\alpha\Delta\theta\}. \qquad [3]$$

A graphical method was developed from Equation [3]. First increments of solid angle for a hemisphere were found using the relationship of infinitesimal solid angle, $d\omega = \sin\theta \, d\alpha d\theta$. The incremental steps were taken as the difference between cones starting at the center of a sphere of which the hemisphere is a part. Another approach which yields the same result stems from defining a solid angle as the ratio of the area on a circumscribed sphere of radius r intercepted by the cone starting from the center of a sphere and outlining the area, $\omega = A/r^2$. Therefore incremental zones of a hemisphere can be calculated by the relationship:

$$S = 2\pi rh \qquad [4]$$

where

S = area of each zone

r = radius of the sphere, and

h = altitude of each zone.

The second step was to multiply each of these values by the cosine of the zenith angle for each increment as expressed in Equation [3]. These values were then plotted *vs* zenith angle as seen in Figure 2 and the integrated area was divided into 10 equal areas. The angles at the intersections of the equal areas were then plotted on polar coordinate paper as shown in Figure 3. Each alternating ring (clear or stippled) represents the angular interval that 10 percent of the energy is received

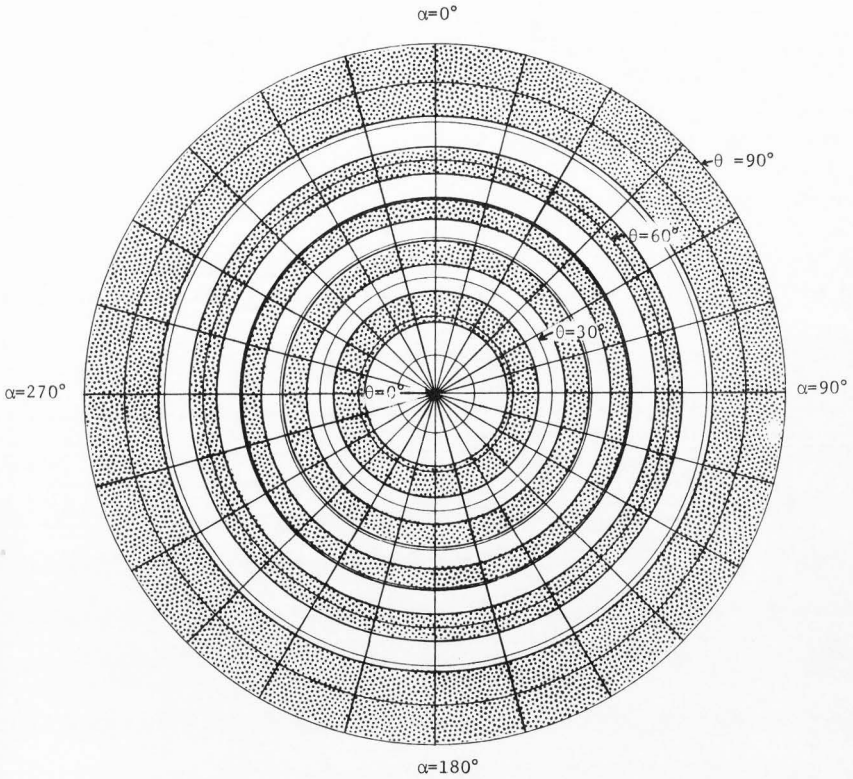

Figure 3. Angular intervals (clear or stippled) representing equal amounts of energy received by a 2π hemispherical sensor.

by an instrument with a 2π solid angle receiver such as a pyranometer. This diagram shows that the greatest amount of power received per zone is at zenith angle of 45° and diminishes toward both zones at 0° and 90° zenith angles. The same diagram allows the plotting of a reflectance at any combination of nadir and solar azimuth angle. The indicatrices were developed from measurements of reflectances at various azimuth and nadir angles over each surface.

The Nimbus F-2 medium resolution infrared radiometer (MRIR) was used for most of the measurements. It is a scanning instrument and produces eight scans per minute. Radiation is reflected from a rotating aluminum mirror oriented at 45° to the axis of rotation and collected by a Cassegrainian optical system. The channel used has a bandpass of 0.2-4.0 μm. The instrument has a field of view of 50 milliradians (2.86°) and was mounted on a rotating boom from the top of a 10-foot high triangular tower. The boom was positioned in order that the instrument would scan a path across each feature in a vertical plane and then was repositioned for successive 10° increments in azimuth angles.

The signal was recorded on a high speed strip chart recorder and the data were removed from the charts at intervals of 15° nadir angles by utilizing a plastic overlay with a gridwork etched on it. The data were then normalized by using the nadir angle 0° value as 100 percent. These values were then plotted on diagrams such as Figure 3, isolines were drawn of equal reflectances and a weighted overall value was obtained by planimetering each area. This weighted value if related to a single beam measurement is equivalent to the integrated directional

reflectance obtained by a 2π steradian instrument. The relationship can be expressed as:

$$(\text{reflectance value for nadir angle} = 0°)\begin{bmatrix}\text{integrated } 2\pi \text{ factor} \\ \text{determined from indicatrices}\end{bmatrix} = (2\pi \text{ value as measured by a hemispherical receiver}).$$

A TIROS (television and infrared observation satellite) five-channel radiometer was used over the snow surface. This instrument is of the fixed-beam type and has an opening angle of 5° at the half-power point. The 0.2-4.5 μm channel was operated. This instrument was used in preference to the Nimbus MRIR because of its greater portability and the delicate nature of a snow surface which would be disturbed if a tower was mounted. The TIROS radiometer was hand-held for successive nadir angles of 15° and several azimuth angles. The signal was also recorded on a strip chart recorder and the data points plotted and analysed similar to that described above.

Photographs were taken utilizing a fish-eye lens to supplement the measurements of the indicatrices. The photographs were not analysed quantitatively but display qualitatively the reflection patterns examined.

For comparison to the 2π values derived from the satellite instruments, measurements were simultaneously taken with a pyranometer. The pyranometer was used for both global and reflected radiation in order to determine the daily variation of albedo.

There are two processes and one instrumental error responsible for a daily variation of albedo. The first process is due to the anisotropy of a surface with respect to its pattern of reflected radiation. If the

indicatrix is found to vary with solar angle, there will be a daily variation of albedo.

The second process is a change in the actual surface itself such as a change in surface soil moisture, deposition of a foreign substance such as dust or moisture, wilting of a plant cover or a metamorphism of the crystal structure of a snowpack.

The instrumental error is caused by the failure of pyranometers to respond correctly at all solar angles. Since the sensor is generally horizontal, the instrument should respond to the cosine of the zenith angle of a similar direct beam component. A deviation of this value is known as a "cosine error" and occurs with most pyranometers at zenith angles greater than 70°. In a comparison of measured values between pyranometers and those derived from measurements utilizing the TIROS or Nimbus radiometers, agreement should be found when considering the two processes discussed, but the "cosine error" of a pyranometer will cause a deviation when comparing values at high zenith angles. The Nimbus-MRIR obtained values should be correct with the pyranometer being slightly in error.

Calibration of the Instruments

In this study a calibration constant for each surface was independently derived. Using the relationship (reflectance value for nadir angle = 0°) (integrated 2π factor derived from indicatrices) = (2π values measured by the pyranometer), the pyranometer values were used as the absolute values and the equation was solved for the reflectance values

normal to the surface. This procedure is exact since the integrated 2π factors were normalized to the reflectances normal to the surface. Linear regression analysis was used to find the best-fit line between the normal reflectance values derived from the pyranometer values accounting for anisotropy and the corresponding signal in voltage from the MRIR. Table 1 shows the slopes (b), standard coefficients (r), and degrees of freedom (df) for each feature. Since the slopes of the regression analysis represent the calibration constants of the MRIR for each surface, possible factors influencing the slopes were examined.

The pyranometer was calibrated with an Ångstrom pyrheliometer a standard instrument. These calibrations were carried out under clear sky conditions for various solar angles in Logan, Utah. Since the pyranometer was used as the measurement standard in the field, it was necessary to verify if the pyranometer has a "flat response," i.e., responds equally for all wavelengths. The pyranometer was compared with an Ångstrom pyrheliometer using two short-wavelength cutoff long-wavelength pass (SCLWP) filters, each 2 mm thick. The filters are described in Farb and Filter Glas (1965) as OG5 and RG5 filters. The filter transmittances were checked on a Beckman DK-2A spectrophotometer and the cutoff wavelengths were found to occur at 550 nm and 650 nm at the 50 percent transmittance values. Several comparable measurements were taken between the pyranometer and pyrheliometer with no filter and with the filters. A mean of all values shows the ratio of radiant flux density to that without a filter as in Table 2.

Table 1. Results of linear regression analysis to determine calibration constants for the Nimbus MRIR

Features	Slopes (b_1)	Standard Coefficient (r)	Coefficient of Determination (r^2)	Degree of Freedom (df)
1973 Bonneville Salt Flats	1.26	0.9992	0.9984	7
1974 Bonneville Salt Flats	1.25	0.9996	0.9992	5
1973 + 1974 Bonneville Salt Flats	1.25	0.9980	0.9960	14
Alkali Flats	1.25	0.9990	0.9980	6
Nibley Silty Clay loam	0.78	0.9963	0.9926	3
Sugar Beets	1.10	0.9928	0.9856	5
Alfalfa	1.07	0.9999	0.9998	3
Corn	0.90	0.9949	0.9899	4
Sagebrush	1.17	0.9971	0.9942	5
Crested Wheatgrass	0.94	0.9995	0.9990	4

Table 2. Comparison of pyrheliometer and pyranometer spectral response

	Pyrheliometer	Pyranometer
550 nm cutoff	0.680	0.693
650 nm cutoff	0.559	0.535

Thus the pyranometer responds 4.5 percent less than the pyrheliometer at wavelenths greater than 650 nm and 1.9 percent less than the pyrheliometer for wavelengths less than 550 nm.

Temperature effects were considered as an explanation for the variation of slopes but were rejected due to the high standard coefficient (r) values as shown in Table 1, indicating linearity. If the MRIR varied with temperature changes, each daily set of values would have shown a curvilinear effect. The range of temperature during any given day of measurement is in general greater than the temperature variability found between different surface features at similar solar angles. While no temperature effect could be found in the field calibrations, laboratory tests had shown a change of 4.5 percent in calibration when the scanner and module were changed from 10 to 25 C (Malinowski, 1966). Since this temperature change is probably in excess of that found during the field measurements, this would represent an extreme upper limit in estimating temperature effect.

Also the possible change of calibration of the MRIR due to degradation or drifting of its sensitivity was considered. The Bonneville Salt Flats were measured twice at a one-year interval and testing the hypothesis for a difference between the slopes derived from the two separate sets of data failed to show a difference at the 95 percent probability level. Thus it was concluded that the MRIR did not change its sensitivity during the measurement period.

Another possible factor explaining the variation of slopes is a change in the spectral sensitivity of the MRIR from the time of manufacture. The spectral sensitivity shown in Figure 4 (Raschke et al, 1973) was found when the instrument was new in 1964. Visible oxidation is found on the previously polished aluminum scan mirror. Although the

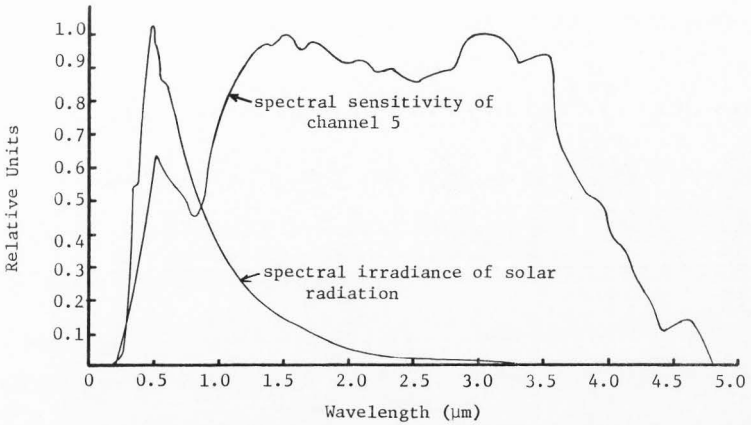

Figure 4. Spectral sensitivity of channel 5 and the extraterrestrial spectral irradiance of the sun.

MRIR mirror itself could not be measured, the reflection characteristics of samples of both oxidized and freshly polished aluminum were found with a Beckman DK-2A spectrophotometer. Normalizing the curves showed agreement at wavelengths greater than 1.5 μm wavelength, but the oxidized aluminum surface displayed a reflection approximately 17 percent less than the clean aluminum surface for wavelengths less than 0.8 μm wavelength. Since the MRIR contains three reflecting surfaces, the scan mirror and two in the Cassegrainian optical system, the total effect of change in spectral sensitivity due to oxidation of reflecting surfaces was estimated as three times that found with a single sample measured with the spectrophotometer.

Another possible explanation for the different slopes investigated is the interaction of the spectral sensitivity of the Nimbus MRIR and the spectral characteristics of the measured surfaces. The spectral sensitivity of the MRIR is shown in Figure 4 while spectral characteristics of several surfaces are found in Figure 5 (Dirmhirn, 1967) and Figure 6. As seen in Figure 4, Channel 5 is only about one-half as sensitive in the visible and near infrared as it is for wavelengths greater than 1.5 μm. This will cause an overweighting in the near infrared part of the spectrum in relation to the shorter wavelengths. Also as seen in Figure 4, the solar spectrum has its maximum power in the shorter wavelenths. In order to evaluate the degree of this effect, a graphical technique was employed combining the effects of a generalized solar spectrum at sea level and the MRIR spectral sensitivity with the spectral characteristics of some of the curves from Figures 5 and 6.

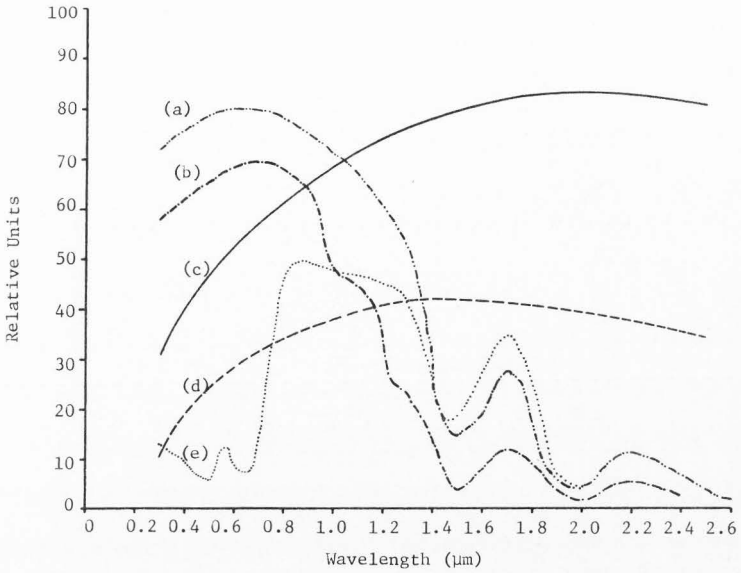

Figure 5. Spectral characteristics of some natural surface materials: (a) fresh fallen snow, (b) old snow, (c) limestone, (d) sand and (e) green plants. After Dirmirn, 1967.

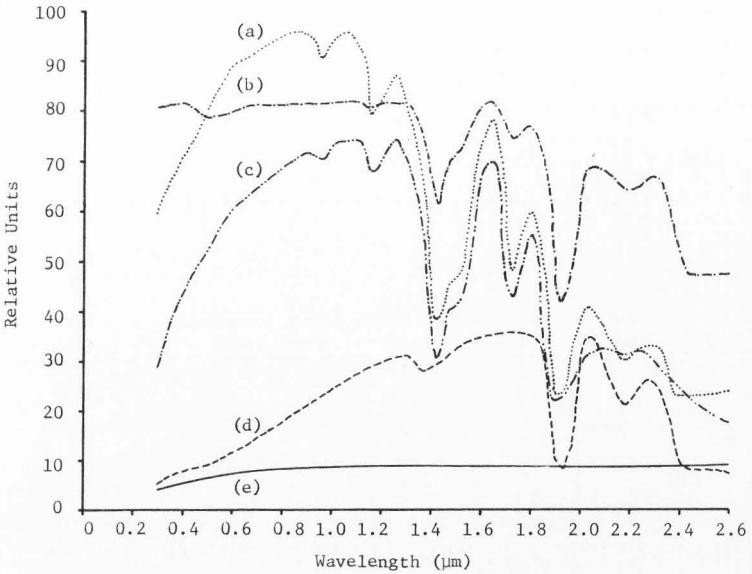

Figure 6. Spectral characteristics of the natural surfaces: (a) White Sands gypsum sand, (b) Bonneville Salt Flats, (c) Alkali Flats, (d) Nibley silty clay loam and (e) lava bed rock measured with a Beckman DK-2A spectrophotometer with a reflectance attachment.

Comparisons were made of these calculated values to values assuming a "flat response" such as assumed to be found with a pyranometer. The comparisons are shown in Table 3. The gypsum sand, Alkali Flats, Bonneville Salt Flats, and snow surfaces show an underestimation of reflectances as compared with green plants or bare soil when measured with the MRIR due to the deviation from unity of the spectral sensitivity. This generally agrees with the calibration constants displayed in Table 1 but other factors are necessary to explain the complete effect.

Table 3. Estimated effect of spectral sensitivity of channel 5 for the MRIR for various surfaces using an idealized solar spectrum

Feature	A[a]	B[b]	A/B (%)
White Sands gypsum sand	.5224	.8429	62.0
Alkali Flats	.3841	.6022	63.8
Bonneville Salt Flats	.4940	.7945	62.1
New Snow	.4265	.7111	60.0
Green Plants	.1536	.2331	65.9
Soil	.1197	.1728	69.3

[a] A = (solar spectrum) (spectral sensitivity of channel 5) (spectral characteristics of the surface)

[b] B = (solar spectrum) (spectral characteristics of the surface)

Values presented are represented by an integrated solar spectrum (0.3-4.0 μm) = 1.00

The greatest range in the calibration constants (slopes) is found to be between the Bonneville Salt Flats and bare soil data. The salt flats constant is found to be 38 percent greater than the bare soil constant. A green plant calibration constant is represented as the mean of the alfalfa and sugar beets values since both of these crops showed almost complete coverage of the soil. The salt flats calibration constant is found to be 13 percent greater than for the green plants.

The total effects for the individual factors possibly contributing to the variation of constants between specific surfaces can be developed. For each surface, the Bonneville Salt Flats, the green plants and the bare soil, the interaction of the estimated effect of the spectral sensitivity of the pyranometer, and the effect of oxidation of the MRIR reflecting surfaces with the previously discussed combined effect of the solar spectrum, spectral characteristics of the surfaces and spectral sensitivity of the MRIR was developed.

Table 4 is a summary and estimates of the possible effects which can contribute to a deviation of the calibration constants (slopes) of the different surfaces. As presented, there is still some unexplained contribution, particulary when comparing the salt flats to bare soil calibrations. Possibly part of the unexplained contribution is due to the pyranometer values not being representative of the overall bare soil area. The radiant flux density values were quite low for the reflected component over the soil surface and a local situation may have influenced the pyranometer values. Other possible contributions to the different calibrations are a change in the spectral sensitivity of the Infrasil Quartz filter and drift in the electronics.

Table 4. Estimates of possible effects producing differences in the calibration constants (slopes) for different surfaces

Possible Effects	Possible error due to effect (%)	
	Salt Flats *vs* Green Plants	Salt Flats *vs* Soil
Temperature effect	+ 0.0-4.5	+ 0.0-4.5
Degradation of instrument during study period	0.0 (negligible)	0.0 (negligible)
Pyranometer spectral response	- 0.4	- 0.3
Spectral characteristics of surface interacting with spectral sensitivity of MRIR	+ 6.1	+11.6
Change in spectral sensitivity of MRIR from time of manufacture		
a) oxidation of reflecting surfaces	+ 3.3	+ 5.7
b) degradation or drift of Infrasil Quartz Filter, electronics, etc.	?	?
Total (temperature effect included)	14.3	22.1
Total (temperature effect not included)	9.8	17.6
Slope of curve (actually measured)	12.8	37.6
Unexplained (temperature effect included)	- 1.5	15.5
Unexplained (temperature effect not included)	3.0	20.0

RESULTS AND DISCUSSION

Land Surfaces

The land surfaces examined were the Bonneville Salt Flats, White Sands Alkali Flats and a plowed field of Nibley silty clay loam soil.

Bonneville Salt Flats

The indicatrices of reflected solar radiation for the Bonneville Salt Flats were determined for August 9, 1973 and August 8, 1974. In 1973, indicatrices were found for solar angles of 3.0°, 8.9°, 19.0°, 27.4°, 39.1°, 40.7°, 47.3°, 58.4°, and 62.6° as seen in Figures 7-1[illegible] All measurements were made in the morning except for the 39.1° and 58.4° solar angle values. In these and all successive figures, solar azimuth angle α = 0 is at the top of the diagram.

In Figure 7, the forward scatter exceeds the back scatter indicating a high degree of specular reflection. The maximum forward scatter for nadir angles greater than 80° is shown to be greater than 200 percent of the reflectance value for nadir angle = 0°. In Figure 8, the forward scatter is almost equal to the backward scatter, but the successive diagrams show the former diminishing with relation to the later as solar angle increases. At solar angles greater than 47.3°, the backscatter is the only anisotropic characteristic.

Figure 16a shows albedo *vs* solar angle measured with a pyranometer. Most of the values were measured in the vicinity of the tower except for the two points labelled "very bright area" and "wet area." These were measured at the edge of the uniform salt field near a body of water.

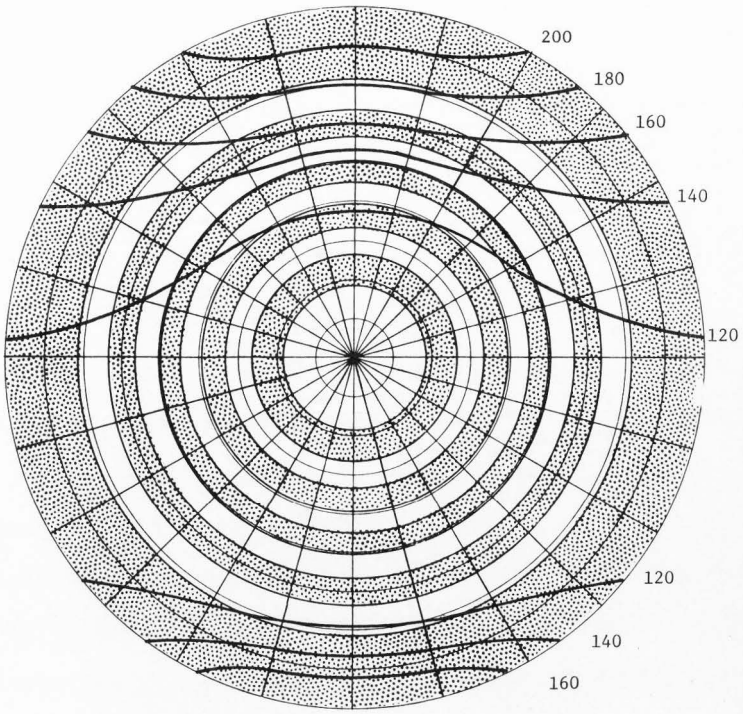

Figure 7. Isolines of reflectance over the Bonneville Salt Flats at solar angle = 3.0° for 1973. Values are based on a reflectance value normal to the surface (nadir angle = 0°) of 100.

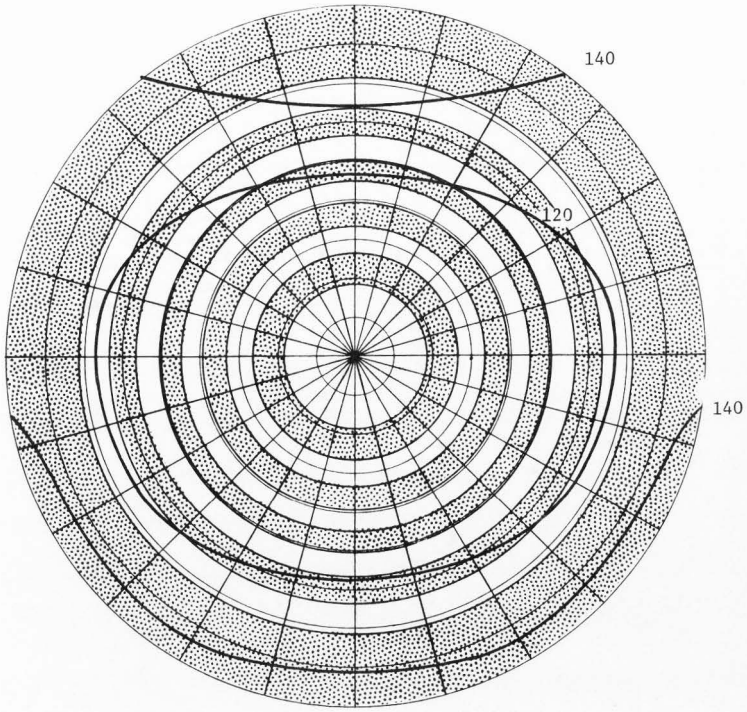

Figure 8. Isolines of reflectance over the Bonneville Salt Flats at solar angle = 8.9° for 1973. Values are based on a reflectance value normal to the surface (nadir angle = 0°) of 100.

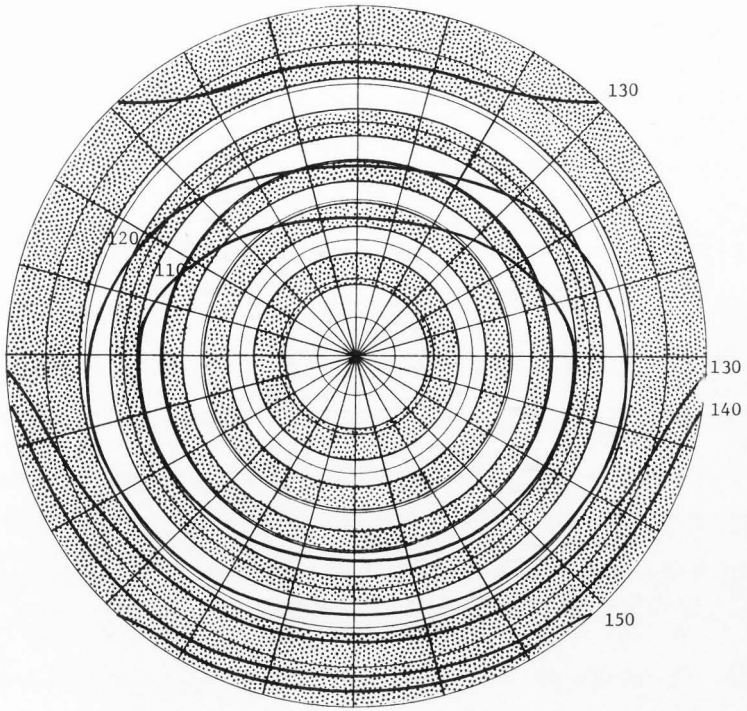

Figure 9. Isolines of reflectance over the Bonneville Salt Flats at solar angle = 19.0° for 1973. Values are based on a reflectance value normal to the surface (nadir angle = 0°) of 100.

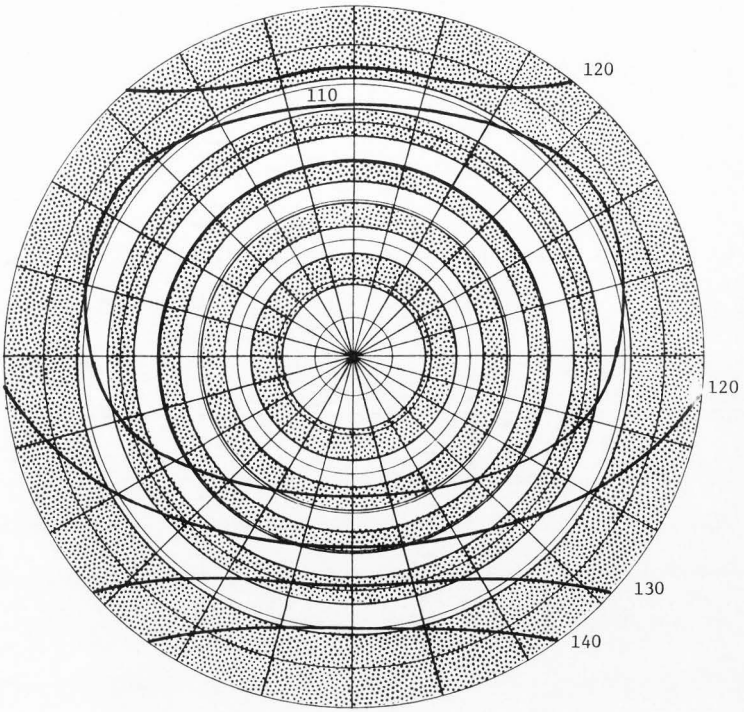

Figure 10. Isolines of reflectance over the Bonneville Salt Flats at solar angle = 27.4° for 1973. Values are based on a reflectance value normal to the surface (nadir angle = 0°) of 100.

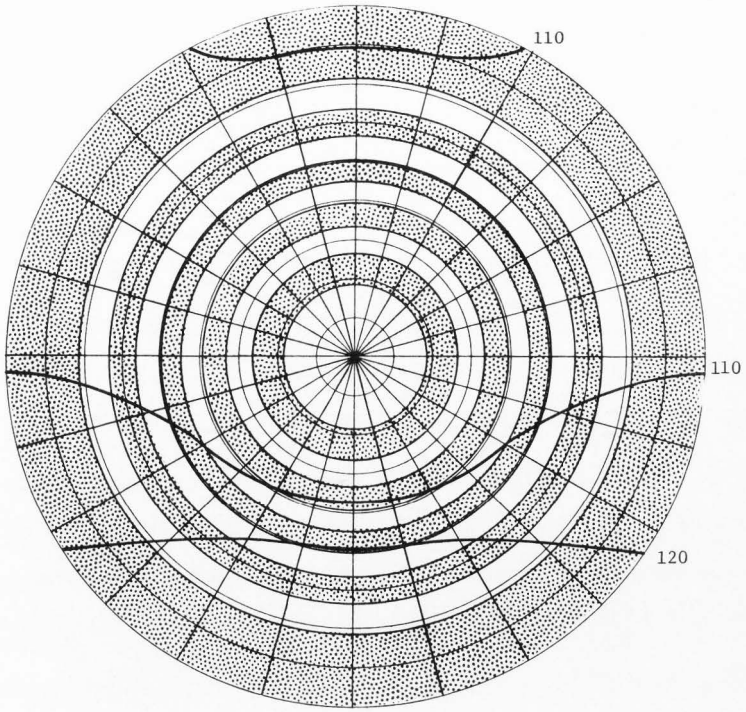

Figure 11. Isolines of reflectance over the Bonneville Salt Flats at solar angle = 39.1° for 1973. Values are based on a reflectance value normal to the surface (nadir angle = 0°) of 100.

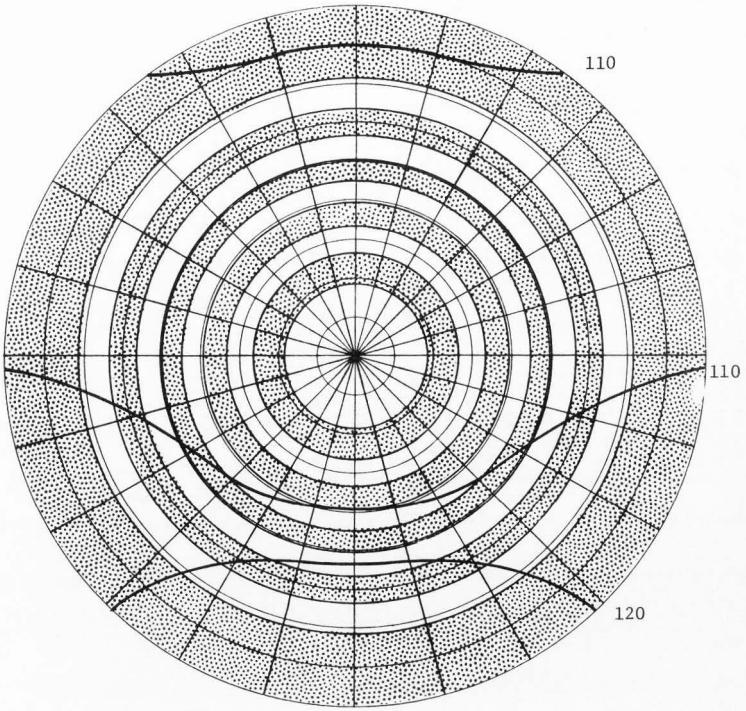

Figure 12. Isolines of reflectance over the Bonneville Salt Flats at solar angle = 40.7° for 1973. Values are based on a reflectance value normal to the surface (nadir angle = 0°) of 100.

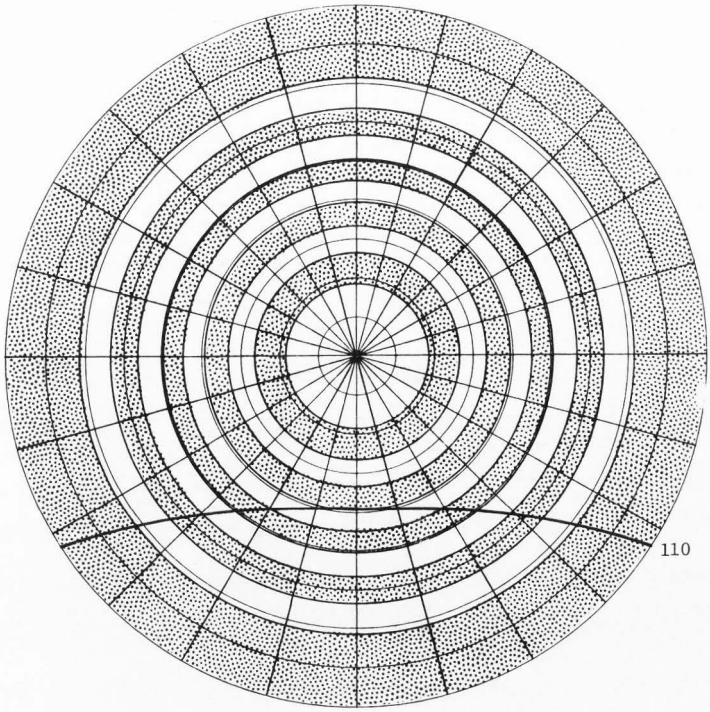

Figure 13. Isolines of reflectance over the Bonneville Salt Flats at solar angle = 47.3° for 1973. Values are based on a reflectance value normal to the surface (nadir angle = 0°) of 100.

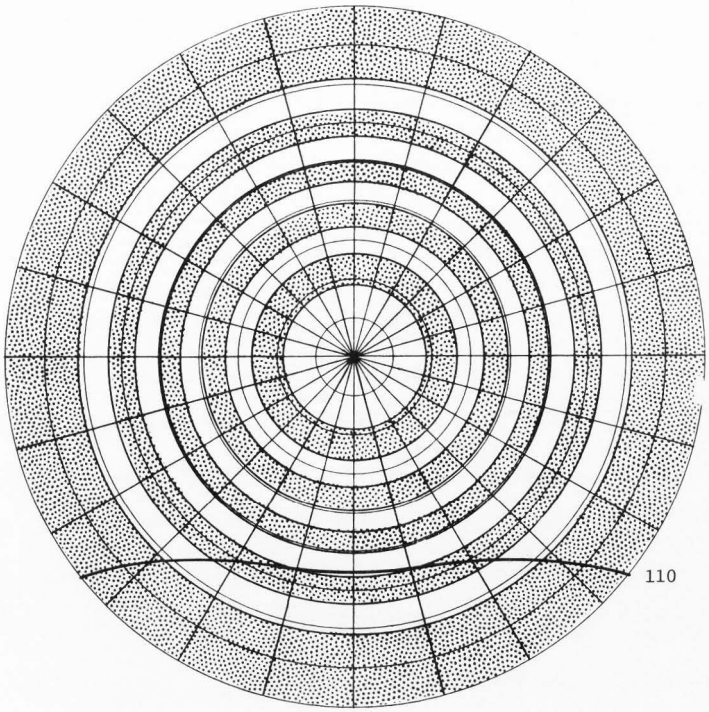

Figure 14. Isolines of reflectance over the Bonneville Salt Flats at solar angle = 58.4° for 1973. Values are based on a reflectance value normal to the surface (nadir angle = 0°) of 100.

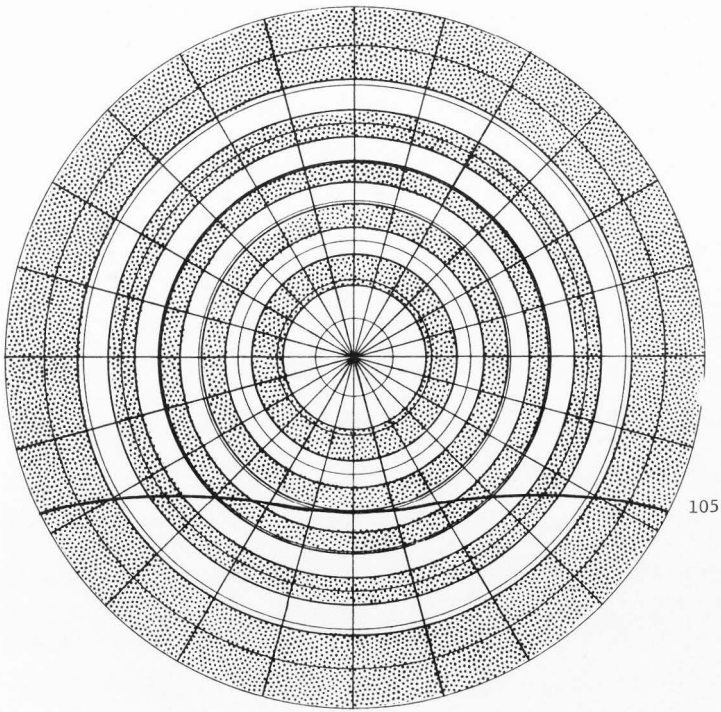

Figure 15. Isolines of reflectance over the Bonneville Salt Flats at solar angle = 62.6° for 1973. Values are based on a reflectance value normal to the surface (nadir angle = 0°) of 100.

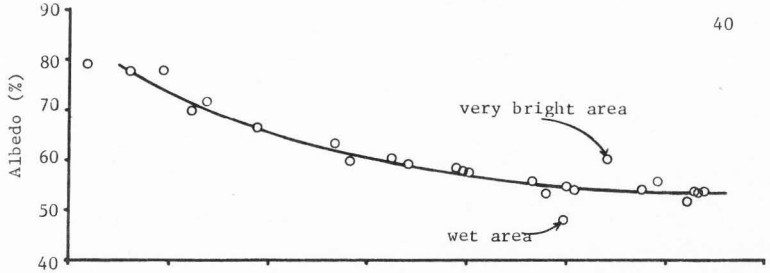

Figure 16a. Albedo vs solar angle for Bonneville Salt Flats, 1973.

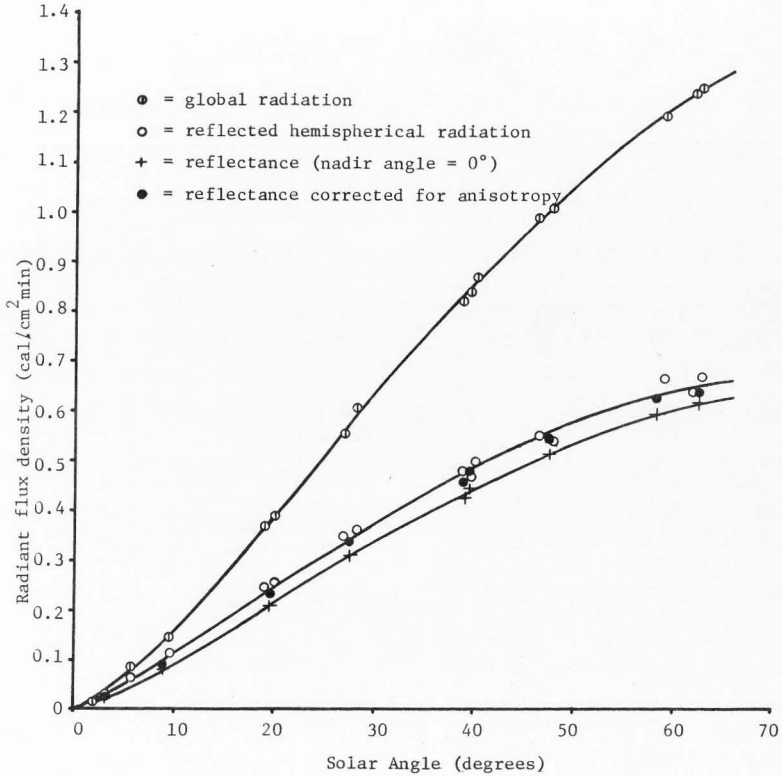

Figure 16b. Global, reflectance and reflected hemispherical radiation values for Bonneville Salt Flats, 1973.

The "very bright area" consisted of new fresh crystals while the "wet area" was partially submerged.

Figure 16b shows the incoming global radiation and reflected radiation values found with a pyranometer. Also the reflectance values for nadir angle = 0° from the MRIR are plotted. These values multiplied times the integrated correction factor for anisotropy from Figure 7-15 are also shown which produce a 2π reflectance equivalent to the values found with a pyranometer. Thus two curves were fitted, one for the nadir angles = 0° values and another for all 2π values.

The 1974 Bonneville Salt Flats indicatrices of reflected solar radiation were found for solar angles of 1.7°, 10.3°, 21.7°, 33.0°, 44.5°, 56.2°, and 64.7° as shown in Figures 17-23. As mentioned before, the antecedent precipitation from October to the date of measurement was considerably less during 1974 than during 1973 at the Bonneville Salt Flats.

Visual observation showed the surface to have a rougher texture in 1974 as compared with 1973. The data for 1974 do not show the specular effect as strongly in 1974 as was seen in 1973 for low solar angles. It is assumed that the antecedent moisture is responsible for this difference possibly from both the standpoint of genesis of the surface crystals and the actual presence of more moisture at the surface during 1973 producing a specular component. However, the general trend between the two years is similar. The backscatter and anisotropy diminishes with increasing solar angle as seen in the development of the indicatrices from Figure 17-23.

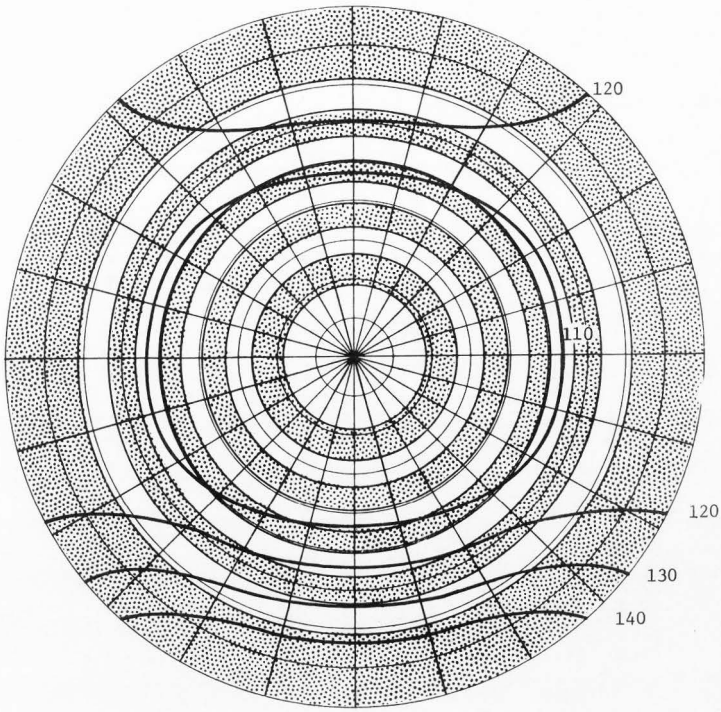

Figure 17. Isolines of reflectance over the Bonneville Salt Flats at solar angle = 1.7° for 1974. Values are based on a reflectance value normal to the surface (nadir angle = 0°) of 100.

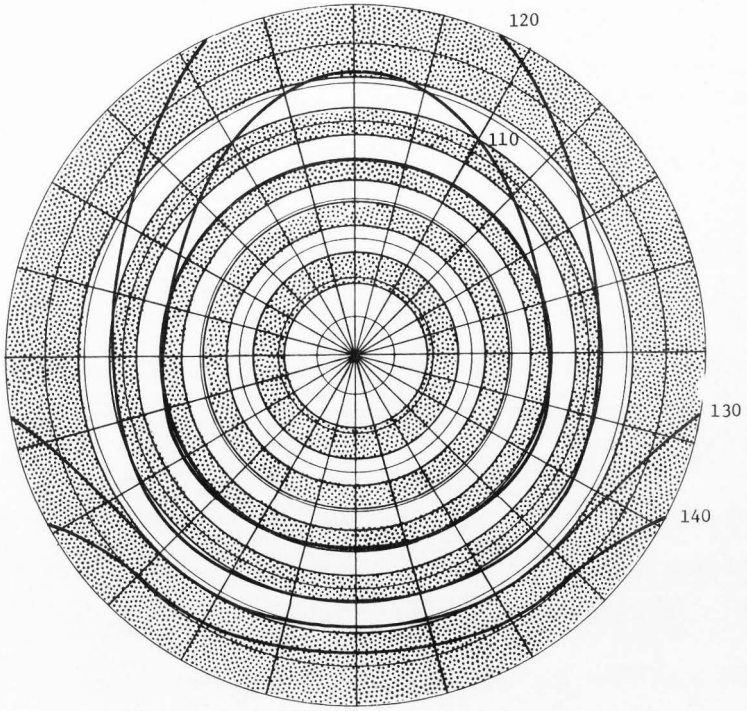

Figure 18. Isolines of reflectance over the Bonneville Salt Flats at solar angle = 10.3° for 1974. Values are based on a reflectance value normal to the surface (nadir angle = 0°) of 100.

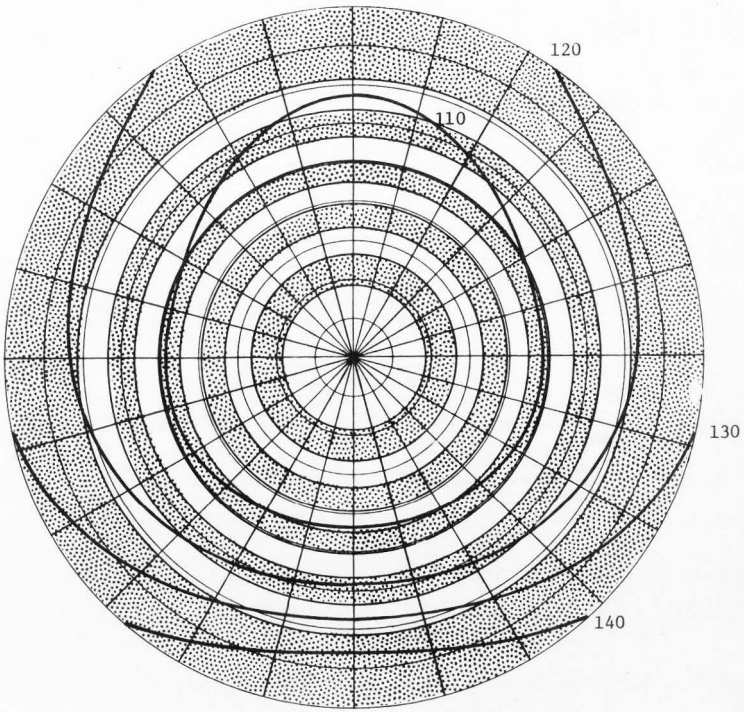

Figure 19. Isolines of reflectance over the Bonneville Salt Flats at solar angle = 21.7° for 1974. Values are based on a reflectance value normal to the surface (nadir angle = 0°) of 100.

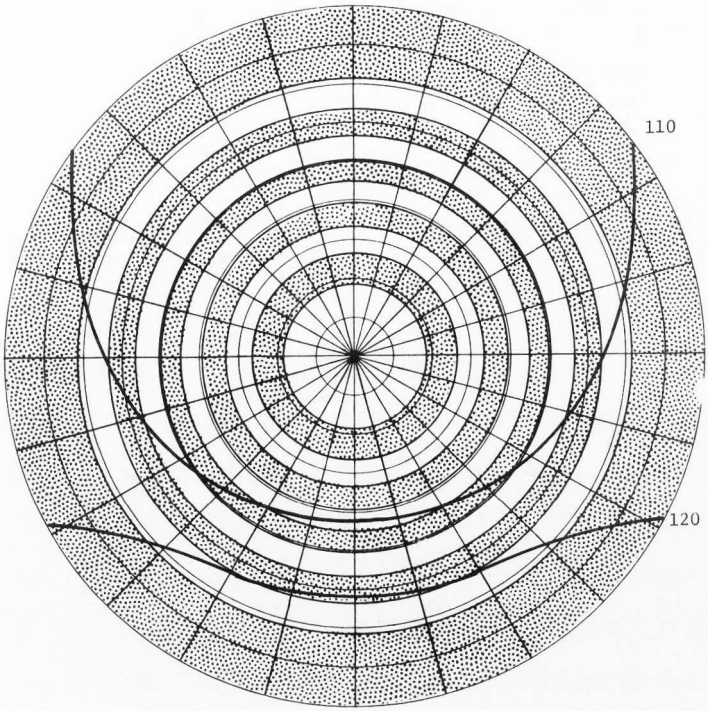

Figure 20. Isolines of reflectance over the Bonneville Salt Flats at solar angle = 33.0° for 1974. Values are based on a reflectance value normal to the surface (nadir angle = 0°) of 100.

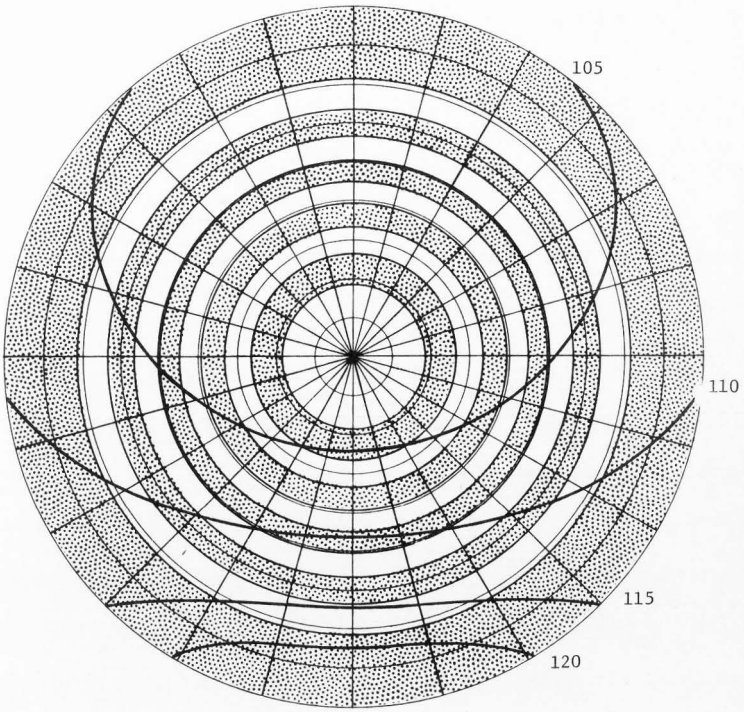

Figure 21. Isolines of reflectance over the Bonneville Salt Flats at solar angle = 44.5° for 1974. Values are based on a reflectance value normal to the surface (nadir angle = 0°) of 100.

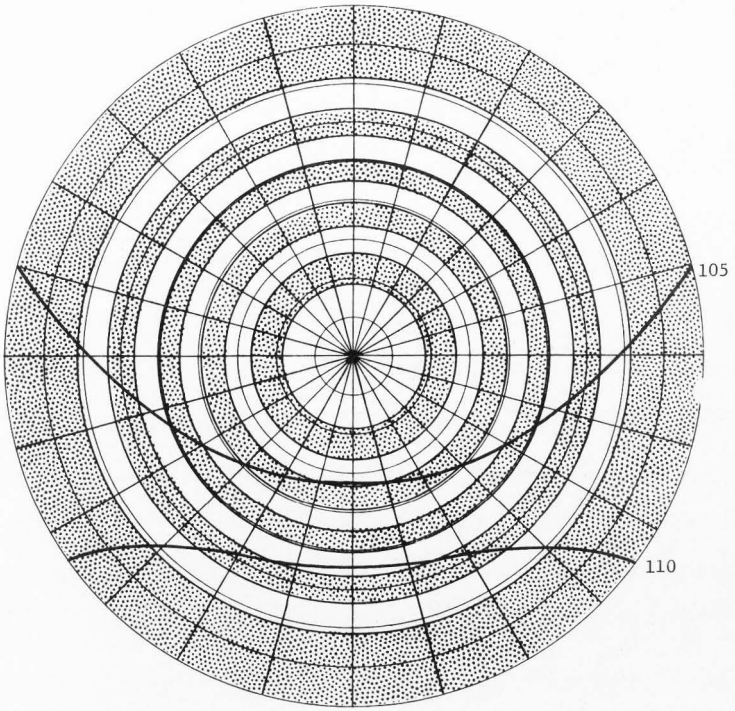

Figure 22. Isolines of reflectance over the Bonneville Salt Flats at solar angle = 56.2° for 1974. Values are based on a reflectance value normal to the surface (nadir angle = 0°) of 100.

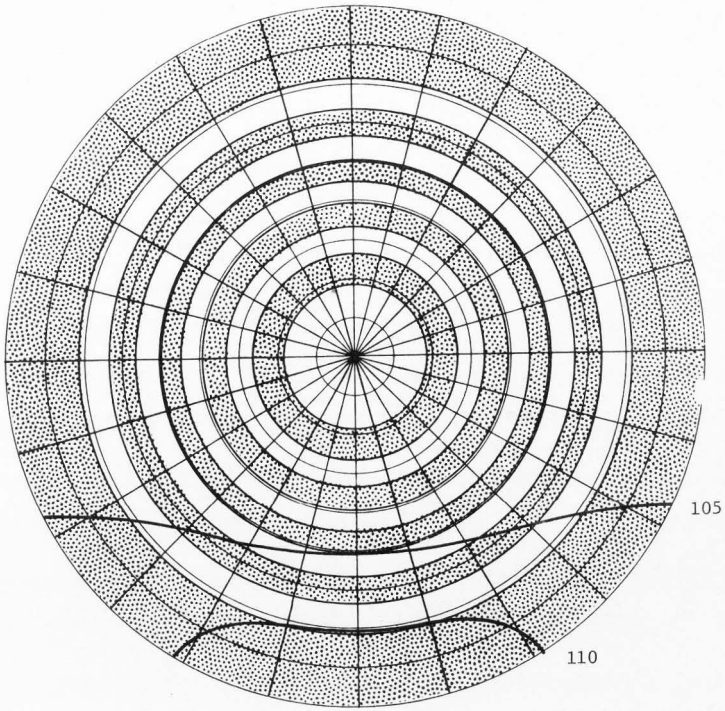

Figure 23. Isolines of reflectance over the Bonneville Salt Flats at solar angle = 64.7° for 1974. Values are based on a reflectance value normal to the surface (nadir angle = 0°) of 100.

Figure 24a shows albedo *vs* solar angle which resembles that found for the previous year. Figure 24b displays the pyranometer values for global and reflected radiation as well as the Nimbus MRIR values for nadir angle = 0° and the 2π reflectance derived values. Curves were fitted similar to those in Figure 16b. In both years the maximum deviation between the two lower curves is seen to be at approximately 40° solar angle. There is a convergence at higher solar angles of the two lower curves and is similar for both years measured at the Bonneville Salt Flats.

Alkali Flats at the White Sands area

Indicatrices of reflected solar radiation for the Alkali Flats at the White Sands area were found on May 20, 1974 for solar angles of 3.3°, 6.2°, 9.9°, 16.6°, 24.2°, and 31.0°, as seen in Figures 25-30.

Measurements taken on May 21, 1974 for solar angles of 69.7° and 73.7° failed to show anisotropy due to the high solar angles.

Figures 25-30 show both forwardscatter and backscatter. The forwardscatter does not disappear at higher solar angles as was found for the Bonneville Salt Flats. It is assumed that the forwardscatter is specular in nature and is produced at higher solar angles by the smoother surface found on the Alkali Flats than found on the Bonneville Salt Flats. All of the diagrams show the backscatter exceeding the forwardscatter in both absolute value and areal extent.

Figure 31a shows albedo *vs* solar angle for the Alkali Flats which is similar to that found for the Bonneville Salt Flats.

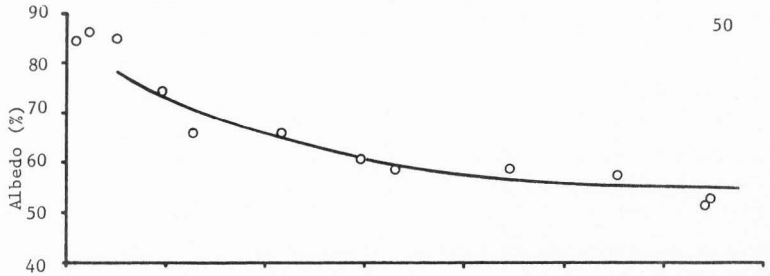

Figure 24a. Albedo vs solar angle for Bonneville Salt Flats, 1974.

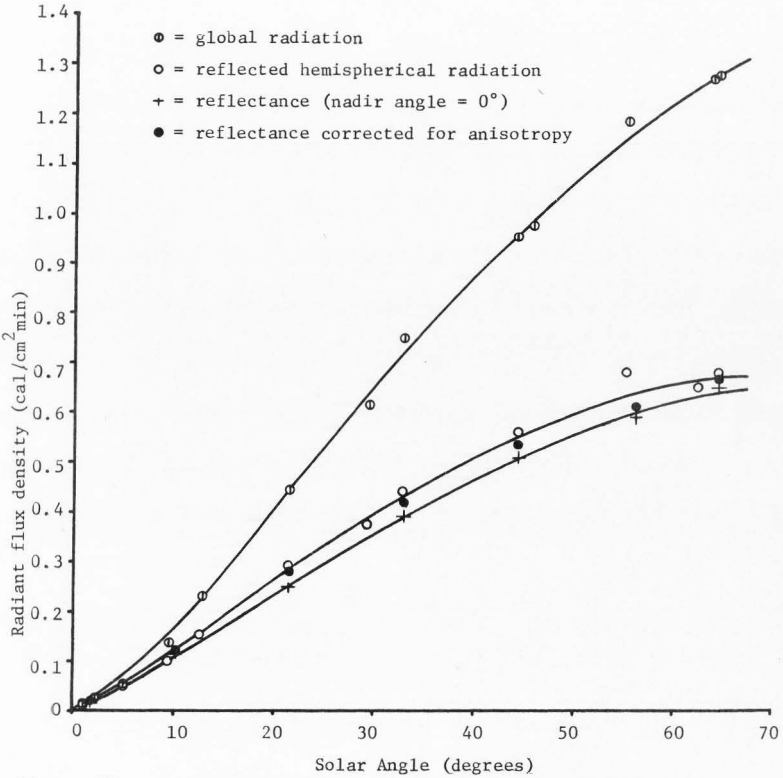

Figure 24b. Global, reflectance and reflected hemispherical radiation values for Bonneville Salt Flats, 1974.

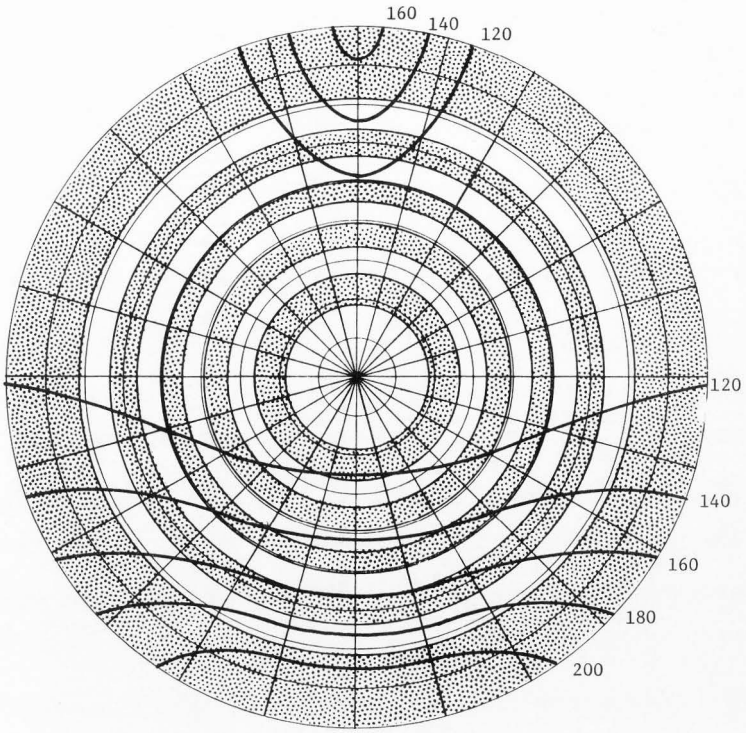

Figure 25. Isolines of reflectance over the Alkali Flats, Holloman Air Force Base, New Mexico on May 20, 1974 for solar angle = 3.3°. Values are based on a reflectance value normal to the surface (nadir angle = 0°) of 100.

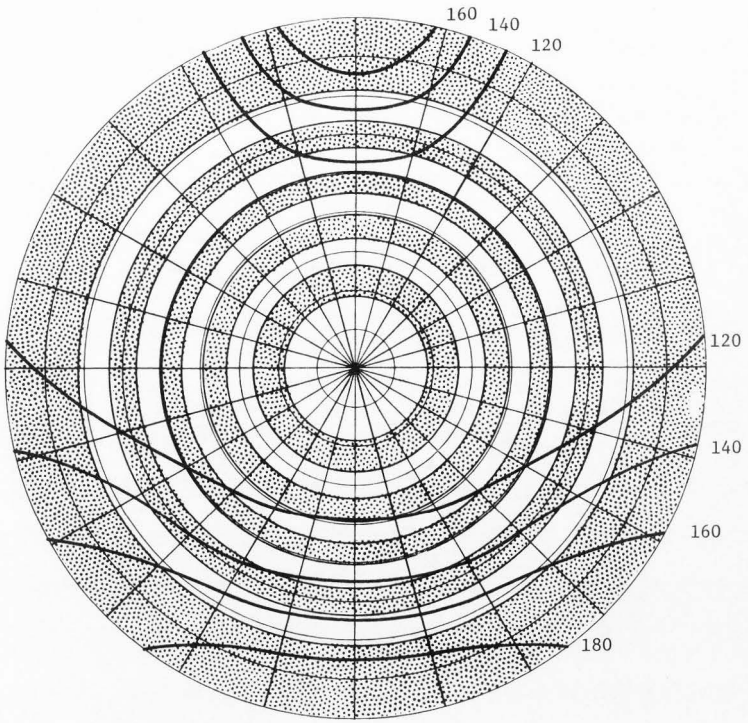

Figure 26. Isolines of reflectance over the Alkali Flats, Holloman Air Force Base, New Mexico on May 20, 1974 for solar angle = 6.2°. Values are based on a reflectance value normal to the surface (nadir angle = 0°) of 100.

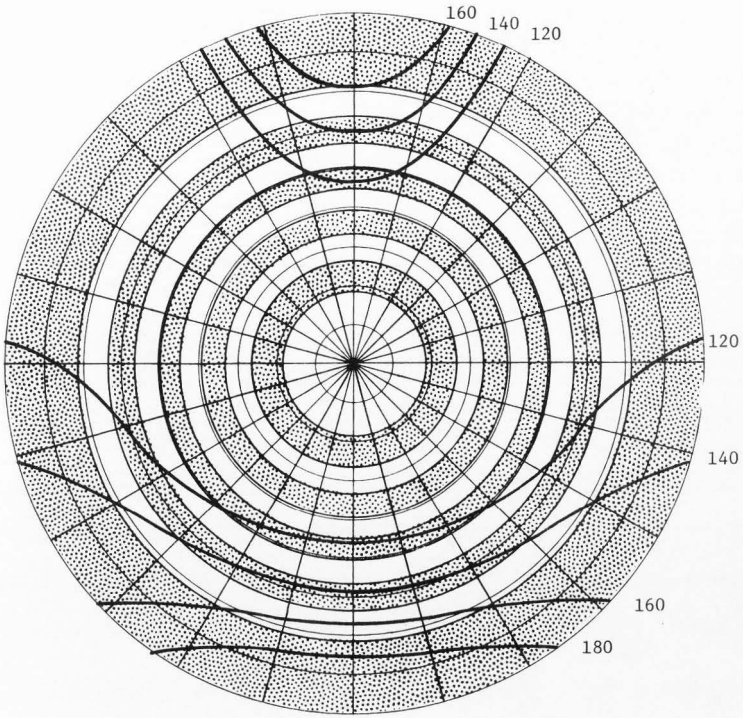

Figure 27. Isolines of reflectance over the Alkali Flats, Holloman Air Force Base, New Mexico on May 20, 1974 for solar angle = 9.9°. Values are based on a reflectance value normal to the surface (nadir angle = 0°) of 100.

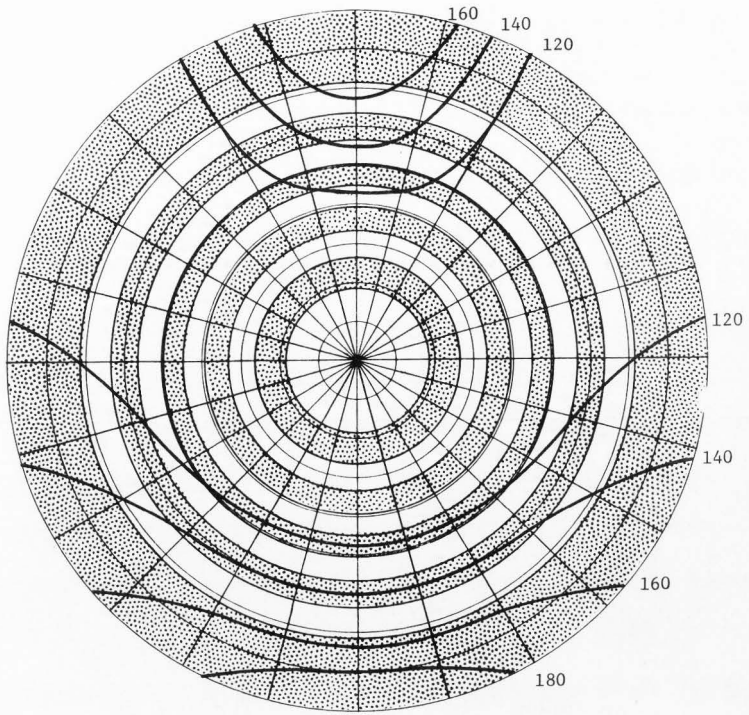

Figure 28. Isolines of reflectance over the Alkali Flats, Holloman Air Force Base, New Mexico on May 20, 1974 for solar angle = 16.6°. Values are based on a reflectance value normal to the surface (nadir angle = 0°) of 100.

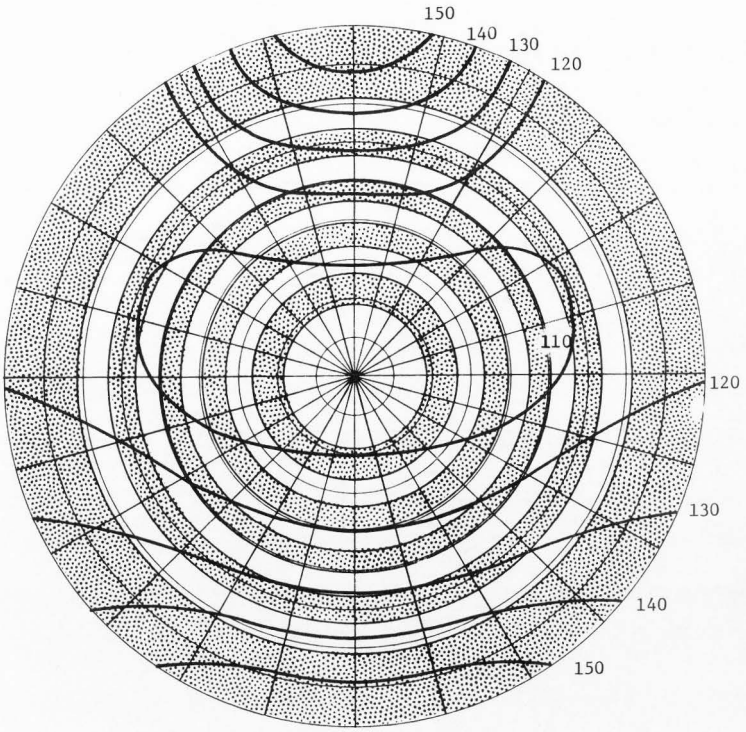

Figure 29. Isolines of reflectance over the Alkali Flats, Holloman Air Force Base, New Mexico on May 20, 1974 for solar angle = 24.2°. Values are based on a reflectance value normal to the surface (nadir angle = 0°) of 100.

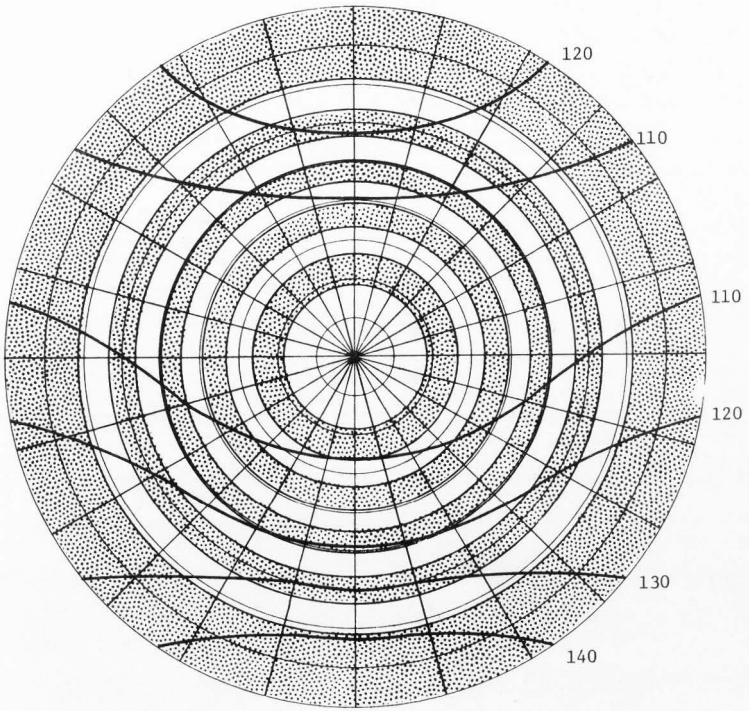

Figure 30. Isolines of reflectance over the Alkali Flats, Holloman Air Force Base, New Mexico on May 20, 1974 for solar angle = 31.0°. Values are based on a reflectance value normal to the surface (nadir angle = 0°) of 100.

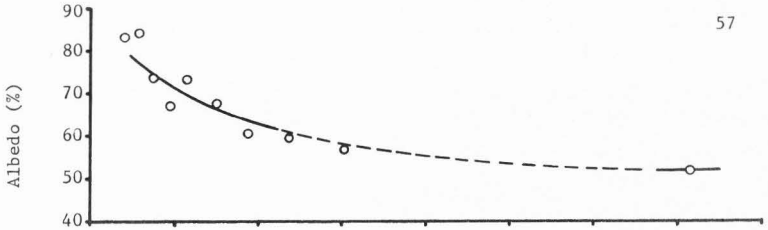

Figure 31a. Albedo vs solar angle over the Alkali Flats.

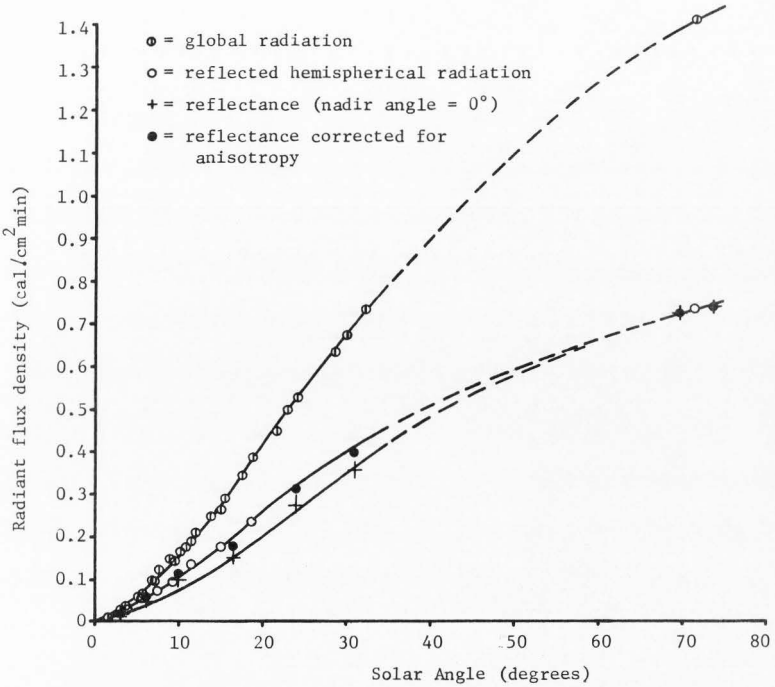

Figure 31b. Global, reflectance and reflected hemispherical radiation values for the Alkali Flats.

Figure 31b displays global and reflected radiation values as well as the Nimbus normal reflectance values and the 2π derived reflectances. For this feature the two lower curves are seen to show the maximum deviation at approximately 25° solar angle. Since (reflectance value for nadir angle =0°) (integrated 2π factor determined by indicatrices) = (2π value measured by a pyranometer), and the integrated 2π factor = 1.00 under isotropic conditions, there will be found convergence to the same curve under isotropic conditions. This is seen in the extrapolation to 69.7° solar angle from the 31.0° solar angle value.

Plowed field

The plowed field of Nibley silty clay loam was examined on October 5, 1973 to determine the indicatrices of reflected radiation for solar angles of 12.5°, 17.5°, 25.0°, 33.4°, and 40.0° as shown in Figures 32-36.

A characteristic of these indicatrices not found in the previously discussed features is the lack of forwardscatter. The plowed field actually shows a decrease in reflectances as the nadir angle increases for the sectors in the sun's direction. The explanation for this effect is the great roughness of the surface producing many shadows when viewing in the forward direction.

The backscatter also shows a different character than previously described with the Alkali Flats and Bonneville Salt Flats. In the backscatter the relative values to the normal reflectance are greater, exceeding 500 percent as shown in Figure 32. Also the pattern of backscatter is more localized and not as broadly distributed. This is also

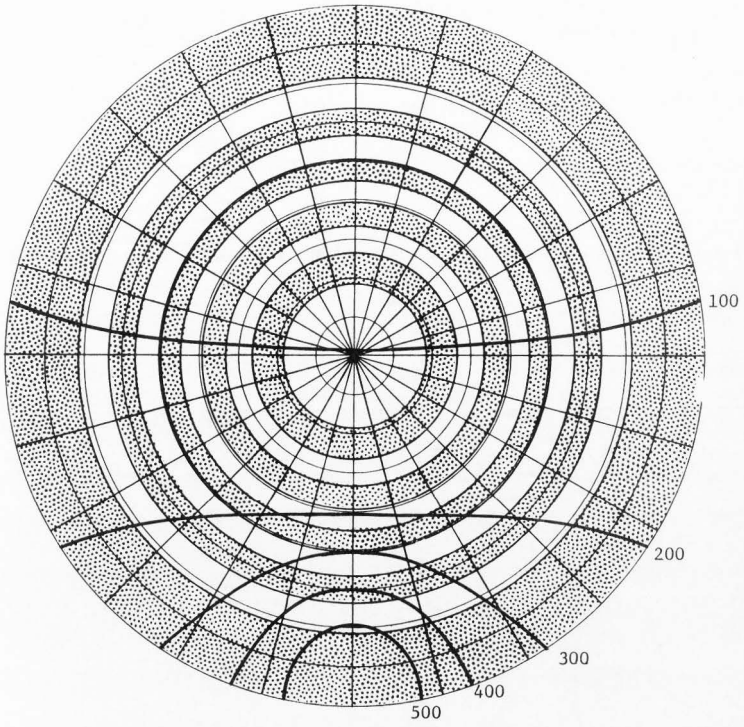

Figure 32. Isolines of reflectance for a plowed field of Nibley silty clay loam for solar angle = 12.5°. Values are based on a reflectance value normal to the surface (nadir angle = 0°) of 100.

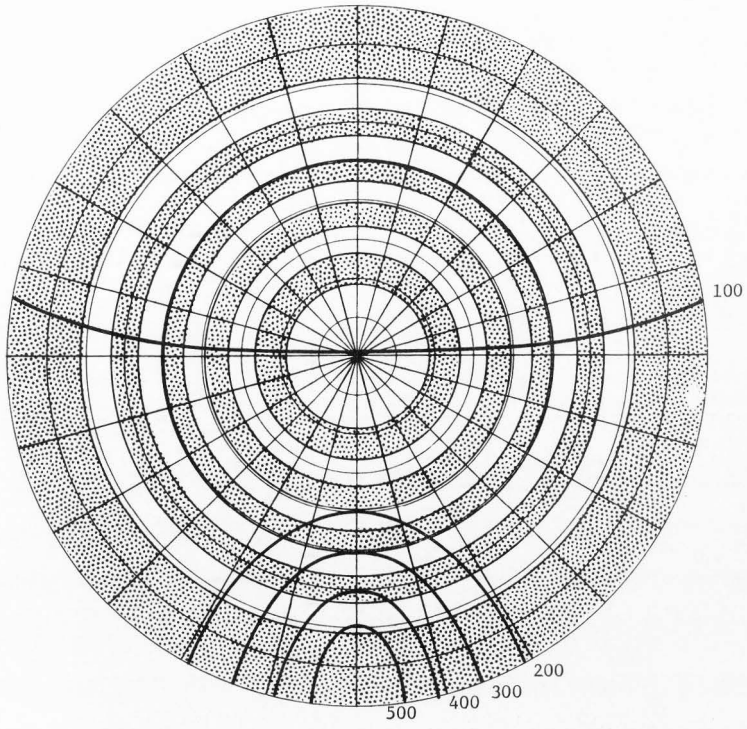

Figure 33. Isolines of reflectance for a plowed field of Nibley silty clay loam for solar angle = 17.5°. Values are based on a reflectance value normal to the surface (nadir angle = 0°) of 100.

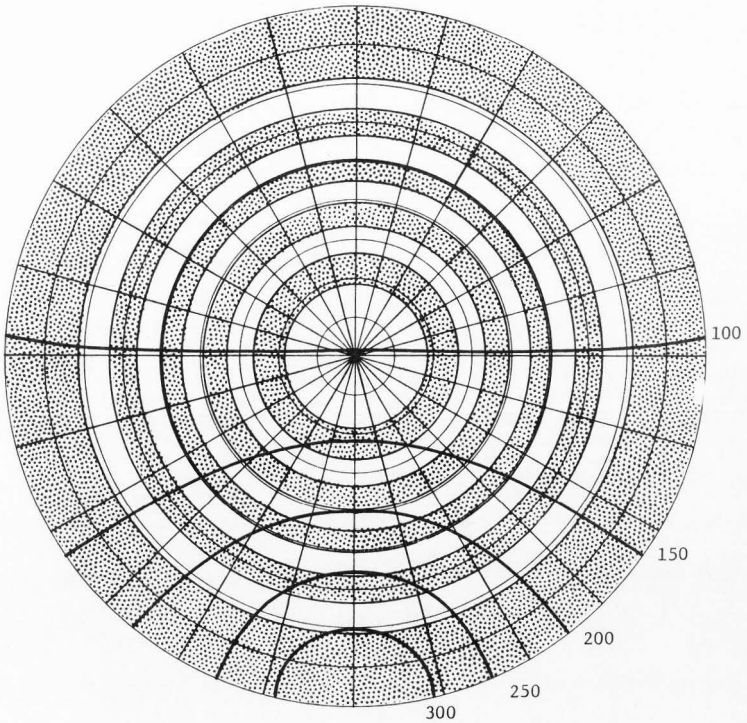

Figure 34. Isolines of reflectance for a plowed field of Nibley silty clay loam for solar angle = 25.0°. Values are based on a reflectance value normal to the surface (nadir angle = 0°) of 100.

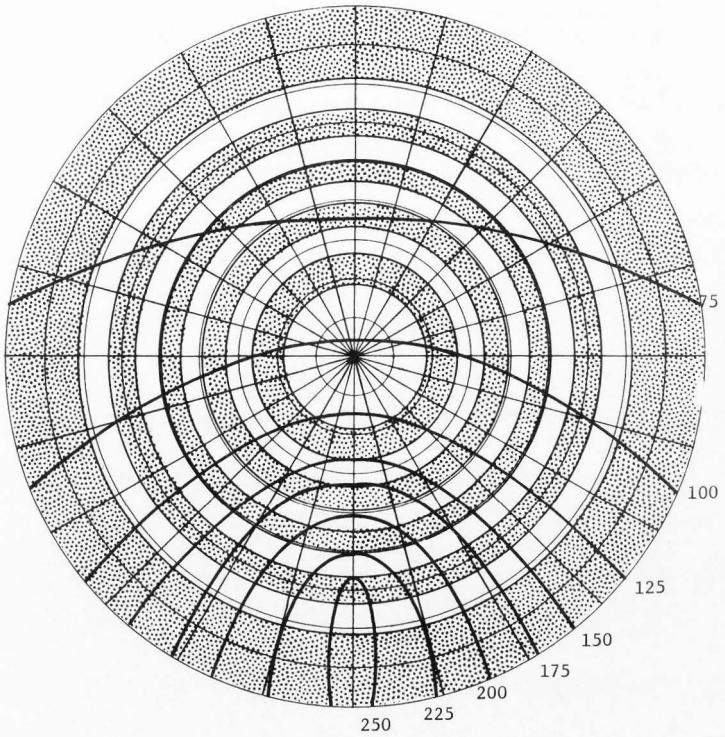

Figure 35. Isolines of reflectance for a plowed field of Nibley silty clay loam for solar angle = 34.3°. Values are based on a reflectance value normal to the surface (nadir angle = 0°) of 100.

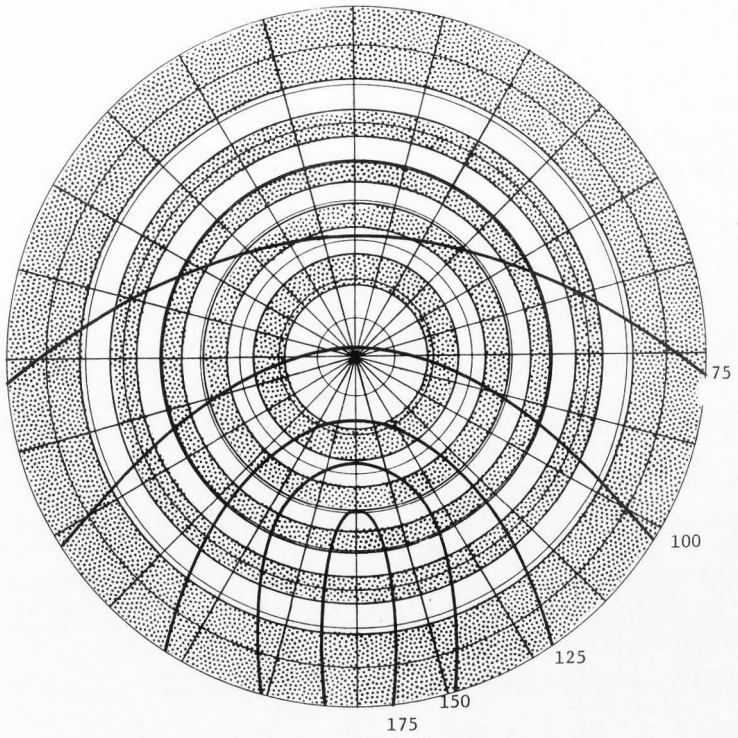

Figure 36. Isolines of reflectance for a plowed field of Nibley silty clay loam for solar angle = 40.0°. Values are based on a reflectance value normal to the surface (nadir angle = 0°) of 100.

explained by the geometry of the rough surface whereby the anti-solar point will now have large clods producing surfaces normal to the direct beam component, thereby increasing the backscatter. In all cases, the anti-solar point falls within the isolines of highest reflectance.

The anti-solar point, referred to as the "hot-spot" by those engaged in aerial photogrammetry, is described in the "Manual of Color Aerial Photography," 1968. This point occurs diametrically opposite to the point of the sun's specular reflection and is found at the same distance from the principal point.

The trend in Figures 32-36 is also toward isotropy with increasing solar angle. Figure 37a shows that the albedo over the plowed field doesn't vary much on a daily basis and is approximately only 10.0 percent. Figure 37b displays the reflected radiation measured with a pyranometer as well as the normal reflectance values and 2π derived reflectance found with the Nimbus MRIR. At 40° solar angle, the integrated value for the correction of anisotropy is less than 100 percent and causes the two curves to cross at about 40° solar angle.

Photography utilizing a fish-eye lens was employed to observe qualitatively the reflection properties of the land surfaces of the Bonneville Salt Flats, White Sands Alkali Flats and the plowed field. The photographs in Figures 38 and 39 show the 1974 Bonneville Salt Flats surface conditions for a low and high solar angle, respectively. Figure 38 agrees with the results shown in Figure 17 whereby there is some forwardscatter but the backscatter predominates. Figure 39 corresponds to the results in Figure 20 where backscatter is evident but there is no apparent forwardscatter. The small visible ridges which are in the

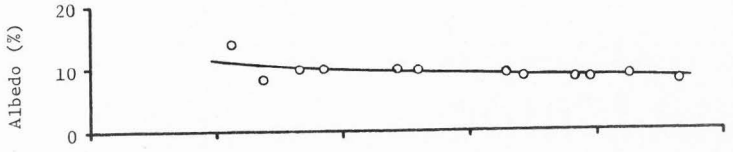

Figure 37a. Albedo vs solar angle for the plowed field.

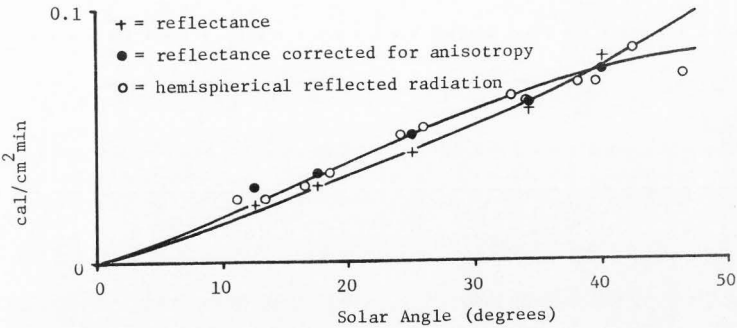

Figure 37b. Reflectance, reflectance corrected for anisotropy and hemispherical reflected radiation values measured with pyranometer for a plowed field.

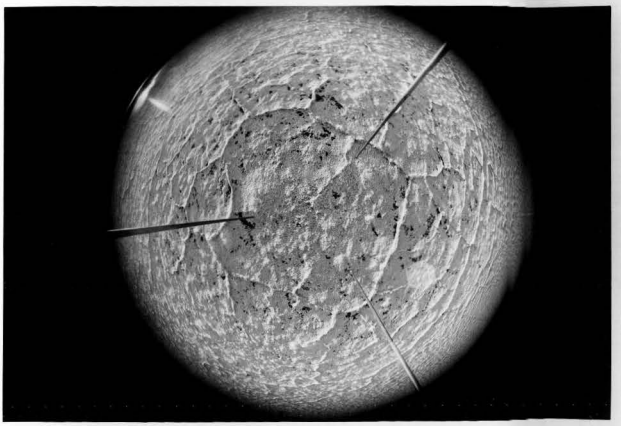

Figure 38. Fish-eye photograph of Bonneville Salt Flatts for a low solar angle.

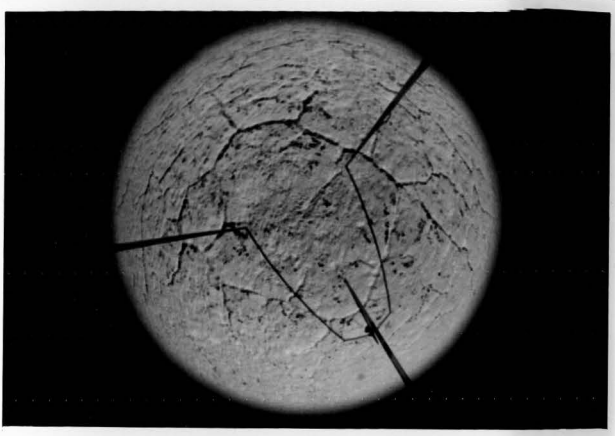

Figure 39. Fish-eye photograph of Bonneville Salt Flatts for a high solar angle.

photographs contribute to the backscatter from a geometrical point of view. The roughness produces a proportion of shaded area when viewing toward the sun while the same surface irregularities produce an increased backscatter.

Figure 40 shows a fish-eye photograph taken from a helicopter over the White Sands Alkali Flats. The backscatter shows the greatest reflectances with the forwardscatter also exceeding the reflectances normal to the surface; these effects agreeing with the measurements over the feature.

Figure 41 is a photograph taken over the plowed field and displays clearly the maximum reflectances within the vicinity of the shadow of the camera which locates the anti-solar point. The photograph also shows the decrease in reflected radiation from nadir angles of 0° to 90° in the direction toward the sun. Both of these effects are shown in the measured indicatrices as seen in Figures 32-36.

Figure 42 shows the percentage of correction that must be applied to reflectances for nadir angle = 0° in order to find the hemispherical or integrated 2π reflection values. Each point represents the overall weighted mean for each indicatrix. A polar planimeter was used to find the areas and a mean for the zones contributing equal power to a hemispherical receiver determined the anisotropic correction factors.

All four land surfaces examined show a trend toward isotropy. The Bonneville Salt Flats and White Sands Alkali Flats show similar slopes and values of their respective curves, indicating similar anisotropic correction factors for corresponding solar angles. The plowed field shows a steeper slope than found for the other features, demonstrating

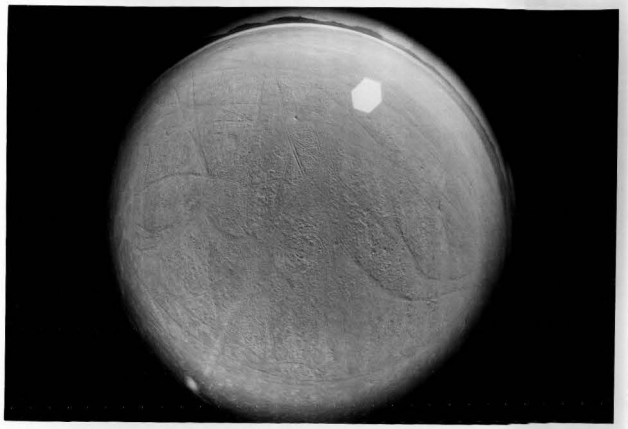

Figure 40. Fish-eye photograph of the Alkali Flats.

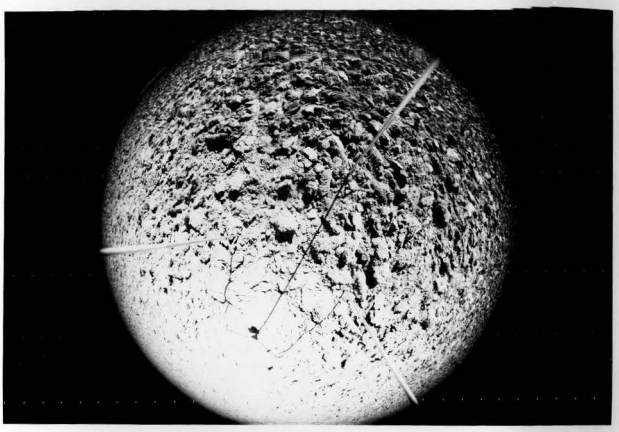

Figure 41. Fish-eye photograph of a plowed field.

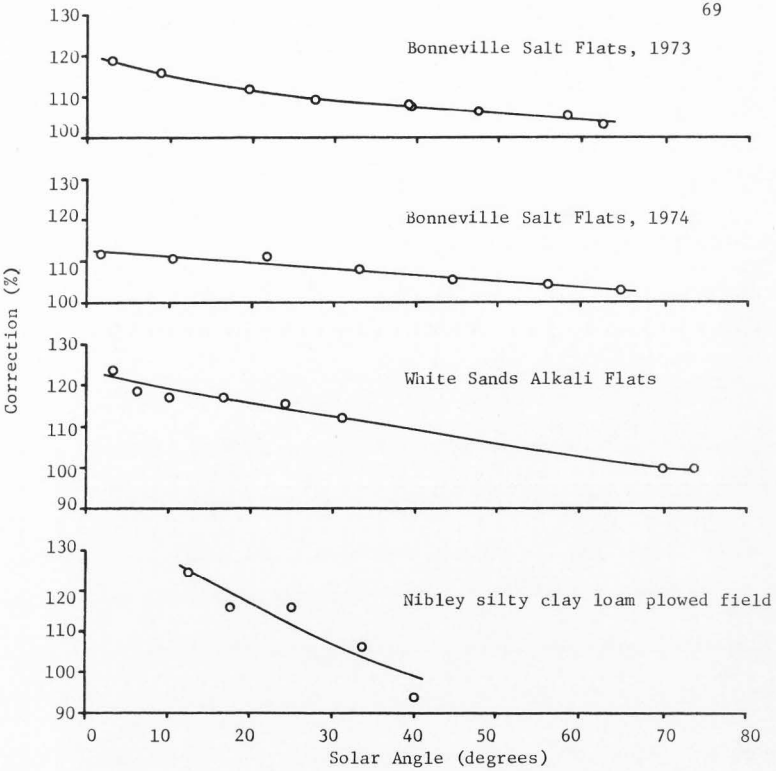

Figure 42. Percentage of correction *vs* solar angle that must be applied to reflectances for nadir angle = 0° to obtain the hemispherical reflection values for the mineral surfaces examined.

a greater change in anisotropy with change in solar angle. This is explained by the greater dimensional roughness of the plowed field than found with the other features which show up in greater range of shadow patterns and backscatter with a corresponding change in solar angle.

Snow surface

The albedo of snow is more complicated than most surfaces because of the metamorphism of the snowpack (Dirmhirn and Eaton, 1975). This is evidenced by the asymmetric daily variation of albedo as shown in Figure 43 whereby the minimum is not at noon but in general is shifted about 2 hours into the afternoon. A snowpack is a very dynamic system and thus the indicatrices of reflected radiation are assumed to change greatly with the condition of the snowpack. A ripe snowpack was measured on April 4, 1973 for solar angles of 13.2°, 17.9°, 25.2°, 42.0°, and 54.4°. In Figure 44 the values for 0°, 30°, 60°, and 90° nadir angles are presented with the radius of the circle equal to 100 and all other values proportioned to this distance. The snow surface had a glazed appearance which produced a broad streak of reflected light in the forward direction. Specular reflection greatly overpowers the backscatter, particularly as the solar angle decreases.

Figures 45-49 show the results of Figure 44 in the same format as previously described. The diagrams show the large gradient of forward scatter but also show that the contribution to the total integrated 2π reflectance isn't very large, particularly for some of the highest values. The trend shown by the indicatrices also is toward isotropy as solar angle increases.

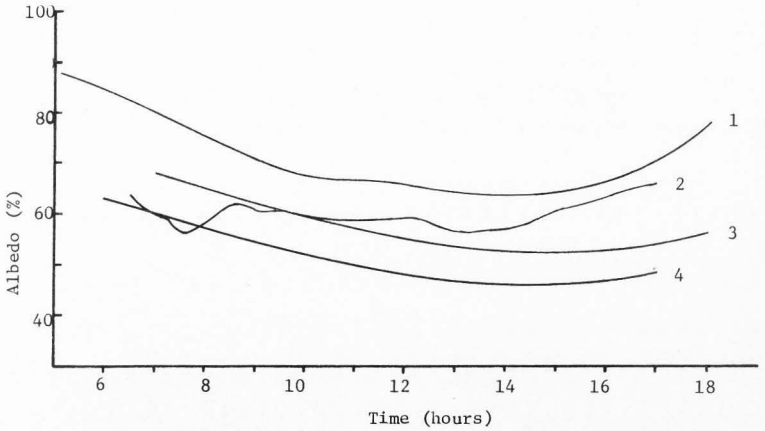

Figure 43. Daily variation of albedo on a clear day:

1. Lemon Creek Glacier, near Juneau, Alaska, Summer 1954 (R.C. Hubley, 1955).
2. Granular snow, Tartu, USSR, March, 1956 (H. Tooming, 1960).
3. Snow and firn, September 1950, and
4. Snow and firn, July, 1950 (F. Sauberer and I. Dirmhirn, 1952).

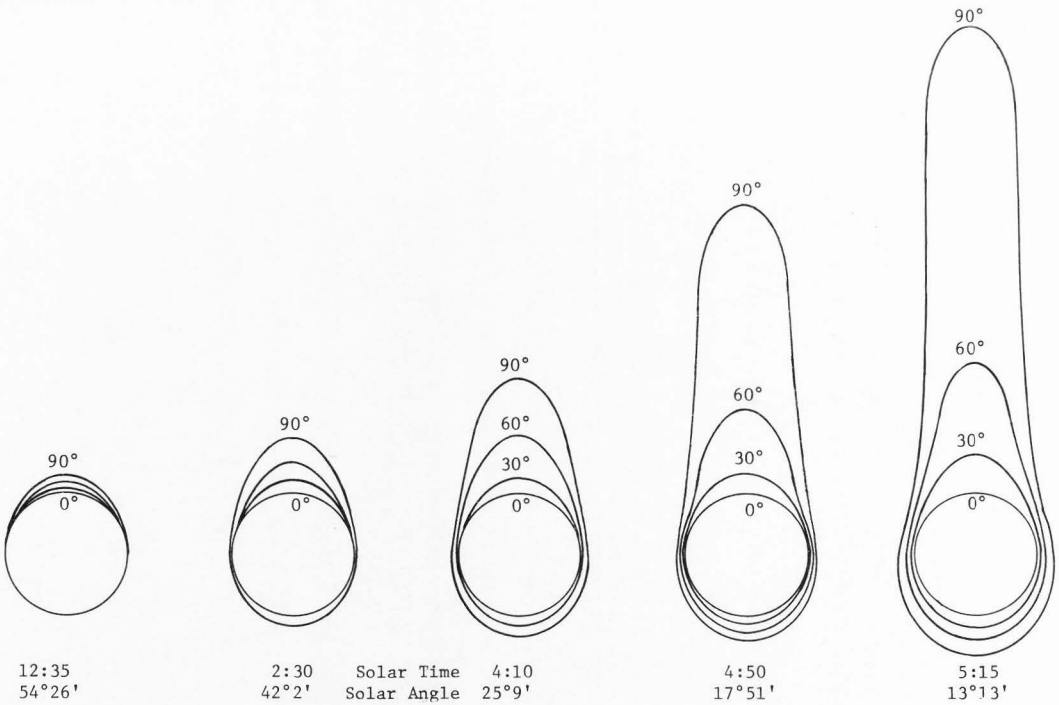

Figure 44. Indicatrices of snow reflectance at different sola. angles on 4 April 1973.

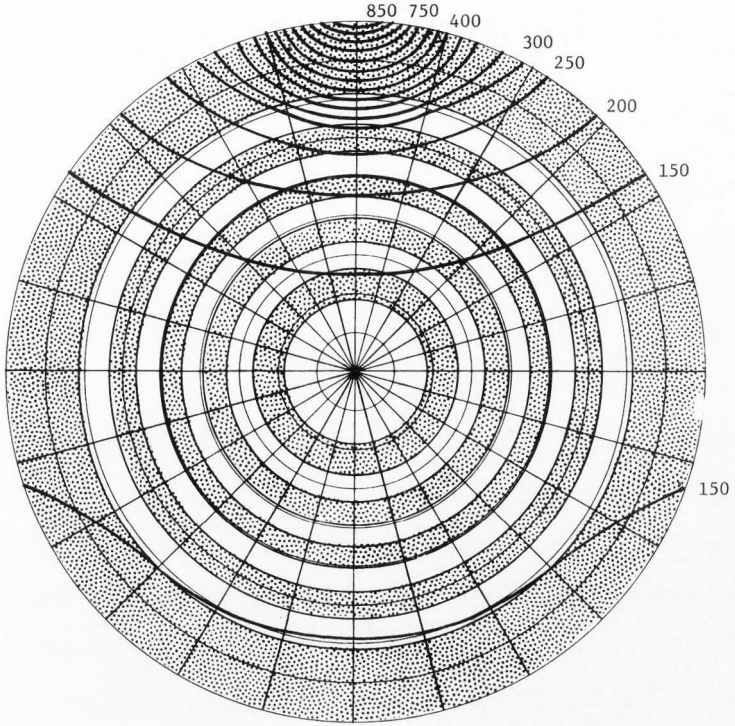

Figure 45. Isolines of reflectance for a glazed snow surface at solar angle = 13.2°. Values are based on a reflectance value normal to the surface (nadir angle = 0°) of 100.

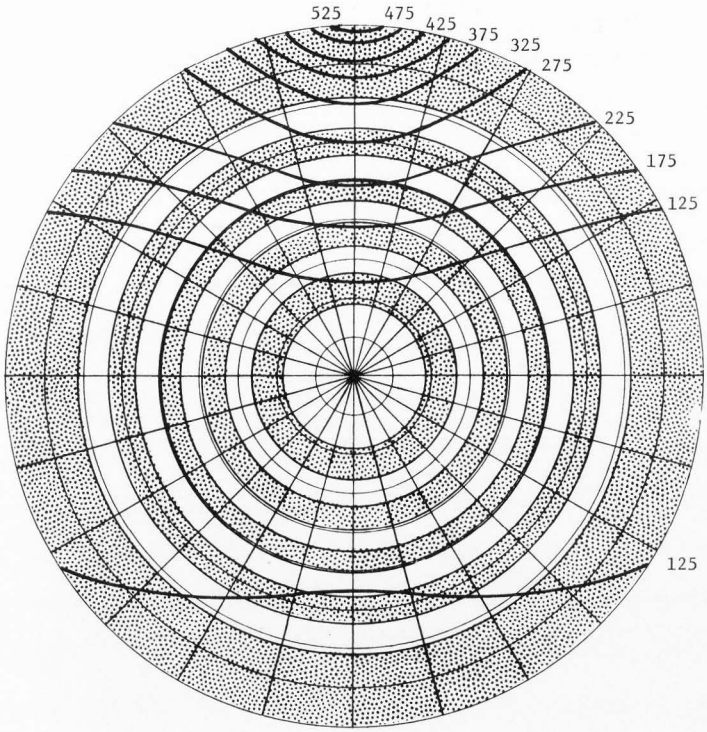

Figure 46. Isolines of reflectance for a glazed snow surface at solar angle = 17.9°. Values are based on a reflectance value normal to the surface (nadir angle = 0°) of 100.

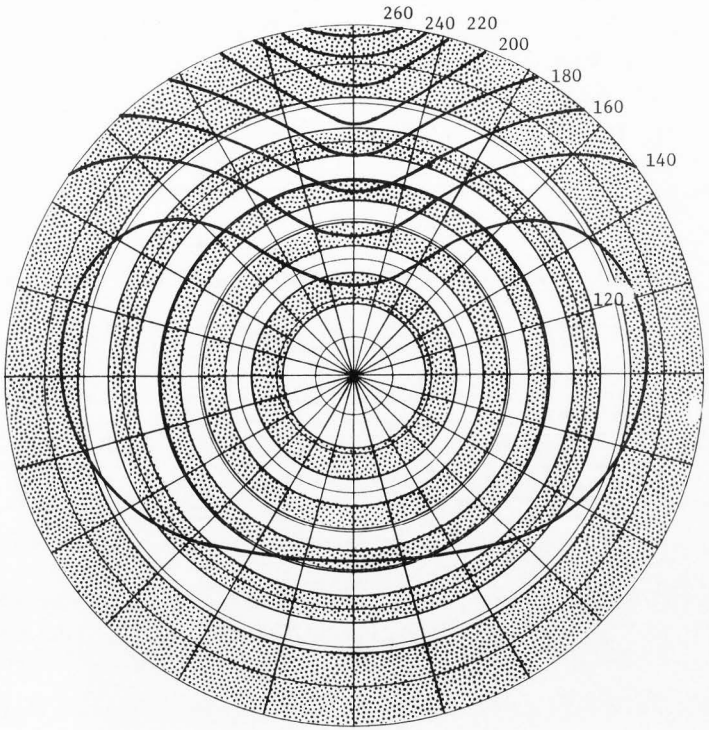

Figure 47. Isolines of reflectance for a glazed snow surface at solar angle = 25.2°. Values are based on a reflectance value normal to the surface (nadir angle = 0°) of 100.

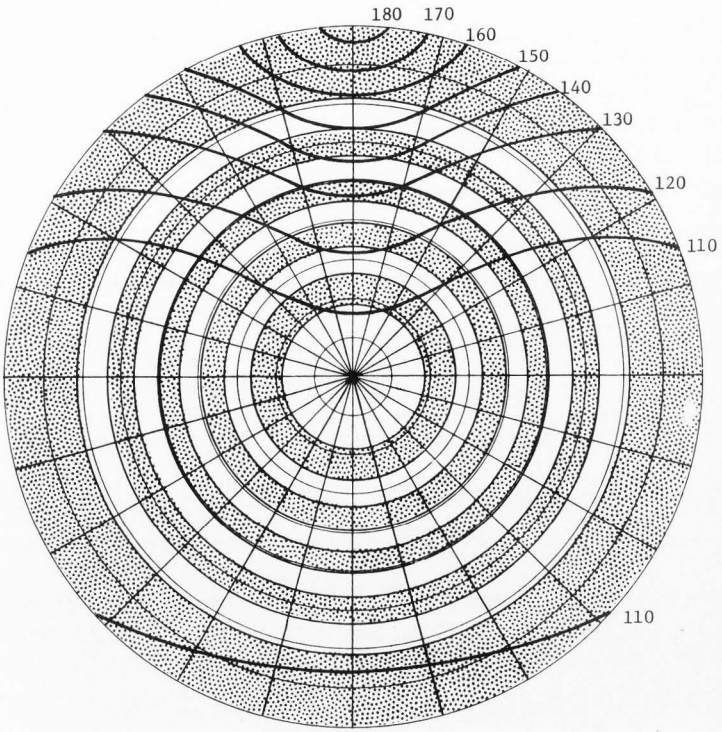

Figure 48. Isolines of reflectance for a glazed snow surface at solar angle = 42.0°. Values are based on a reflectance value normal to the surface (nadir angle = 0°) of 100.

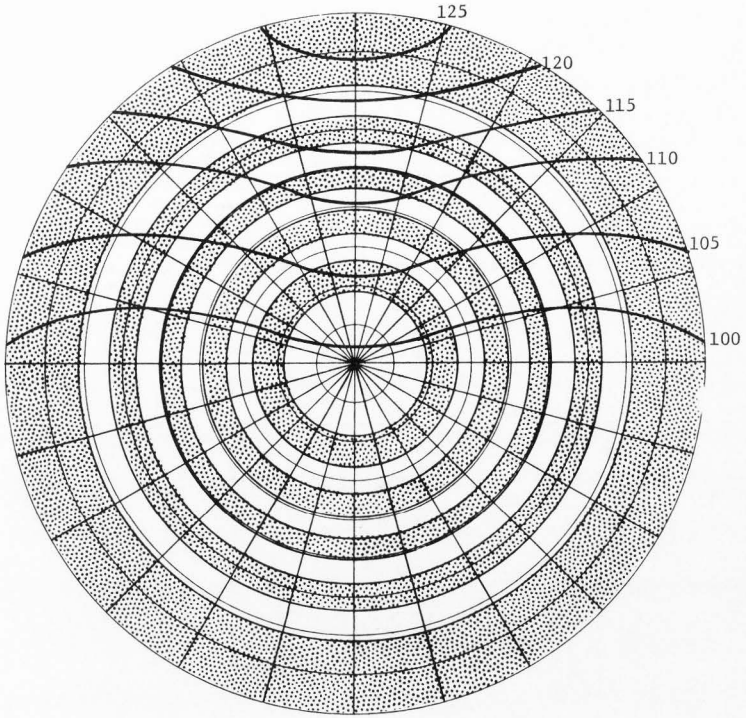

Figure 49. Isolines of reflectance for a glazed snow surface at solar angle = 54.5°. Values are based on a reflectance value normal to the surface (nadir angle = 0°) of 100.

Figure 50 shows reflected radiation *vs* solar angle values determined with a pyranometer as well as the TIROS normal reflectance values and the 2π values derived from the normal reflectance values with their respective corrections for anisotropy.

The maximum deviation between the two curves for the snow surface occurs at about 20° solar angle with a convergence above 40° solar angle, but the two curves never cross.

The TIROS values at 54.4° solar angle had to be slightly adjusted so that the 2π derived value fitted the curve for the pyranometer values. The TIROS radiometer is not as stable as the Nimbus MRIR and apparently performed some irregularity for that individual measurement.

Figure 51 shows the percentage of correction that must be applied to the reflectances of nadir angle = 0° in order to find the hemispherical or 2π reflected radiation values. At the higher solar angles the results show a trend toward isotropy.

Agricultural Crops

Alfalfa

Measurements were taken with the Nimbus MRIR over the alfalfa field on August 23, 1974 at solar angles of 9.7°, 17.0°, 27.7°, 42.2°, and 57.3°. As illustrated in Figure 52, the most pronounced characteristic observed is the strong backscatter which reaches a maximum of over 300 percent of the reflectance value normal to the surface. The anti-solar point is also located within the area of maximum reflectances for Figures 52 and 53 as seen in the plowed field.

Also seen in Figure 52 is a strong forward scatter, exceeding 200 percent of the vertical reflectance. This is probably due to two effects;

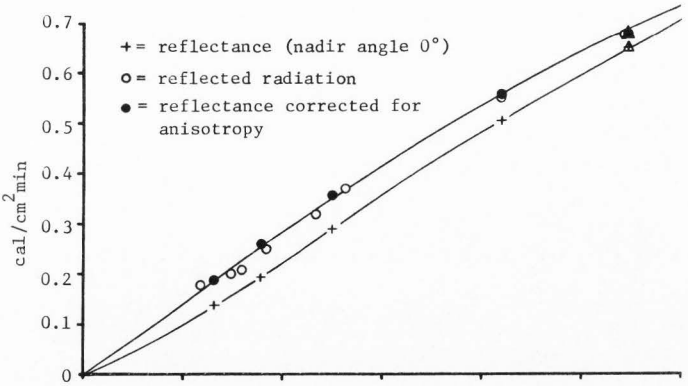

Figure 50. Reflectance (nadir angle = 0°) measured with TIROS radiometer, and reflected radiation measured with pyranometer, for different solar angles for a spring glazed snow surface.

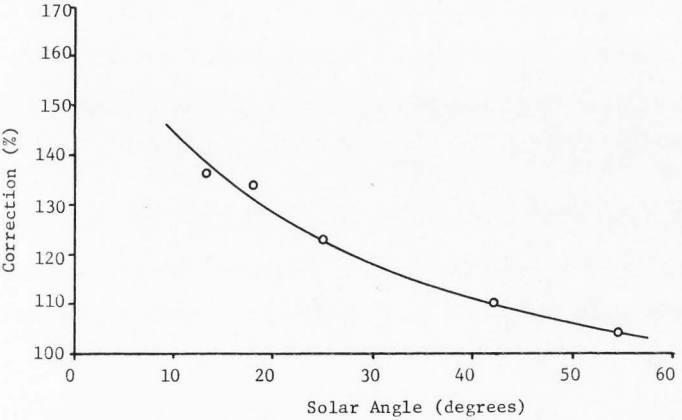

Figure 51. Percentage of correction *vs* solar angle that must be applied to reflectances for nadir angle = 0° to obtain the hemispherical reflection values for a spring glazed snow cover.

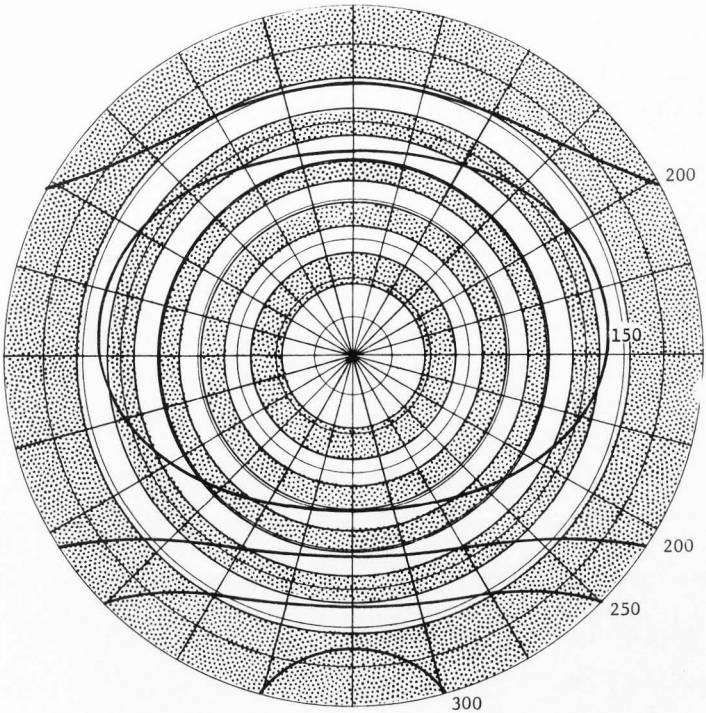

Figure 52. Isolines of reflectance over an alfalfa field at solar angle = 9.7°. Values are based on a reflectance value normal to the surface (nadir angle = 0°) of 100.

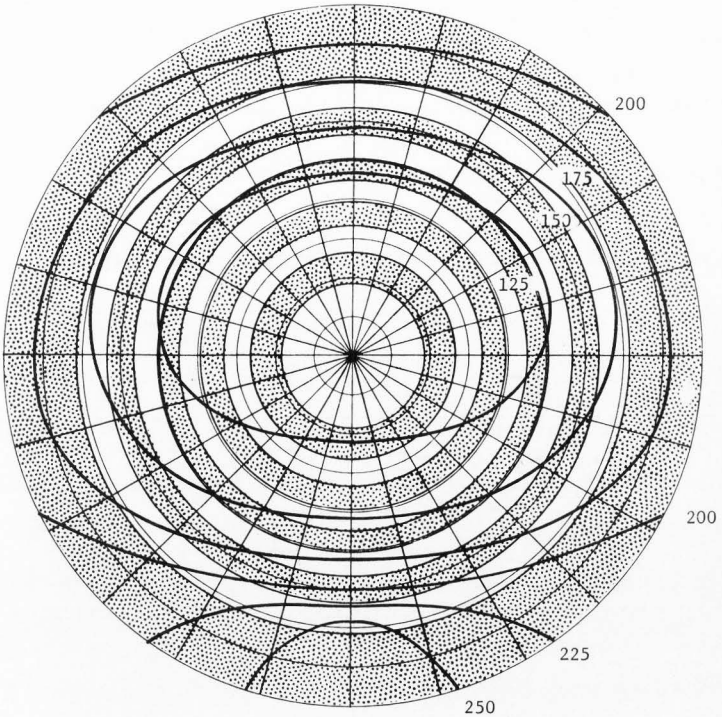

Figure 53. Isolines of reflectance over an alfalfa field at solar angle = 17.0°. Values are based on a reflectance value normal to the surface (nadir angle = 0°) of 100.

a specular component and the angle of viewing the feature. Figures 52-56 show that the reflectance increase with increasing nadir angle for all azimuth angles. The explanation for this effect is that a large proportion of dark interstices to foliage is viewed at small nadir angles while as the nadir angle increases, an increasing proportion of sun-lit foliage to dark interstices is detected. Figures 52-56 also show the development of the indicatrices as a function of solar angle. The trend observed is a decrease in anisotropy with increasing solar angle. As the solar angle increases, there is greater penetration of solar radiation into the interstices between the leaves, thus tending to decrease the contrast between the contribution of solar radiation emerging from the intermittent ground and the solar radiation reflected from the foliage.

In all shown cases for alfalfa, the backscatter exceeds the forward scatter. The alfalfa foliage was observed to display heliotropism during these measurements which probably contributed to the strong backscatter.

As with all previously discussed features, a comparison was made with the reflected radiation measured with a pyranometer to the 2π values derived from multiplying the normal reflectance values for the normalized factors obtained by integrating the indicatrices. Figure 57b presents these interrelationships *vs* solar angle. The lower curve shows the reflectance values measured with the MRIR normal to the surface while the upper curve shows the 2π values.

The maximum deviation between the vertical and hemispherical reflectance values occurs at approximately 35° solar angle with a convergence

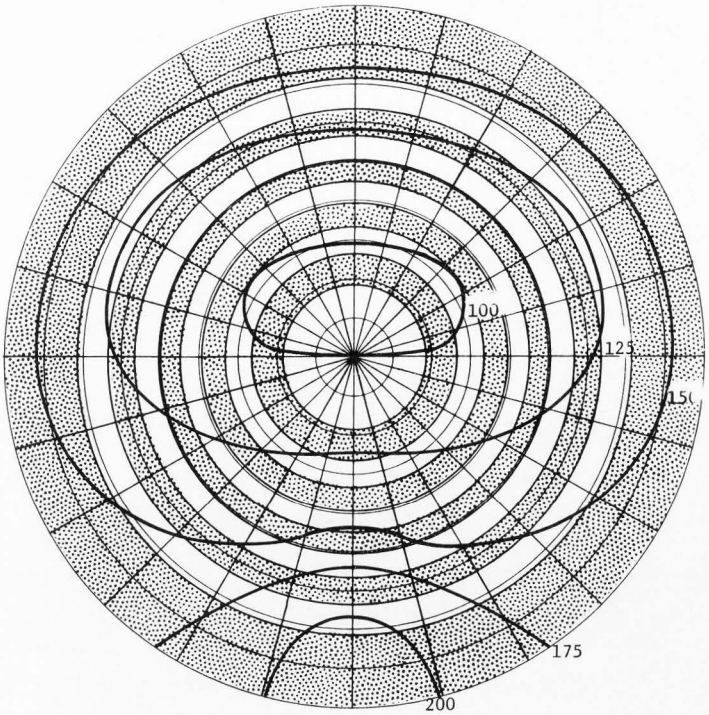

Figure 54. Isolines of reflectance over an alfalfa field at solar angle = 27.7°. Values are based on a reflectance value normal to the surface (nadir angle = 0°) of 100.

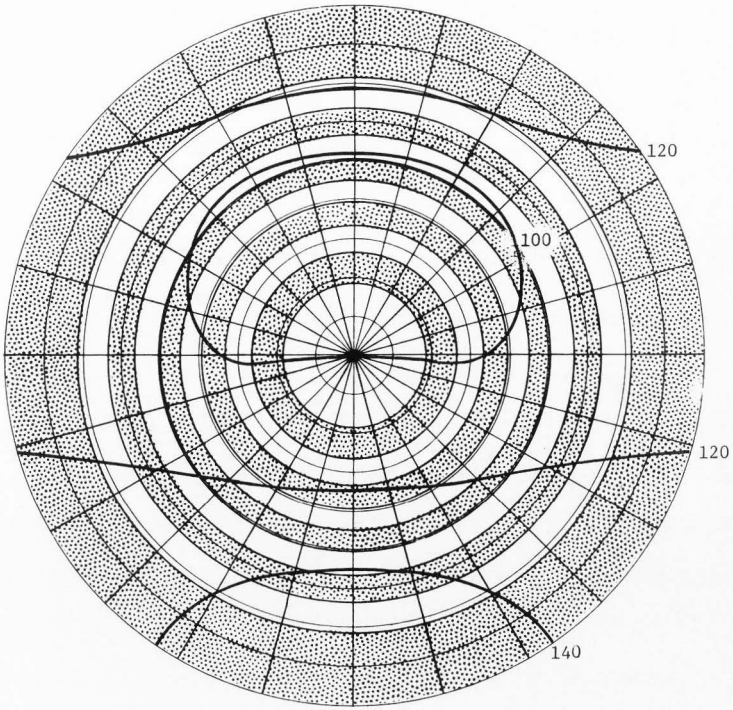

Figure 55. Isolines of reflectance over an alfalfa field at solar angle = 42.2°. Values are based on a reflectance value normal to the surface (nadir angle = 0°) of 100.

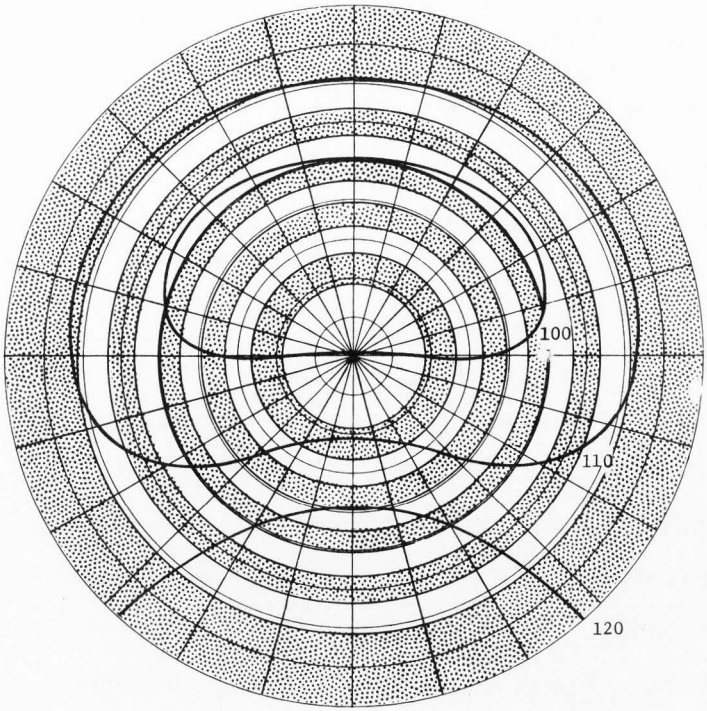

Figure 56. Isolines of reflectance over an alfalfa field at solar angle = 57.3°. Values are based on a reflectance value normal to the surface (nadir angle = 0°) of 100.

of the normal and 2π reflectances at lower and higher solar angles. This pattern is similar to that found for the Bonneville Salt Flats, Alkali Flats, and snow surface.

Figure 57a displays albedo *vs* solar angle for alfalfa with a decrease of albedo as solar angle increases, again similar to the previous features discussed.

The pyranometer value in Figure 57b for 42.7° solar angle is found to be too low while the corresponding albedo value shows good agreement. The corresponding global radiation value was too low, thus indicating some temporary irregularity in the recording.

Sugar beets

The second agricultural crop studied was sugar beets for solar angles 6.3°, 13.6°, 23.9°, 35.6°, 47.4°, 58.0°, and 67.8° as seen in Figures 56-64 on July 13, 1974. Sugar beets were chosen because of their large, broad leaves in contrast with the small, dense foliage of alfalfa. As seen in Figure 58 with a low solar angle, sugar beets produce a reflection pattern similar to that found for alfalfa at a similar solar angle. There is increasing reflectance with increasing nadir angle and the backscatter is the predominant characteristic. The strong backscatter exceeds 600 percent of the normal reflectance while the forward scatter shows values above 200 percent. The trend observed in the succeeding indicatrices is a decrease in anisotropy with increasing solar angle. At solar angles of 47.4°, 58.0°, and 67.8° there are areas in the reflection patterns, centered at approximately 45° nadir angle and 0° azimuth angle, which are less than the normal reflectance values.

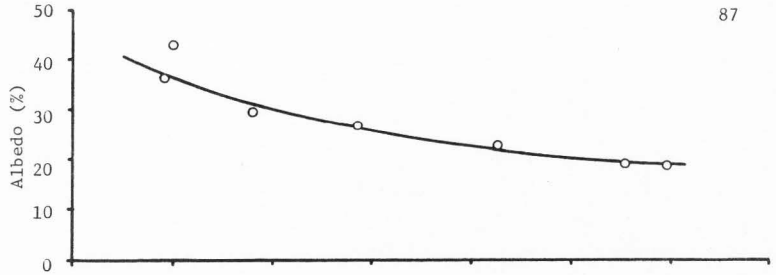

Figure 57a. Albedo vs solar angle for alfalfa.

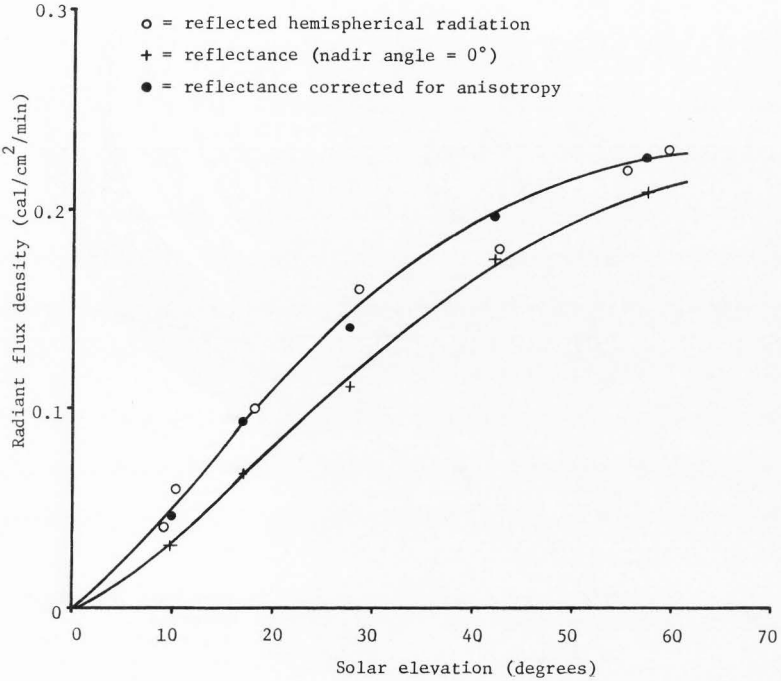

Figure 57b. Reflectance and reflected hemispherical radiation values for an alfalfa field.

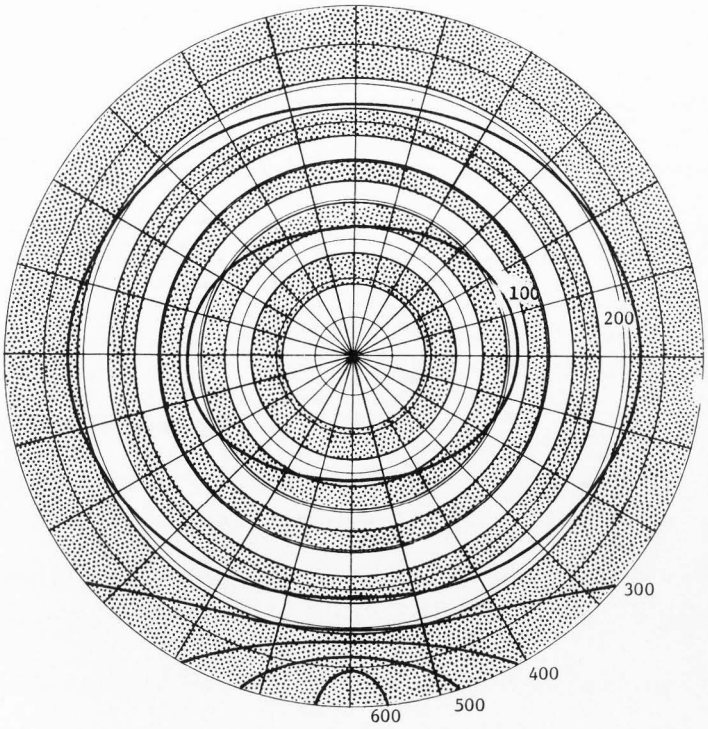

Figure 58. Isolines of reflectance over a sugar beet field at solar elevation of 6.3°. Values are based on a reflectance value normal to the surface (nadir angle = 0°) of 100.

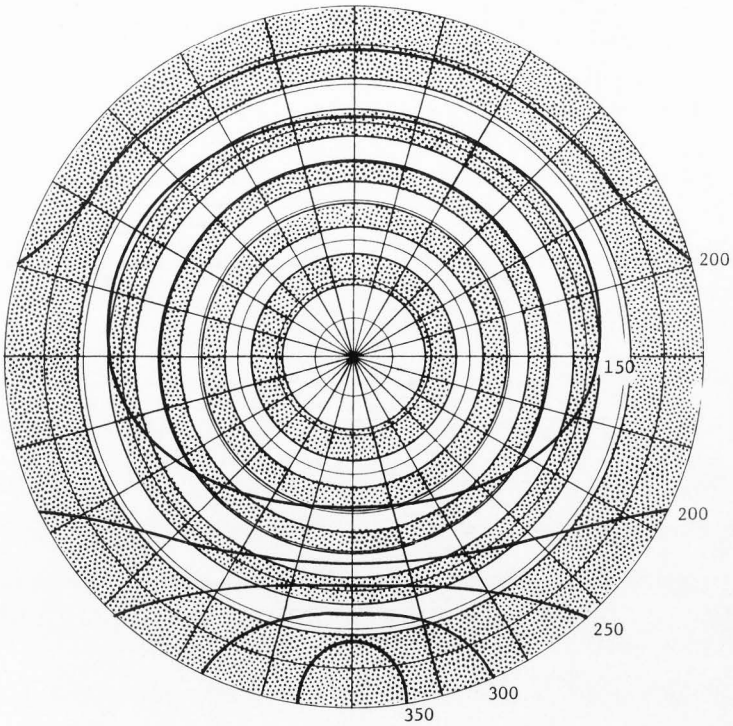

Figure 59. Isolines of reflectance over a sugar beet field at solar elevation of 13.6°. Values are based on a reflectance value normal to the surface (nadir angle = 0°) of 100.

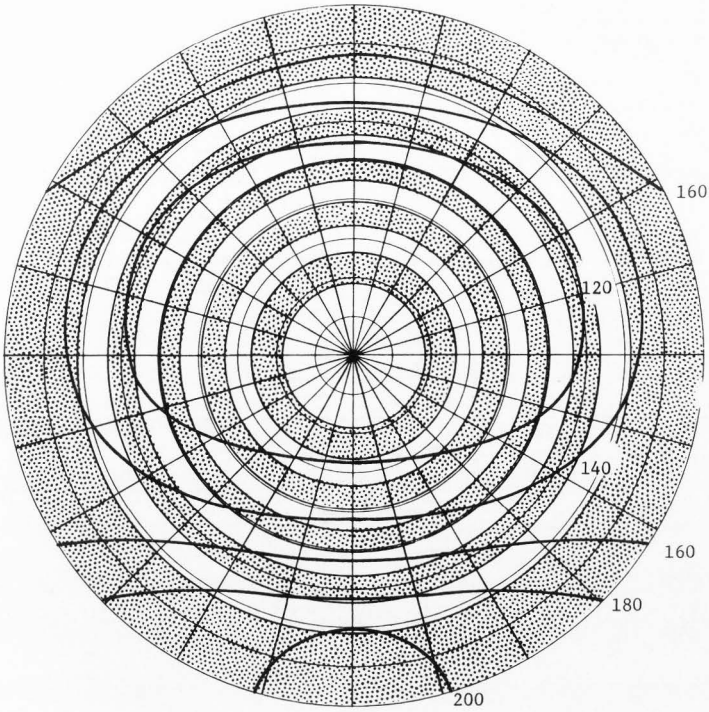

Figure 60. Isolines of reflectance over a sugar beet field at solar elevation of 23.9°. Values are based on a reflectance value normal to the surface (nadir angle = 0°) of 100.

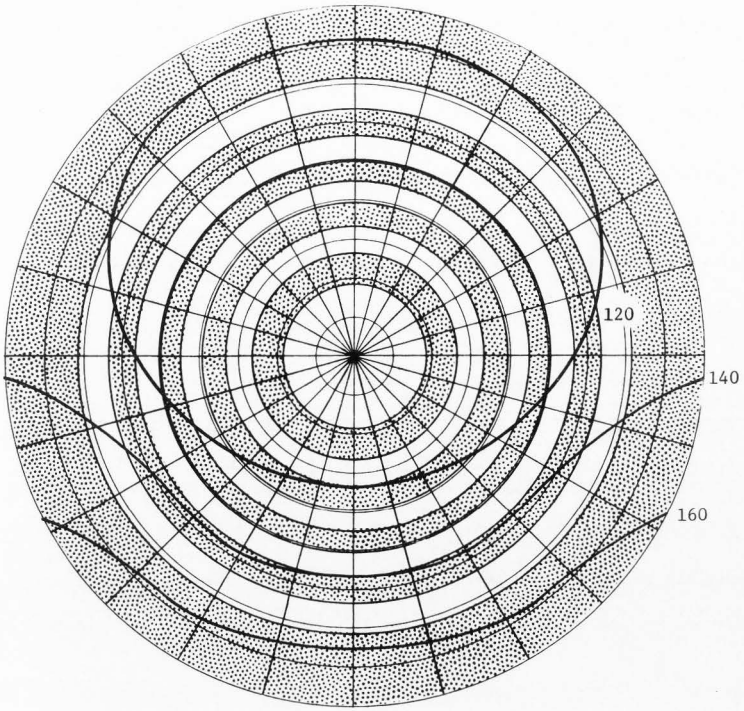

Figure 61. Isolines of reflectance over a sugar beet field at solar elevation of 35.6°. Values are based on a reflectance value normal to the surface (nadir angle = 0°) of 100.

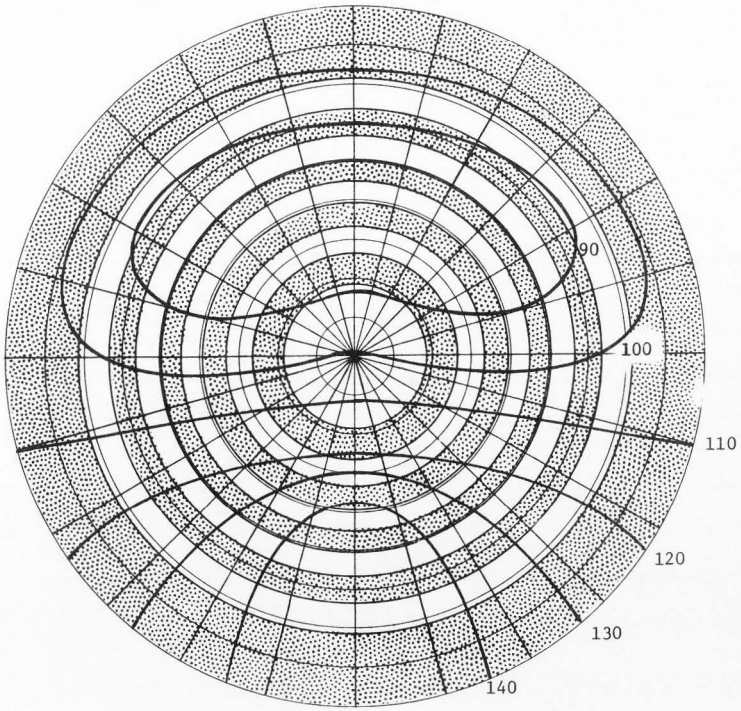

Figure 62. Isolines of reflectance over a sugar beet field at solar elevation of 47.4°. Values are based on a reflectance value normal to the surface (nadir angle = 0°) of 100.

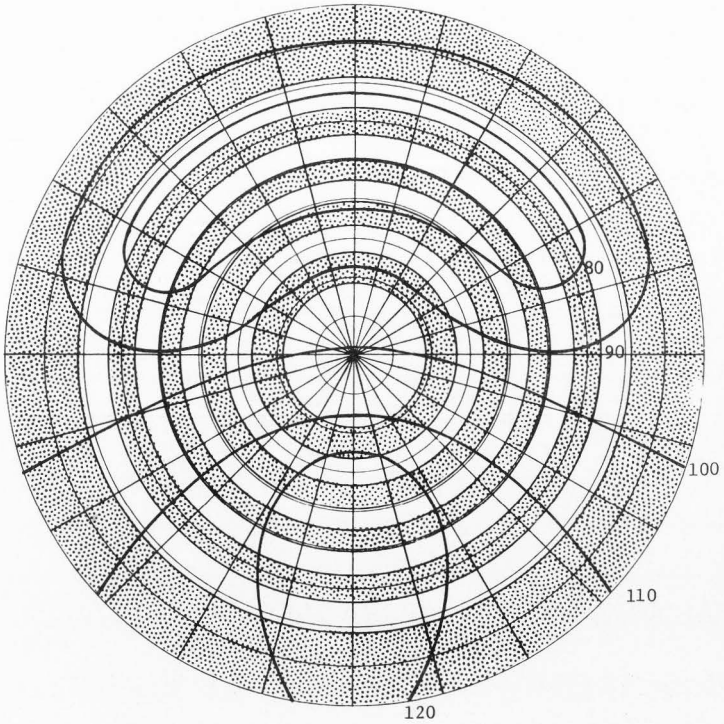

Figure 63. Isolines of reflectance over a sugar beet field at solar elevation of 58.0°. Values are based on a reflectance value normal to the surface (nadir angle = 0°) of 100.

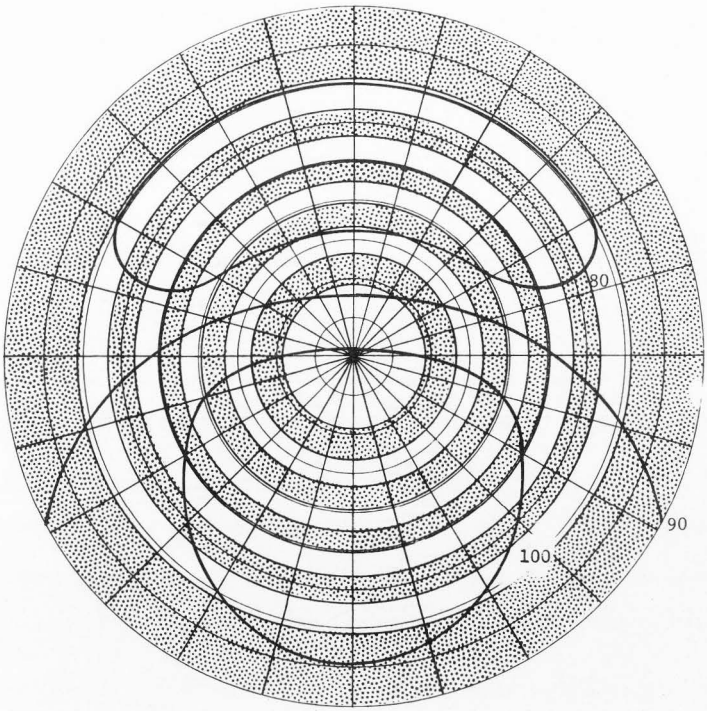

Figure 64. Isolines of reflectance over a sugar beet field at solar elevation of 67.8°. Values are based on a reflectance value normal to the surface (nadir angle = 0°) of 100.

These are explained by viewing the underside of the foliage which is protected from direct illumination of the direct beam component. The anti-solar points agree with the effects on reflectivity to the results discussed for alfalfa.

Figure 65a shows the albedo *vs* solar angle for sugar beets. Figure 65b shows the normal reflectances, 2π values derived from indicatrices and the vertical measurements as well as pyranometer values. The two curves cross since the normal reflectances exceed the 2π integrated value for 58.0° and 67.8° solar angles. In Figure 63, many isolines of reflectance are seen to be less than 100 while all reflectance isolines in Figure 64 are equal to or less than 100. The anti-solar points for both of these figures are seen to lie within their respective areas of maximum reflectivity. Only the plowed field displayed this characteristic in the previously discussed features.

The MRIR normal reflectance value for 35.6° solar angle lies above the curve and it is assumed that the recorder drifted for this measurement. If this value was adjusted to the lower curve, the corresponding 2π integrated value would agree with its respective curve.

Corn

The third agricultural crop chosen to study was corn because of its extreme height and narrow, long leaves. Data were collected on July 4, 1974 for solar angles of 6.1°, 15.9°, 27.9°, 39.2°, 50.3°, and 66.4°. Visual observation showed a large contribution of the soil surface to the reflected radiation which was shaded for lower solar angles and directly illuminated at higher solar angles (Figures 66-71).

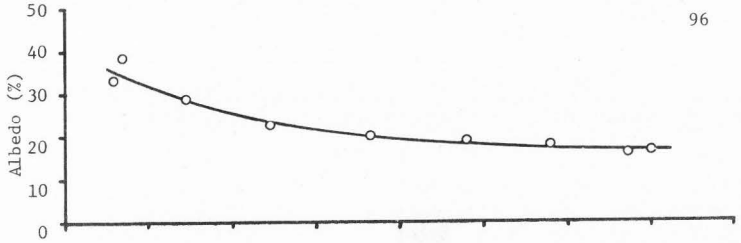

Figure 65a. Albedo vs solar angle for sugar beets.

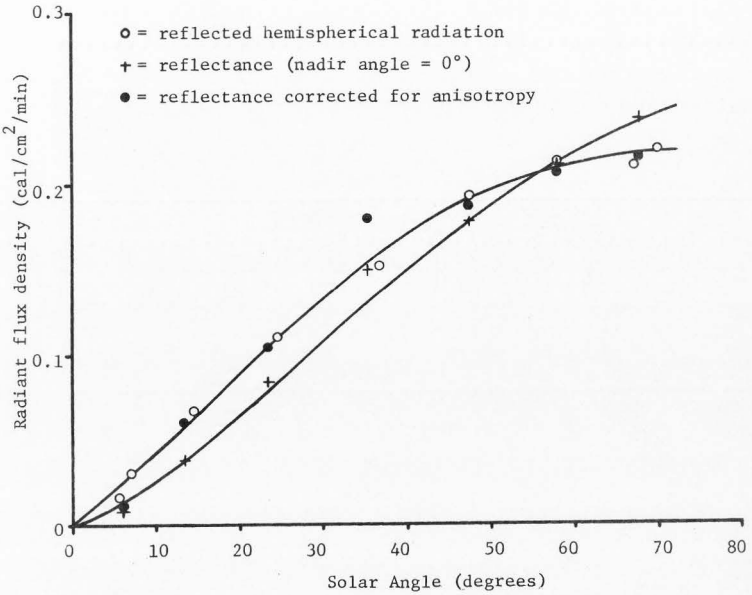

Figure 65b. Reflectance and reflected hemispherical radiation values for a sugar beet field.

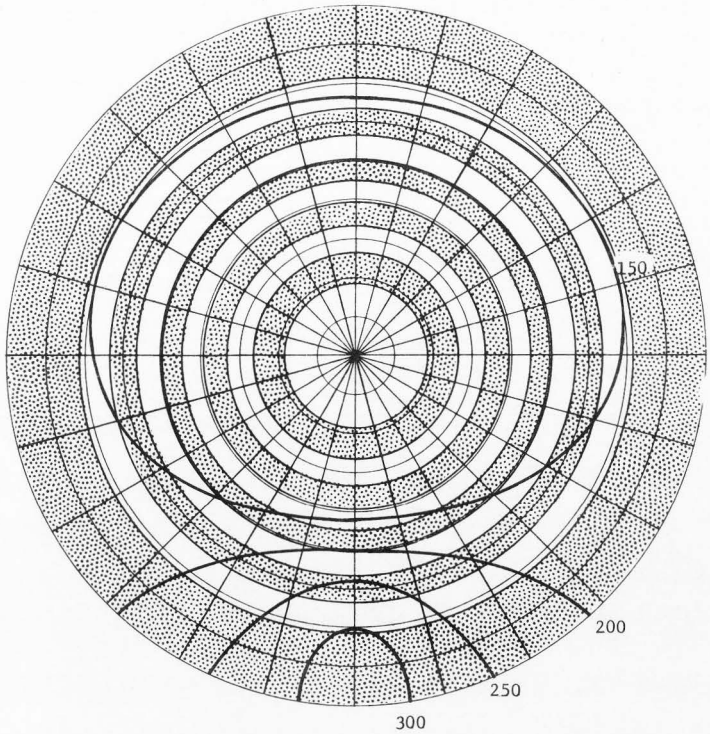

Figure 66. Isolines of reflectance over a corn field at solar elevation = 6.1°. Values are based on a reflectance value normal to the surface (nadir angle = 0°) of 100.

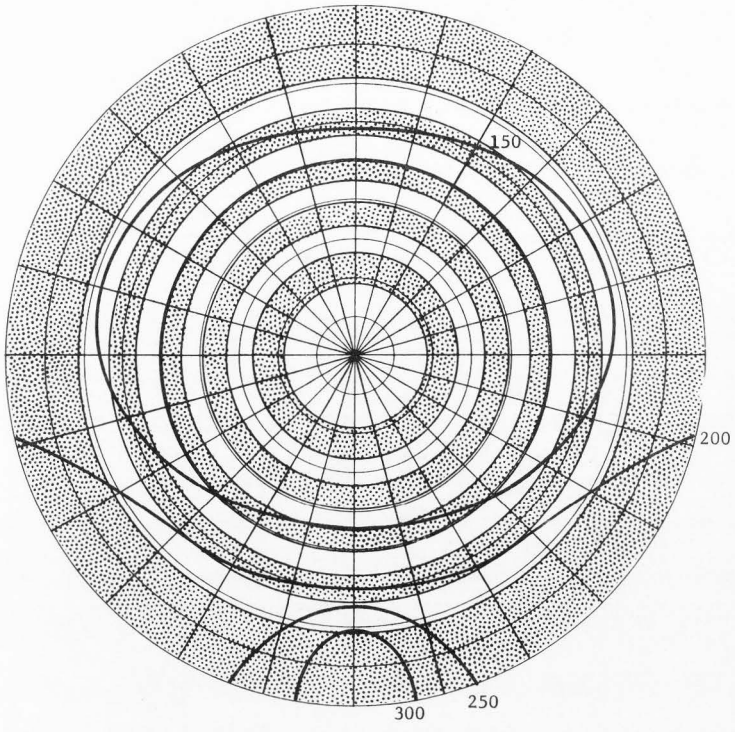

Figure 67. Isolines of reflectance over a corn field at solar elevation = 15.9°. Values are based on a reflectance value normal to the surface (nadir angle = 0°) of 100.

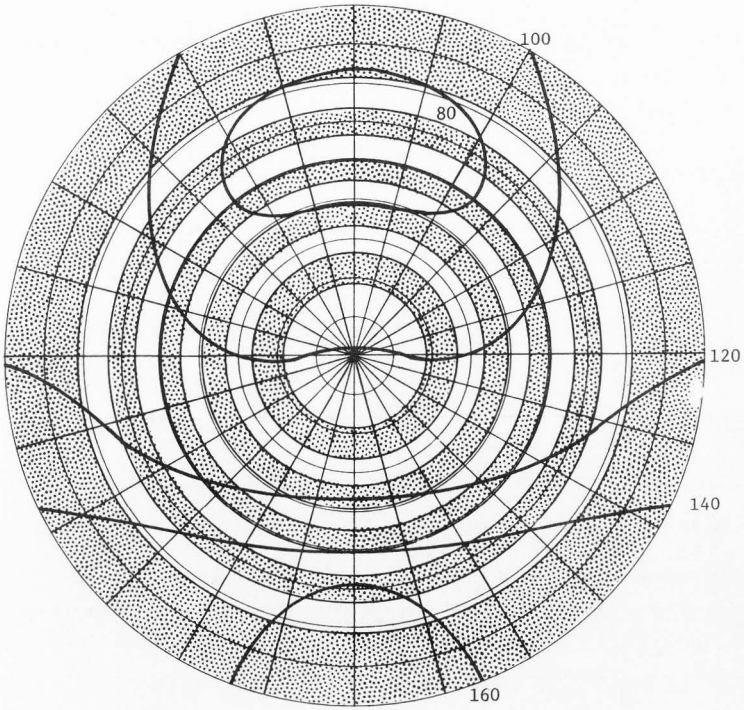

Figure 68. Isolines of reflectance over a corn field at solar elevation = 27.9°. Values are based on a reflectance value normal to the surface (nadir angle = 0°) of 100.

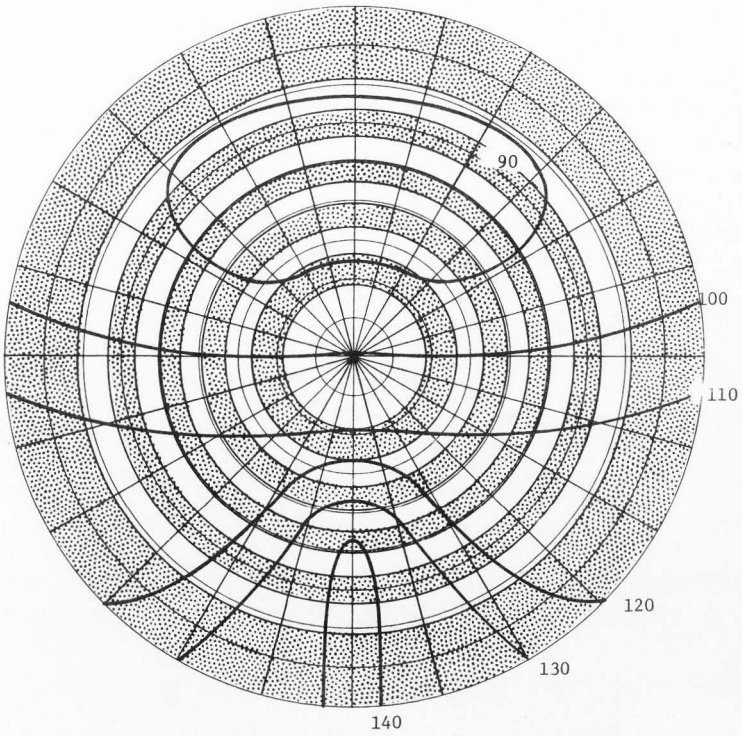

Figure 69. Isolines of reflectance over a corn field at solar elevation = 39.2°. Values are based on a reflectance value normal to the surface (nadir angle = 0°) of 100.

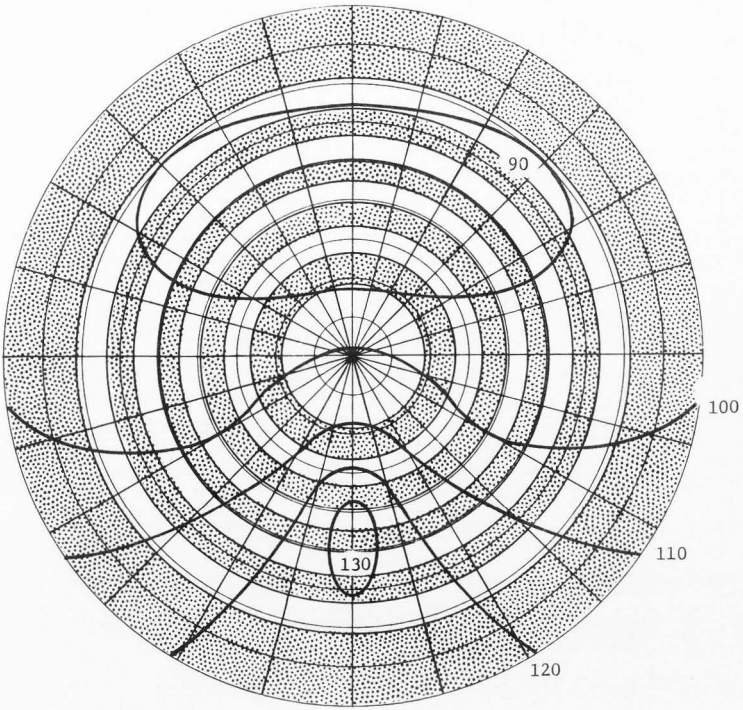

Figure 70. Isolines of reflectance over a corn field at solar elevation = 50.3°. Values are based on a reflectance value normal to the surface (nadir angle = 0°) of 100.

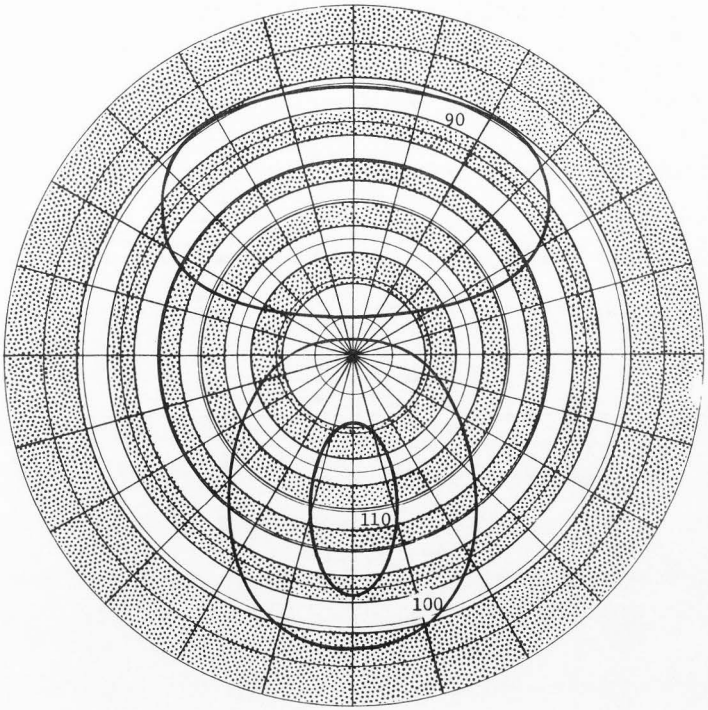

Figure 71. Isolines of reflectance over a corn field at solar elevation = 66.4°. Values are based on a reflectance value normal to the surface (nadir angle = 0°) of 100.

At solar angle 6.1° (Figure 66) the backscatter component is also the predominant characteristic as seen in the other agricultural crops and the plowed field. No appreciable specular component appears in all of the corn indicatrices since the forward scatter doesn't exceed the values at 90 and 270° azimuth angles. In general, there is a decrease in anisotropy with increasing solar angles as seen in all other features previously discussed. For solar angles of 27.9° and greater, areas of reflectance less than that found at nadir angle = 0 are found centered at approximately 45° nadir angle and 0° azimuth angle. This agrees with sugar beets but not with alfalfa. This can be explained by the nature of the foliage of the different crops. Alfalfa forms a nearly uniform carpet on the surface while corn and sugar beets have large spaces between their leaves allowing large shadowed areas to form in the above mentioned zones. Figure 71 (solar angle 66.4°) shows a similar trend to sugar beets at high solar angles whereby the maximum reflectance occurs around the anti-solar point and the integrated 2π value is less than 100 percent of the normal reflectance. This result is displayed in Figure 72b with the crossover of the 2π curve and normal reflectance curve at approximately 50° solar angle, similar to sugar beets and the plowed field.

Another important characteristic of corn is the decreased difference in absolute values between the normal and 2π reflectance values as compared with the other agricultural crops examined. Figure 72a shows the albedo *vs* solar angle is similar to the other crops.

Replications of these crops, alfalfa, sugar beets, and corn were measured in the 1973 growing season. No appreciable differences were

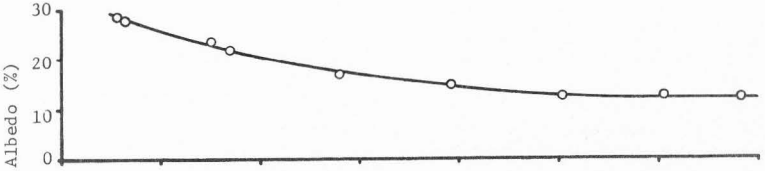

Figure 72a. Albedo vs solar angle for corn.

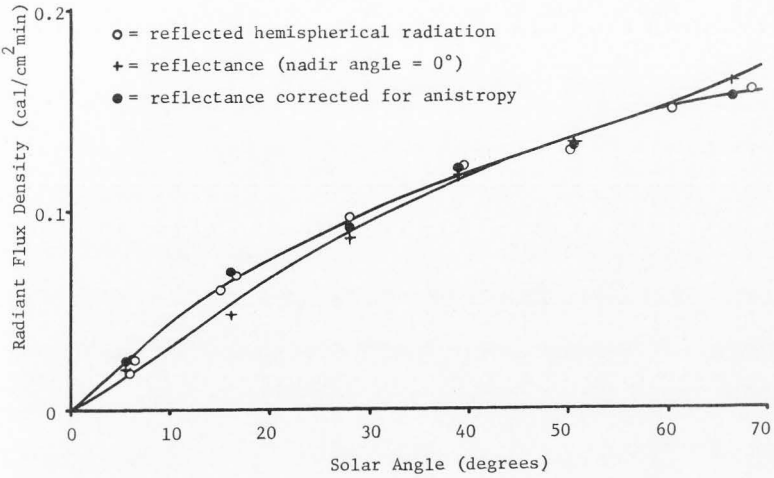

Figure 72b. Reflectance and reflected hemispherical radiation values for a corn field.

observed and all trends appeared the same for the two years. Therefore only one set of data has been reported.

The similarities and difference of the patterns of reflected radiation between the three agricultural crops examined, alfalfa, sugar beets, and corn can be shown qualitatively with photography. Figure 73 displays the indicatrix of reflected radiation over the alfalfa field. The largest reflectance in the imagery is located in the vicinity of the anti-solar point which is identified by the shadow of the camera. Alfalfa with its fine-structured foliage produces a relatively smooth and uniform reflection pattern.

Figure 74 shows the indicatrix of reflected radiation over the sugar beet field taken with a fish-eye camera. Although the large leaves cause a more irregular reflection pattern than shown for alfalfa, the trends observed in the measurements are evident. Here the anti-solar point also shows the greatest reflectance. Also the shadows and dark areas centered around nadir angle = 45° and azimuth angle = 0° show the decreases in reflectance from the reflectance normal to the surface.

Figure 75 and Figure 76 show fish-eye photographs of corn at a low and high solar angle, respectively. At the low solar angle, the exposed soil between the rows of corn is shown to be completely shaded. The anti-solar point also is shown as the greatest reflectance in the indicatrix. However, at high nadir angles, at all azimuth angles, larger reflectances are seen than at nadir angle = 0°. This is explained by sensing only illuminated foliage at large nadir angles while the major contribution of reflected radiation at nadir angle = 0° is from the shaded soil.

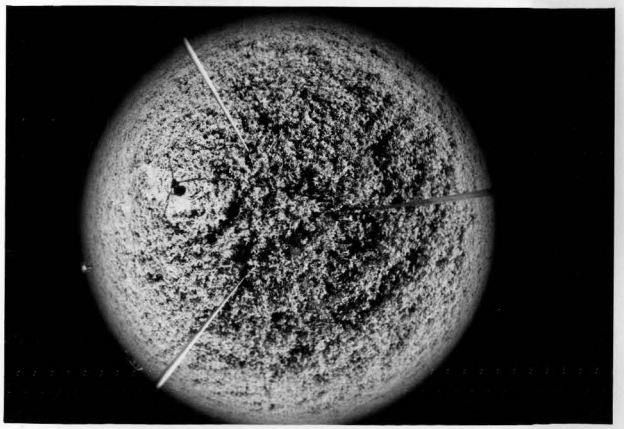

Figure 73. Fish-eye photograph of alfalfa.

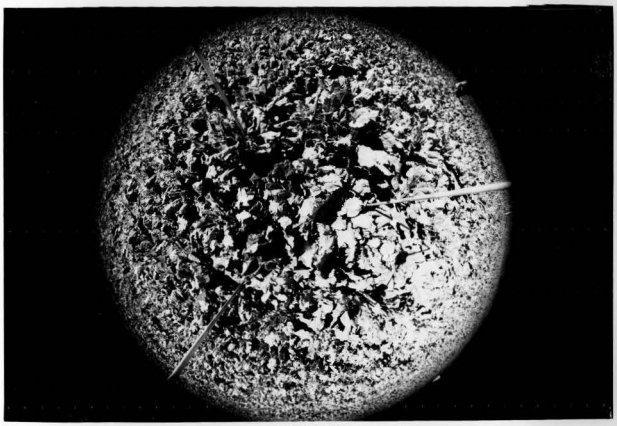

Figure 74. Fish-eye photograph of sugar beets.

Figure 75. Fish-eye photograph of corn under low solar angle.

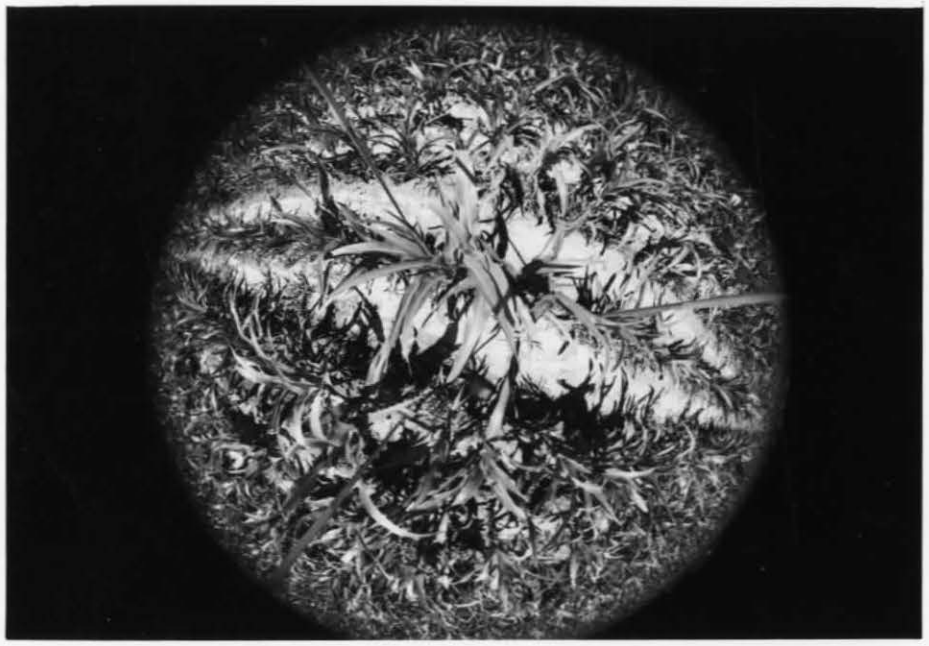

Figure 76. Fish-eye photograph of corn under high solar angle.

At the higher solar angles, the bare soil is largely illuminated by the direct beam of solar radiation as seen in Figure 76. Here the backscatter is seen to exceed the forward scatter with a decrease in reflectance at nadir angle = 45° below the reflectance at nadir angle = 0° for azimuth angles around 0°. This agrees with the results found for sugar beets. Thus the fish-eye photographs taken over the agricultural crops show agreement with the trends and main features found in the measurements.

Figure 77 shows the percentage that the normal reflectance values must be multiplied by to obtain the correct hemispherical reflected radiation values for the three agricultural crops. Alfalfa and sugar beets show close agreement except at the higher solar angles where alfalfa maintains an anisotropic correction factor greater than 100 percent contrasted by a correction factor less than 100 percent for sugar beets. The anisotropic correction for corn is similar to that for sugar beets at the higher solar angles. Corn differs from the other two crops at solar angles between 10° and 30° whereby the anistropic correction decreases more rapidly for corn than is found for alfalfa or sugar beets. This effect is explained by the transition of shaded to sun-lit soil for an increase of solar angle to approximately 30°.

The individual values shown for the anisotropic correction factors for the agricultural crops do not form as smooth a curve as found for the Bonneville Salt Flats, Alkali Flats, or snow surfaces previously discussed. This agrees with the greater surface irregularities found for the agricultural crops as compared with the mineral and snow surfaces,

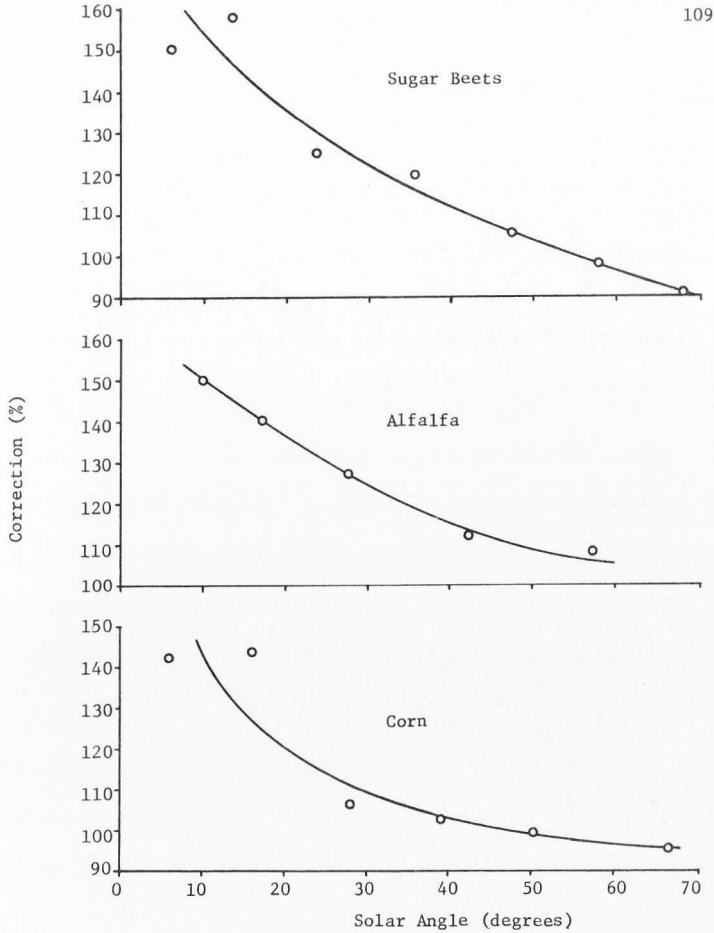

Figure 77. Percentage of correction *vs* solar angle that must be applied to reflectances for nadir angle = 0° to obtain the hemispherical reflection values for the agricultural crop surface examined.

producing greater variability in the plant cover reflectances than found for the mineral and snow surfaces.

Desert Surfaces

Two desert surfaces were examined; a field of crested wheatgrass and a stand of big sagebrush.

Crested wheatgrass

Data were collected over a crested wheatgrass field on June 28, 1974 for solar angles of 3.7°, 9.2°, 23.0°, 36.2°, 60.5°, and 70.9°. Figure 78 (solar angle 3.7°) shows the large backscatter which exceeds 700 percent of the normal reflectance at high nadir angles. No specular reflection can be detected from the results in Figures 78-83. Solar angles 3.7° to 36.2° show forward scatter exceeding the normal values but this is not specular in nature since the values at 90° and 270° solar azimuth are greater than at 0° solar azimuth. The normal reflectance has a larger contribution of shaded ground that found for higher nadir angle reflectances for low sun angles.

However, at high solar angles the effect reverses. Figures 82 and 83 show that at solar angles of 60.5° and 70.9°, respectively, the anti-solar points contribute the greatest reflectances with a decrease in reflectances in all directions from these points. The soil surface has practically no shadow and the soil therefore is able to reflect more than the vegetation with its many reflecting and absorbing parts. This effect is clearly displayed in Figure 84b with the crossover of the normal and 2π reflectance curves at approximately 60° solar angles.

Figure 84a shows albedo *vs* solar angle for crested wheatgrass. The value shown as 87.4 percent is probably not realistic for an overall albedo of the field.

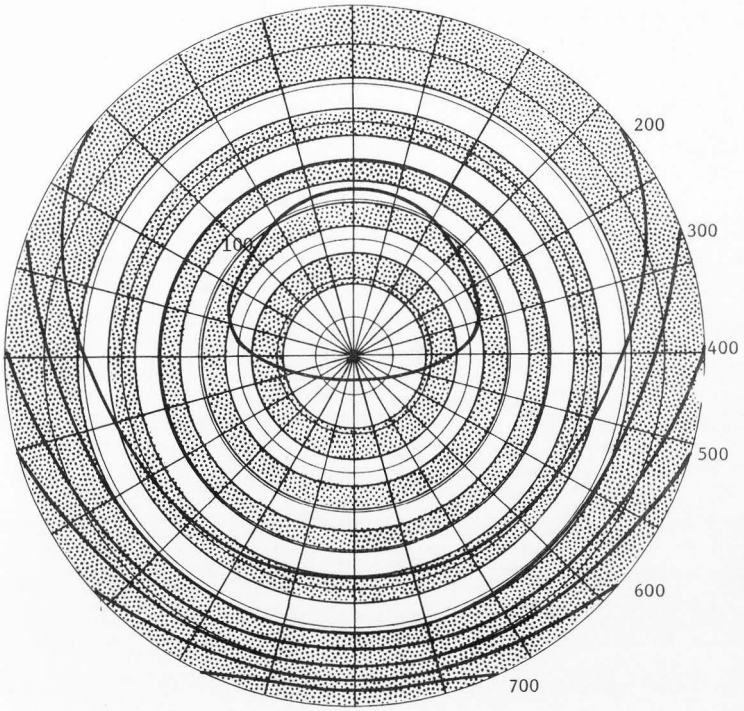

Figure 78. Isolines of reflectance over a field of crested wheatgrass in Curlew Valley, Utah, for solar angle = 3.7°. Values are based on a reflectance value normal to the surface (nadir angle = 0°) of 100.

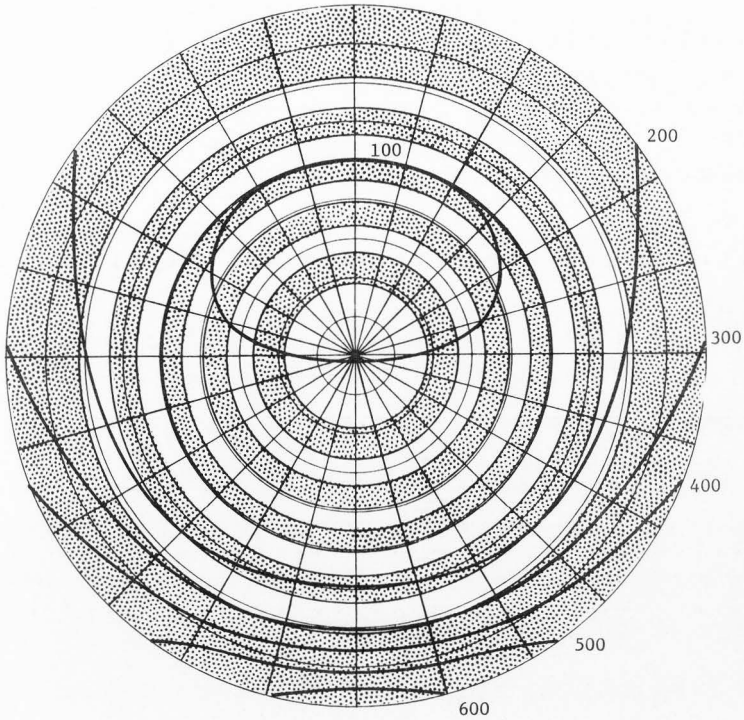

Figure 79. Isolines of reflectance over a field of crested wheatgrass in Curlew Valley, Utah, for solar angle = 9.2°. Values are based on a reflectance value normal to the surface (nadir angle = 0°) of 100.

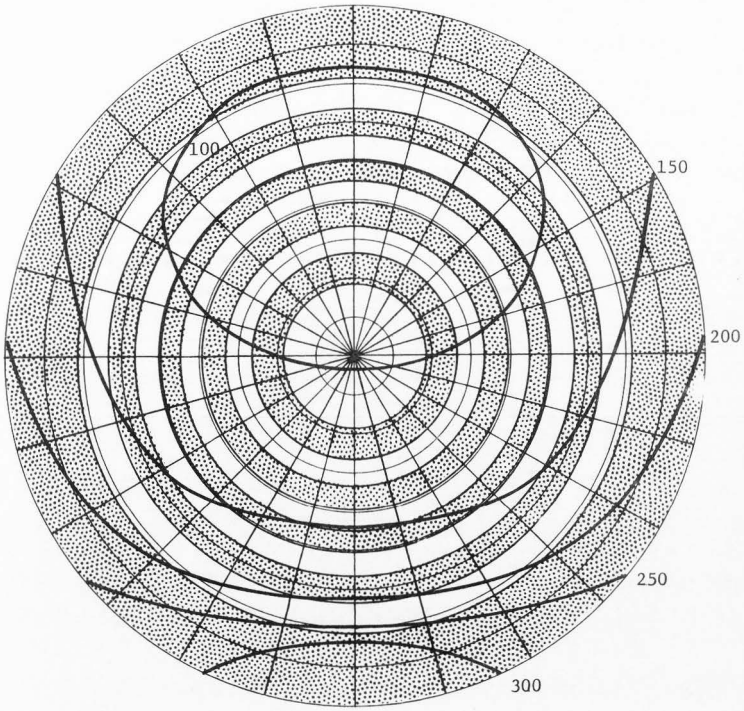

Figure 80. Isolines of reflectance over a field of crested wheatgrass in Curlew Valley, Utah, for solar angle = 23.0°. Values are based on a reflectance value normal to the surface (nadir angle = 0°) of 100.

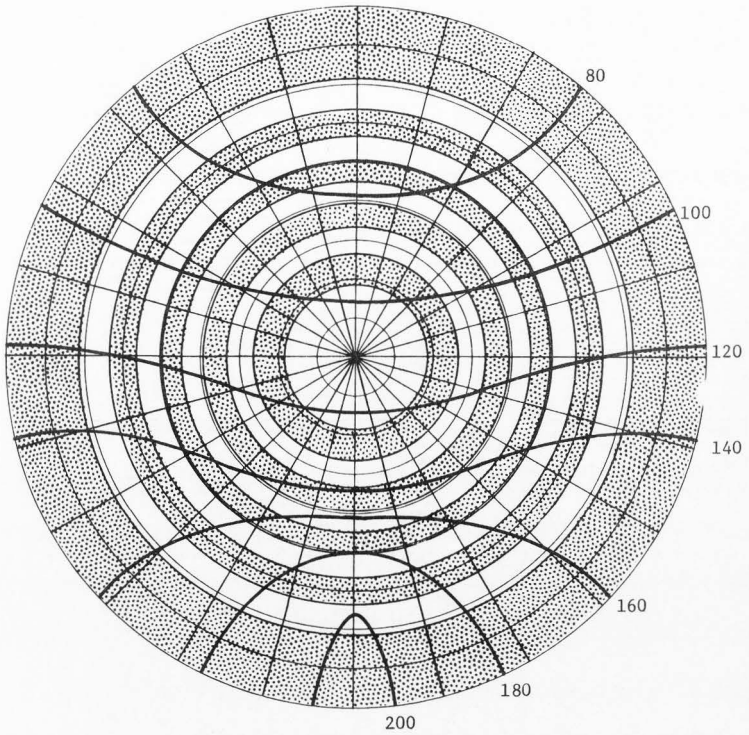

Figure 81. Isolines of reflectance over a field of crested wheatgrass in Curlew Valley, Utah, for solar angle = 36.2°. Values are based on a reflectance value normal to the surface (nadir angle = 0°) of 100.

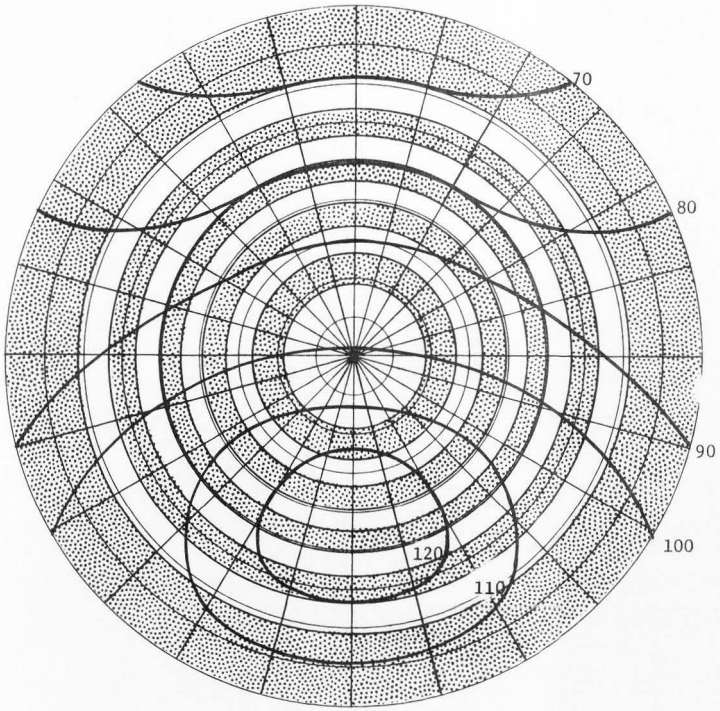

Figure 82. Isolines of reflectance over a field of crested wheatgrass in Curlew Valley, Utah, for solar angle = 60.5°. Values are based on a reflectance value normal to the surface (nadir angle = 0°) of 100.

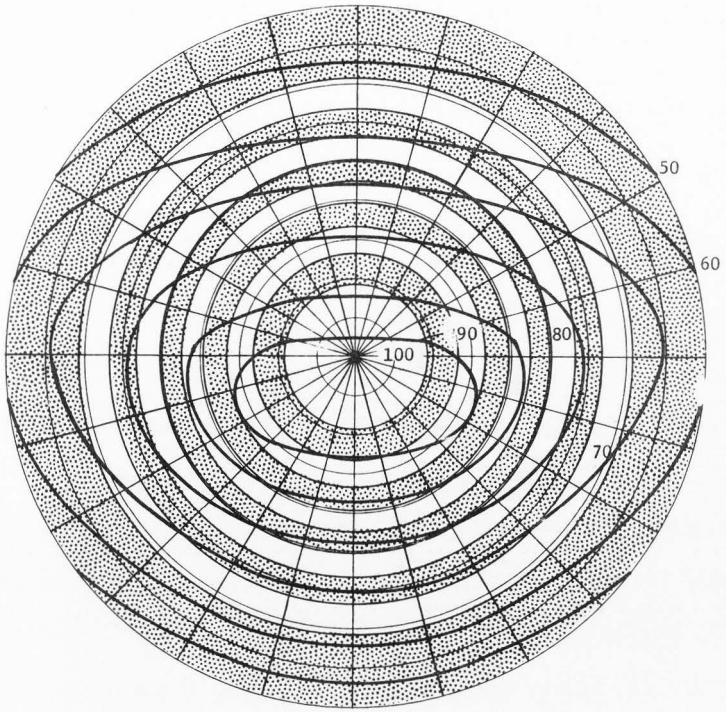

Figure 83. Isolines of reflectance over a field of crested wheatgrass in Curlew Valley, Utah, for solar angle = 70.9°. Values are based on a reflectance value normal to the surface (nadir angle = 0°) of 100.

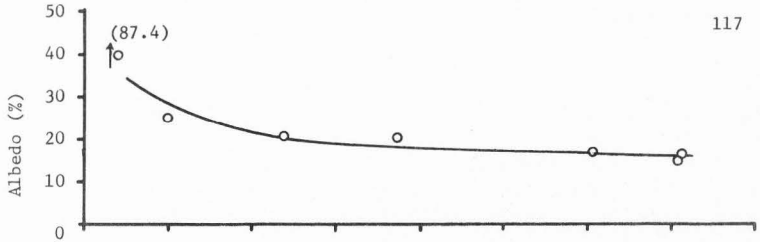

Figure 84a. Albedo vs solar angle for crested wheatgrass.

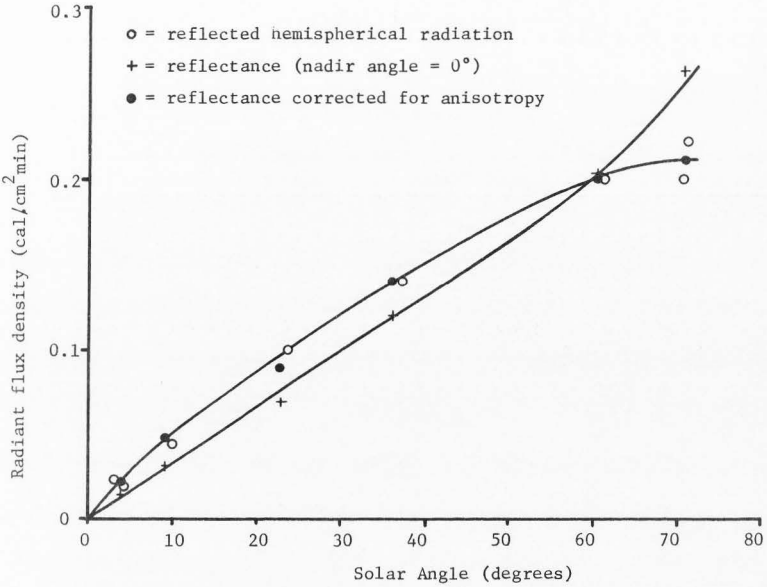

Figure 84b. Reflectance and reflected hemispherical radiation values for crested wheatgrass.

Sagebrush

Indicatrices of reflected radiation were determined with the Nimbus MRIR for solar angles of 6.5°, 9.1°, 20.0°, 33.8°, 47.4°, 61.3°, and 71.3° on June 26, 1974 as shown in Figures 85-91. The sagebrush type was the most difficult to measure of all surfaces examined due to the tremendous irregularities in spacing and height of the vegetation. In all, 12 sets of measurements were taken throughout the day and averages of data were computed for values collected in the morning with values collected in the afternoon for similar corresponding solar angles. This removed a lot of the individual variability and produced more general results.

The results shown in Figures 85-91 agree with those of crested wheatgrass except that the backscatter is not as pronounced in the sagebrush as in the crested wheatgrass. There is no specular reflection apparent in the forward scatter. For solar angles greater than 47.4°, there is the same development as seen for crested wheatgrass whereby the anti-solar point produces the greatest reflectance in the indicatrix with a decrease in all directions from the anti-solar point. Figure 92b also agrees closely with the results obtained with crested wheatgrass. The crossover of the two curves appeared at about 55° solar angle.

Due to the irregulartities of the plant cover, individual reflected radiation values would not produce a representative albedo for sagebrush. The albedo values presented in Figure 92a were derived from measurements taken in the same vicinity on July 21, 1971 (Dirmhirn, 1972). These albedo values were developed by sampling 16 points on a gridwork with a pyranometer on a tripod. The values presented in Figure

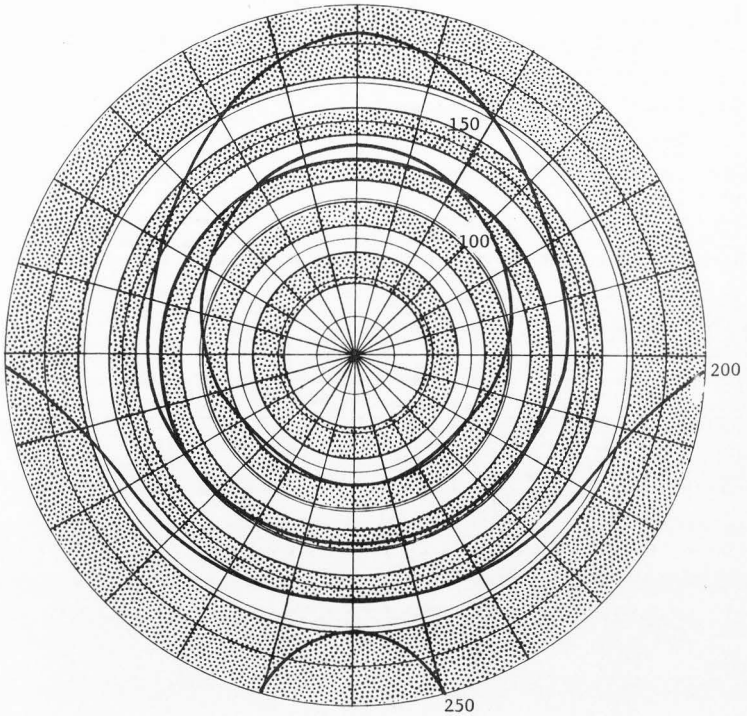

Figure 85. Isolines of reflectance over sagebrush in Curlew Valley, Utah for solar angle = 6.5°. Values are based on a reflectance value normal to the surface (nadir angle = 0°) of 100.

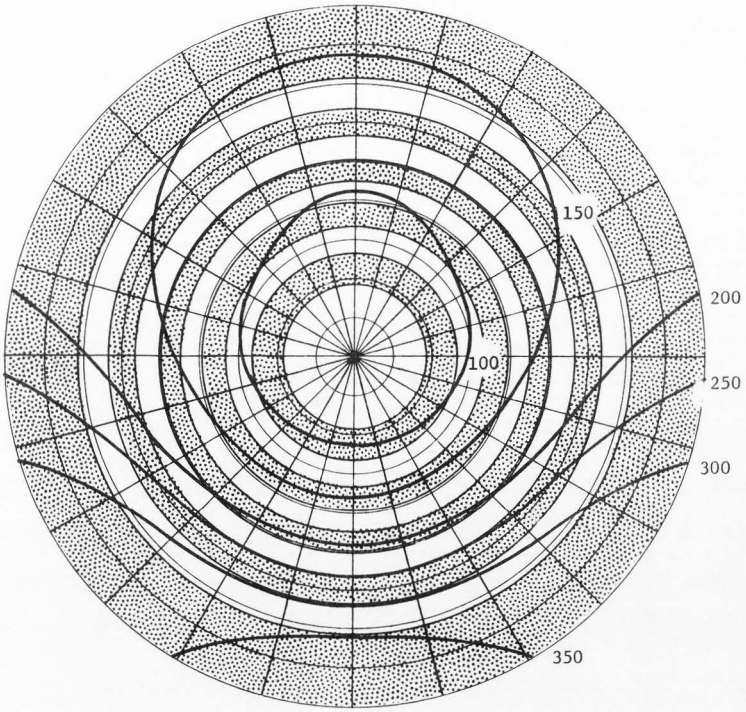

Figure 86. Isolines of reflectance over sagebrush in Curlew Valley, Utah for solar angle = 9.1°. Values are based on a reflectance value normal to the surface (nadir angle = 0°) of 100.

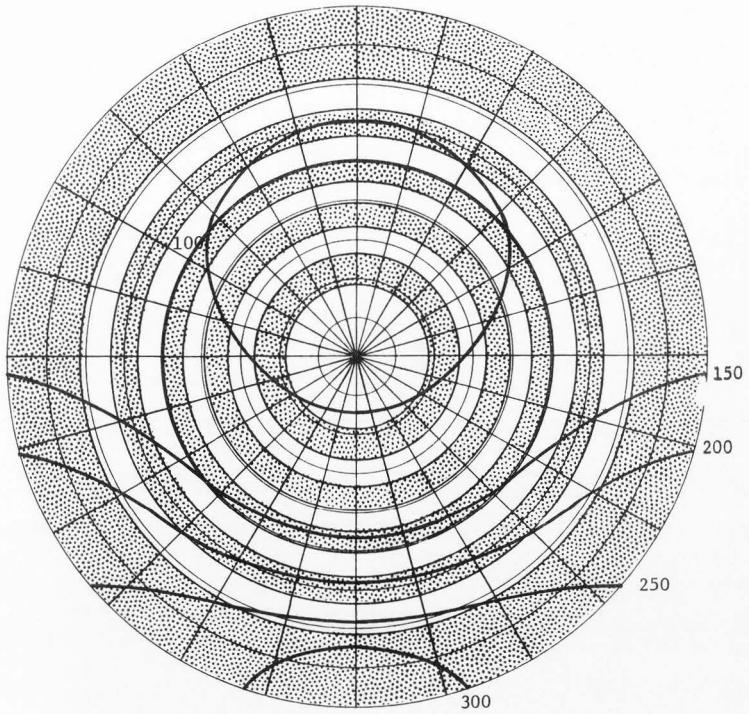

Figure 87. Isolines of reflectance over sagebrush in Curlew Valley, Utah for solar angle = 20.0°. Values are based on a reflectance value normal to the surface (nadir angle = 0°) of 100.

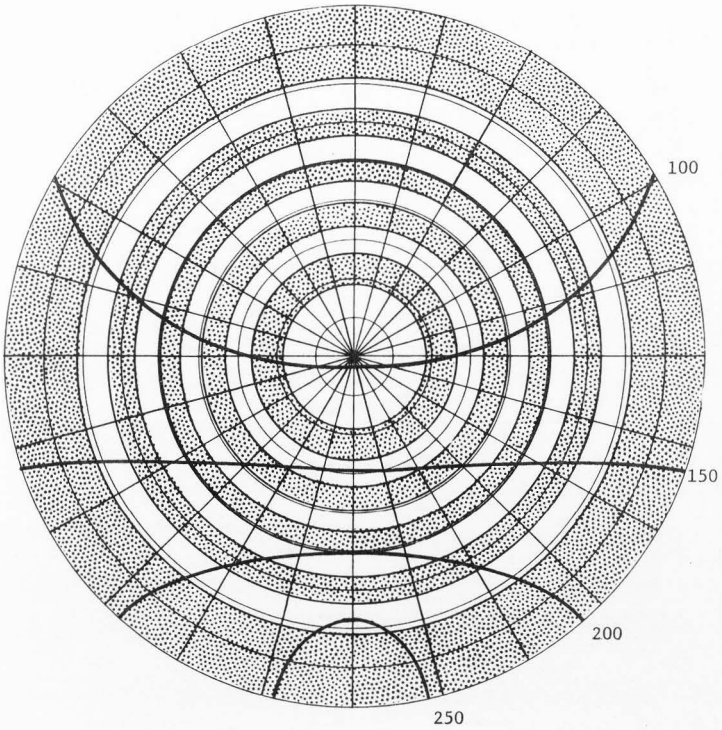

Figure 88. Isolines of reflectance over sagebrush in Curlew Valley, Utah for solar angle = 33.8°. Values are based on a reflectance value normal to the surface (nadir angle = 0°) of 100.

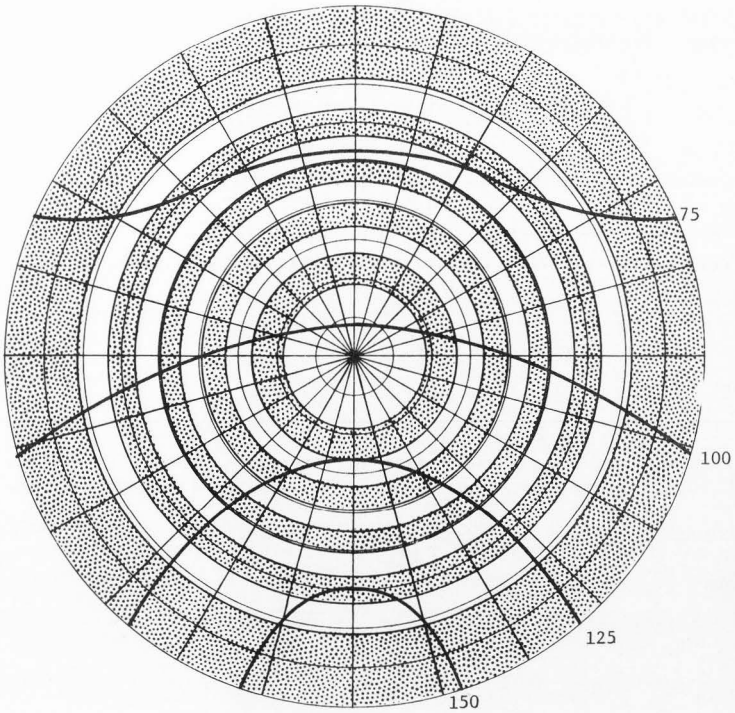

Figure 89. Isolines of reflectance over sagebrush in Curlew Valley, Utah for solar angle = 47.4°. Values are based on a reflectance value normal to the surface (nadir angle = 0°) of 100.

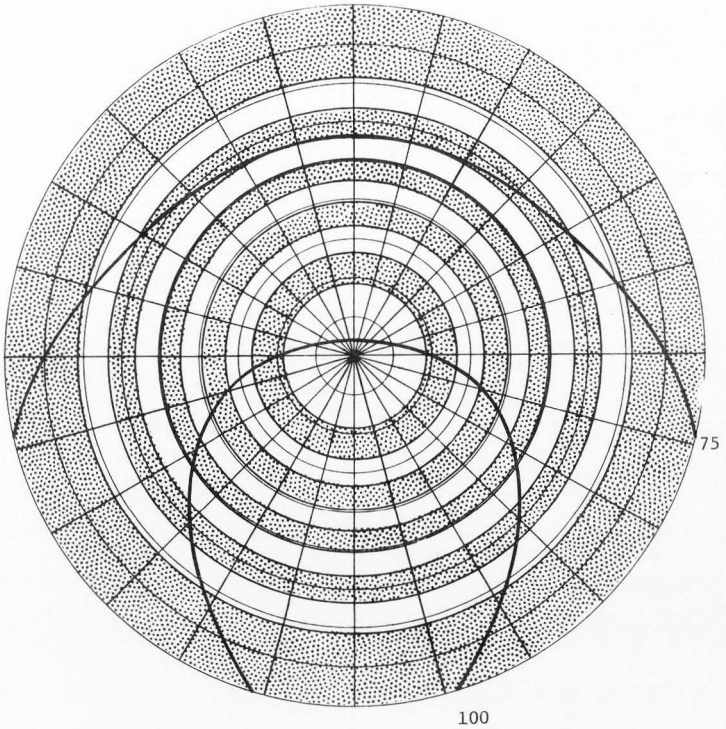

Figure 90. Isolines of reflectance over sagebrush in Curlew Valley, Utah for solar angle = 61.3°. Values are based on a reflectance value normal to the surface (nadir angle = 0°) of 100.

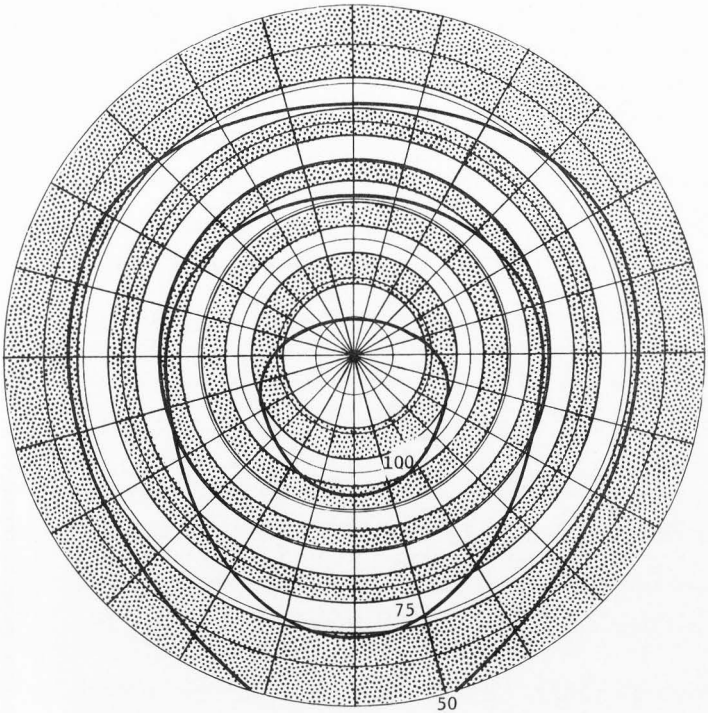

Figure 91. Isolines of reflectance over sagebrush in Curlew Valley, Utah for solar angle = 71.3°. Values are based on a reflectance value normal to the surface (nadir angle = 0°) of 100.

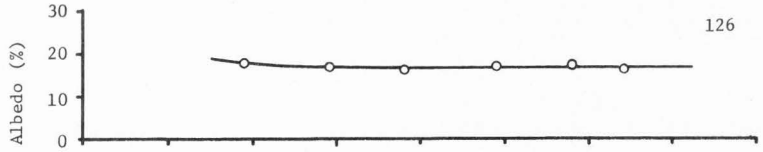

Figure 92a. Albedo vs solar angle for sagebrush.

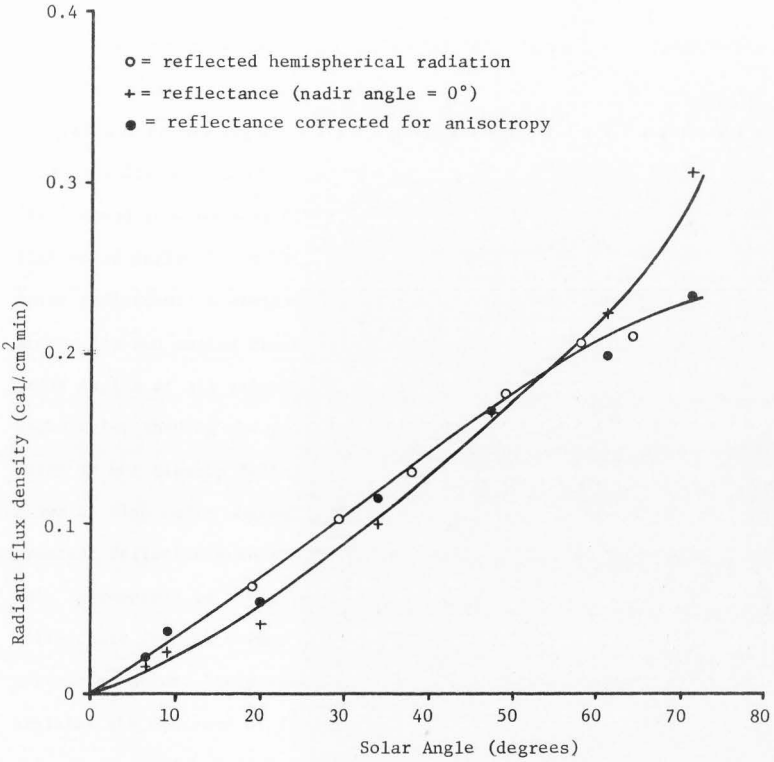

Figure 92b. Reflectance and reflected hemispherical radiation values for sagebrush.

92b were developed from the above mentioned albedo values and global radiation measurements taken on June 26, 1974.

The difficulty in obtaining representative albedo for a natural surface is shown in Figure 93 (Dirmhirn, 1972). The daily variation of albedo can show different trends depending on the shadow patterns for specific features.

Figure 94 and Figure 95 show fish-eye photographs of crested wheatgrass for low and high solar angles, respectively. At a low solar angle the exposed soil between the vegetation is shown shaded while at the high solar angle, it is illuminated by the direct beam component o solar radiation. A similar effect here is shown as was found for corn. At the low sun angles there are greater reflectances found for high nadir angles at all azimuth angles than at nadir angle = 0° with the backscatter showing the predominant reflectance. Here the anti-solar point is not clearly defined. The backscatter exhibits a broad pattern shown at high nadir angles. The high solar angle condition shows the greatest reflectance in the vicinity of the anti-solar point. Since this corresponds to a high nadir angle, there will be a decrease in reflectance for all azimuth angles as the nadir angle increases from the anti-solar point. This effect is verified by the measurements and also explains the decrease of the anisotropic correction factor at higher solar angles which must be applied to reflectances normal to the surface. Both features show similar anisotropic correction factors for the range of solar angles examined. The individual values for the desert surfaces are seen to vary more from the fitted curves than the values found for the mineral and snow surfaces. This effect agrees with that shown for

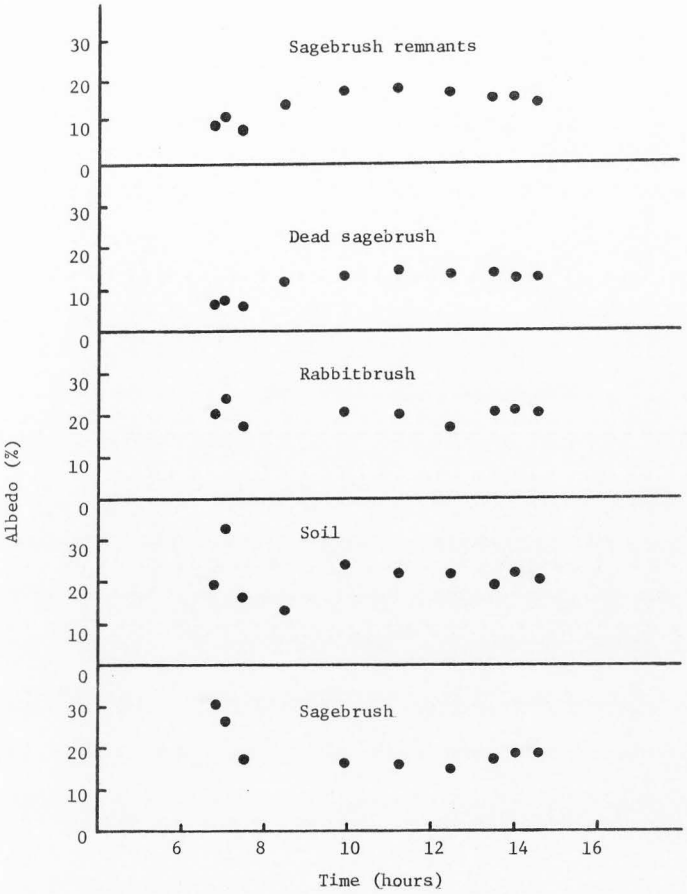

Figure 93. Daily variation of albedo at Curlew Valley, Utah, 11 August 1971.

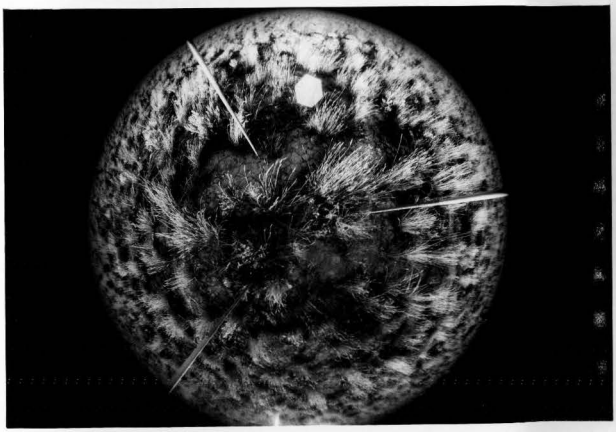

Figure 94. Fish-eye photograph of crested wheatgrass for low sun angle.

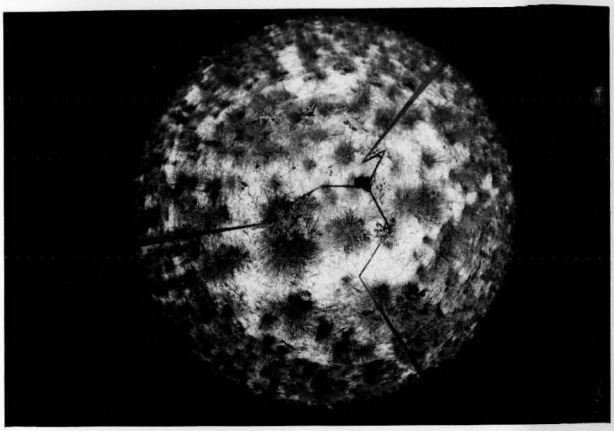

Figure 95. Fish-eye photograph of crested wheatgrass for high sun angle.

the agricultural crops and is explained by the greater variability of reflectances found for the rougher surfaces than found for the mineral and snow surfaces. Figure 96 displays this effect for both crested wheatgrass and sagebrush.

The anisotropic correction factor shown for 6.5° solar angle is shown to be less than for 9.1° solar angle. This agrees with the results shown in Figure 93 where albedo over sagebrush-type decreases at low solar angles.

Aircraft Measurements

Design and instrumentation

In the previously discussed sections, ground measurements were designed to obtain accurate albedo values and indicatrices of reflected radiation for several ground covers. Attempts were made to measure the albedo and indicatrices in the White Sands dune field but it was found that measurements on various points on the ground within the dune field are highly dependent on the position chosen. Figures 97 and 98 show the result of measuring the indicatrices from the top and bottom of a dune, respectively.

These examples of indicatrices illustrate the variability of reflectances produced by the varied slopes of large dimensions found in the dune field. A more general but qualitative display of the reflection pattern over the dune field is shown in Figures 99 and 100 of photographs taken from a helicopter with a normal and fish-eye lens, respectively. These photographs show strong backscatter in the reflection pattern while the reflectances in the forward direction appear relatively low

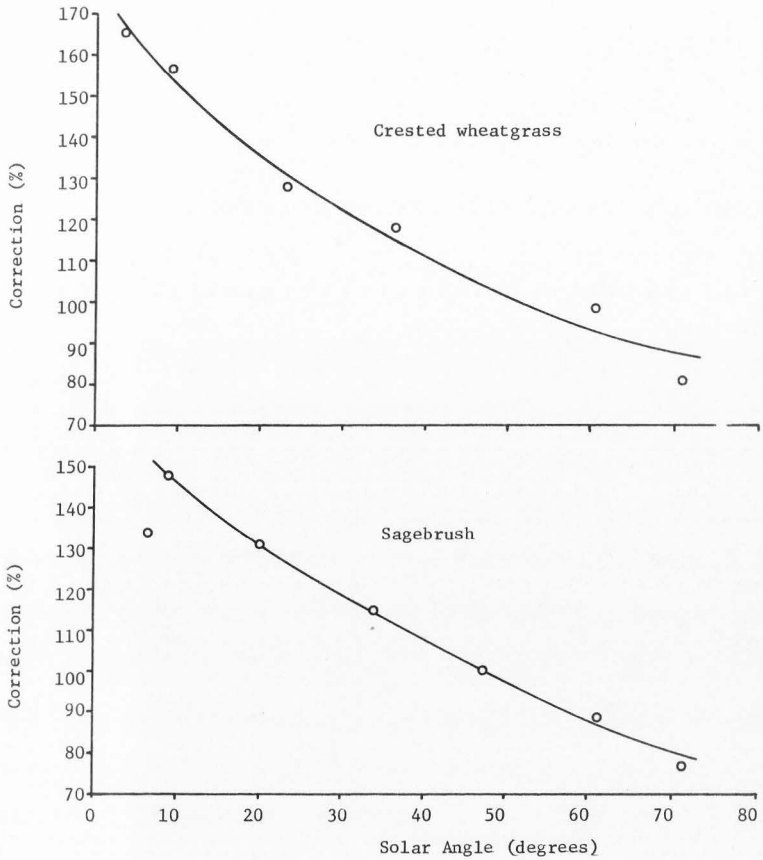

Figure 96. Percentage of correction *vs* solar angle that must be applied to reflectances for nadir angle = 0° to obtain the hemispherical reflection values for the desert surfaces examined.

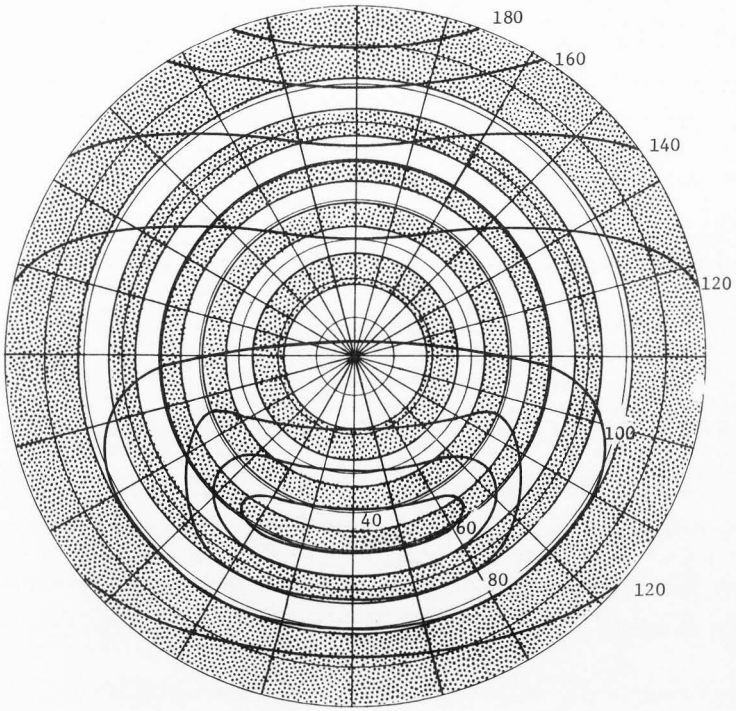

Figure 97. Indicatrix of reflected radiation measured from the top of a sand dune.

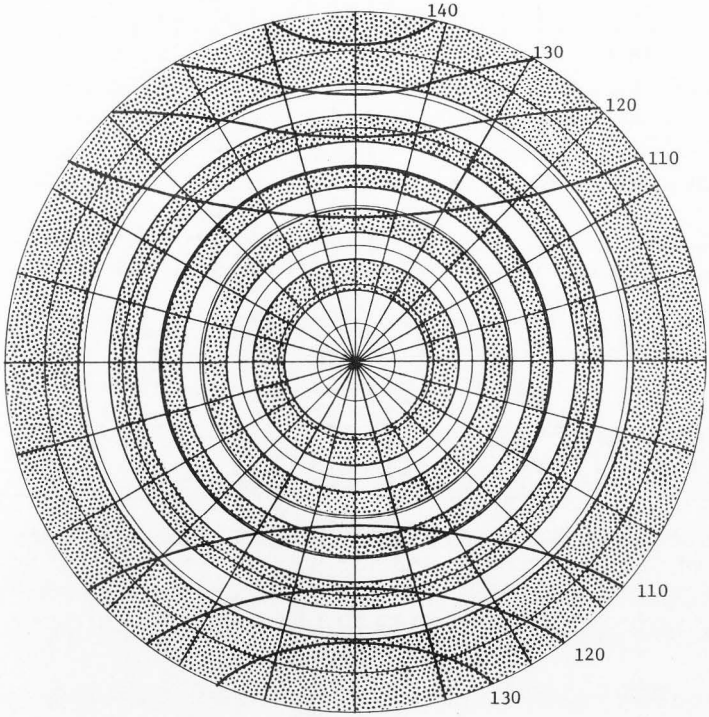

Figure 98. Indicatrix of reflected radiation measured from the bottom of a sand dune.

Figure 99. Photo of White Sands dune field with a ncormal lens.

Figure 100. Photo of White Sands dune field with a fish-eye lens.

due to the extensive shadow patterns produced by the undulating terrain. This reflection pattern agrees with the indicatrices developed over the plowed field. The plowed field, with its irregular surface, showed great backscatter and a similar decrease of forward scatter produced by shadows.

As can be seen from the two examples of indicatrices and photographs over the dune field, the combination of slopes and shadows as well as the large dimensions of each sand dune limit finding an overall albedo of the dune field from ground measurements alone. Therefore it was necessary to combine information obtained from flying platforms with the ground measurements. Flights were made with the TIROS radiometer mounted aligned vertically on a U.S. Army helicopter in order to measure transects showing variability of reflected radiation emerging from the direction normal to the overall surface. Flights were made at several times during the day in order to obtain full coverage of the interaction between solar angle and shadow patterns for the dune field.

Data were also collected from the helicopter at several altitudes over similar flight paths in order to evaluate the effect of integrating larger surface areas in the measurements with increasing altitude. Thus the aircraft flights were designed to determine both spatial effects *vs* solar angles of reflected radiation and the effect of different instantaneous fields of view of an instrument on the sensed reflectances.

Calibration of the TIROS radiometer

Several flight paths extended from the dune field to over the Alkali Flats. Ground observers, positioned on the Alkali Flats,

simultaneously measured the hemispherical reflected radiation with a pyranometer as the helicopter passed overhead. The indicatrices which were developed over the Alkali Flats were used to convert the pyranometer values to reflectances normal to the surface by the relationship, (reflectance value for nadir angle = 0°)(integrated 2π factor determined from indicatrices)=(2π value measured by the pyranometer), as described on page 18. These values were then used to calibrate the TIROS radiometer for in-flight conditions.

Flights for measuring the reflectance normal to the surface of the White Sands dunes were made on October 30, 31, and November 1, 1973 Two flights, each on October 30 and October 31, 1973 were arranged for shortly after sunrise and at noon in order to determine the reflected radiation for the lowest and highest solar angles at that time of the year. All of these transects were flown at 500 feet (A.G.L.). On November 1, 1973, flights were made at 10, 170, 500, 1000, 2000, and 5000 feet (A.G.L.) during the middle of the morning for solar angles ranging from 28.0° to 37.5°.

Figure 101b presents the actual measurements obtained from the TIROS radiometer *vs* solar time for the three days of investigation. Each of the transects flown is shown as one point which was obtained as the mean of integrating one-half inch intervals of the strip chart recordings.

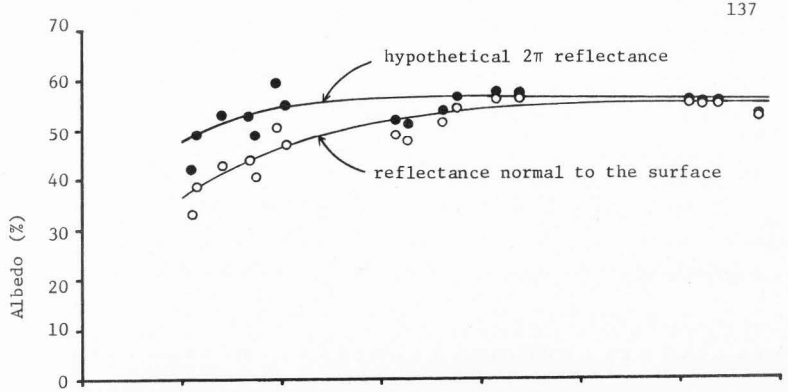

Figure 101a. Daily variation of albedo over sand dunes.

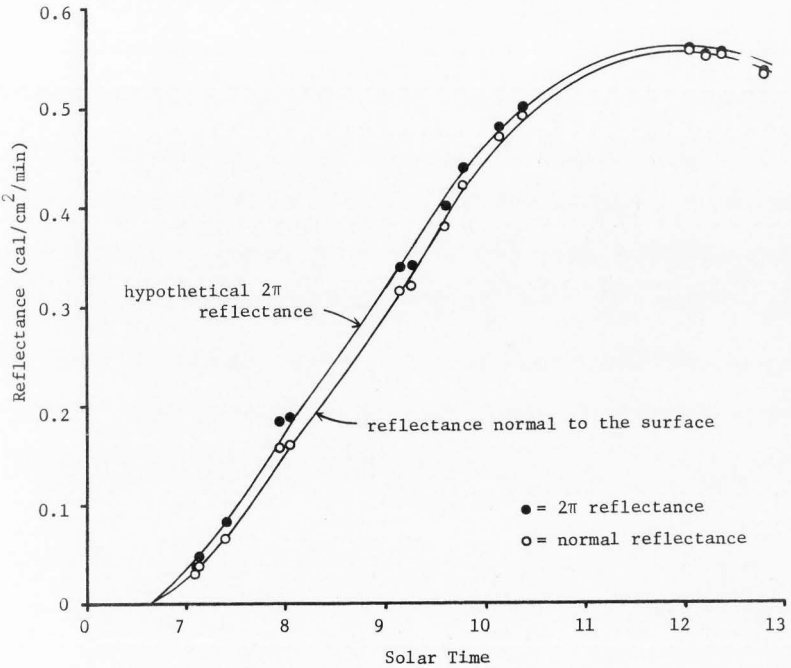

Figure 101b. Normal and 2π reflectances *vs* time over sand dunes.

As was previously discussed, the plowed field is the feature for which indicatrices were developed which most closely match the reflection characteristics of the dune field. Thus the reflectances normal to the overall surface measured by the TIROS radiometer over the dune field were adjusted to obtain hemispherical reflected radiation values by multiplying the measured values by the anisotropic correction factors derived from the plowed field. The curve fitted for the 2π reflected radiation is thus hypothetical.

As shown in Figure 31a, the albedo over the Alkali Flats increases as solar angle decreases. However, Figure 101a shows an opposite trend than found for the Alkalai Flats; a decrease in albedo as solar angle decreases. This trend for the dune field is explained by the large areas of the dune field which are not illuminated by the direct solar beam component of global radiation for low solar angles. Under these conditions only a small proportion of the surface area is contributing to the reflected radiation from direct beam illumination. As solar angle increases more surface area is directly illuminated with an associated increase in albedo.

The decrease in albedo with a decrease in solar angle is also shown in Figure 93 (Dirmhirn, 1972) for sagebrush remnants, dead sagebrush, and soil in Curlew Valley, Utah. The live sagebrush is directly illuminated at low solar angles and shows a trend of the daily variation of albedo similar to that found for the Alkali Flats. However the spacing of the individual bushes is generally such that a similar trend of the

daily variation of albedo for the sagebrush desert area is similar to the trend found for the dune field. For both features the relationship of shaded areas to solar angle determines the daily variation of albedo.

The TIROS radiometer has a field of view of 5° and for the lowest flight (10 feet A.G.L.) on November 1, the instruments I.F.O.V. was 0.9 feet while at the highest altitude (5000 feet A.G.L.), the I.F.O.V. was 436.6 feet. The I.F.O.V. is plotted *vs* altitude, A.G.L., in Figure 102 for the TIROS radiometer.

The minimum, mean and maximum reflectances measured for each altitude are plotted in Figure 102. The mean reflectances were derived by integrating one-half inch intervals of the strip chart recordings over each flight path while the minimum and maximum values were derived by averaging the highest and lowest values from the charts. The increase of the average values with height is due to progressing time during the morning measurements and consequently an increase in solar angle. Thus the results shown in Figure 102 actually show the mean and range of reflectances depending on the altitude. The data indicate the dependence on aperture size by integrating over larger areas as altitude is increased.

Table 5 shows a comparison of the mean reflectances, standard deviations and sample sizes of the measurements between the Alkali Flats and dune field. The standard deviation is seen to be approximately an order of magnitude greater for the dune field than for the Alkali Flats at the lower altitude but converges toward the same value as altitude

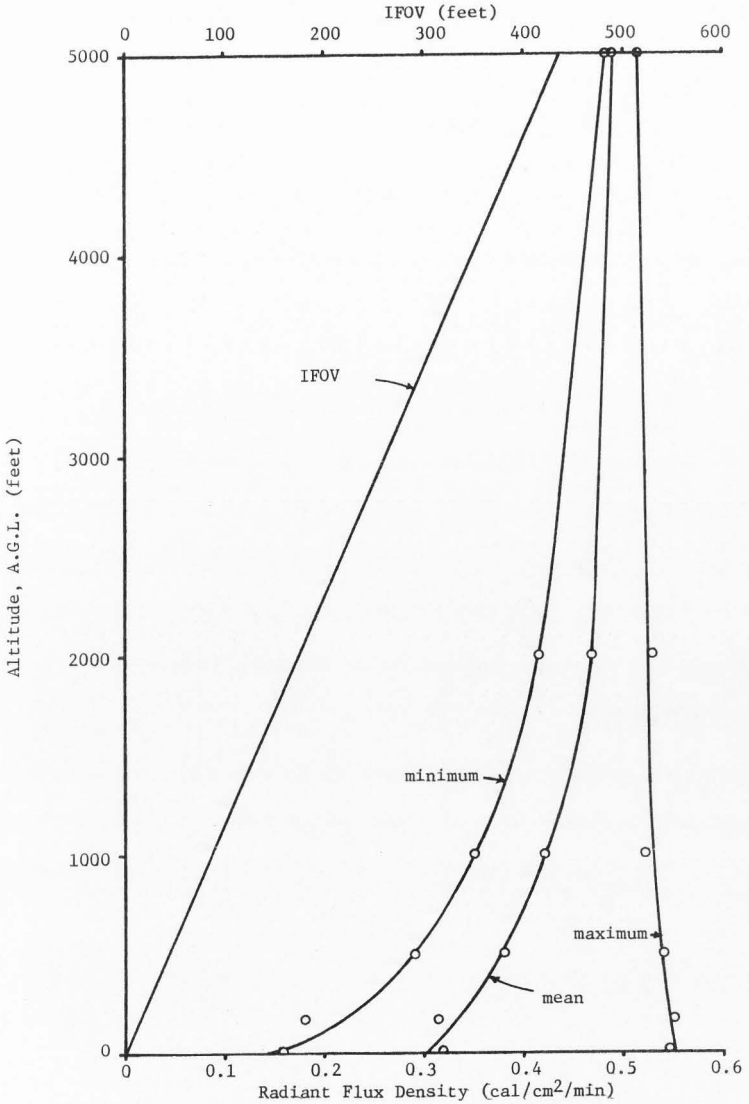

Figure 102. Effect of IFOV on range of radiant flux density over the White Sands dunes area.

is increased. These values in addition to the results shown in Figure 102 show the effect of integrating increasing surface areas in flying platform measurements over the two discussed features.

Table 5. Means, standard deviations, and sample sizes for reflectances over sand dunes and Alkali Flats

Ht. A.G.L. (feet)	Feature	Sample size	Mean (ly/min)	Standard deviation (ly/min)
10	S. dunes	118	0.318	0.097
	A. Flats	10	0.298	0.009
170	S. dunes	79	0.314	0.095
	A. Flats	10	0.270	0.017
500	S. dunes	71	0.380	0.065
	A. Flats	10	0.337	0.037
1000	S. dunes	61	0.421	0.052
	A. Flats	10	0.354	0.015
2000	S. dunes	76	0.468	0.031
	A. Flats	10	0.390	0.010
5000	S. dunes	61	0.489	0.014

Estimation of radiation emerging from the top of the atmosphere

The theory of radiative transfer in a scattering medium was first put on a sound mathematical basis by Rayleigh (1899) in accounting for the blue color of the sky. Van de Hulst (1957) further explained light scattering by small particles and applied his results to specific fields of interest. Chandrasekhar (1950) made significant advances in the

theory of radiative transfer in planetary atmospheres. He incorporated the effects of reflected radiation from a plane surface as one boundary of the scattering medium as well as accounting for all orders of multiple scattering within the scattering medium itself. Sekera (1956) provided several mathematical formulations for treating the scattering and polarization in Rayleigh atmospheres. Coulson (1959) followed this work by computing the flux of radiation emerging from the top of the earth's atmosphere considering only Rayleigh scattering.

With the advent of the space satellite programs, interest was generated for developing more realistic solutions for the extraterrestrial fluxes of radiation from planetary atmospheres by incorporating the effects of multiple scattering, aerosols and clouds into the solutions. With these additional considerations, the mathematics needed for the calculations of radiative transfer becomes extremely laborious and involved.

Bullrich et al. (1965) computed the radiation emerging from the top of the cloudless atmosphere considering both Rayleigh scattering and scattering on large particles. Radiation intensities were computed for various wavelengths as functions of the turbidity, the solar elevation, and the reflectivity of the earth's surface.

Bullrich et al. (1969) considered multiple scattering and found distinct departures in the results between single and triple scattering and concluded it would be desirable to calculate another order to scattering. However, the numerical instability and increasing computer time requirement are serious handicaps against the accomplishment of

this task. Hegar (1971) also compared results of primary, secondary and third order scattering in a turbid atmosphere and found a considerable increase in the albedo at the edge of the atmosphere as the order of scattering increases.

Numerical solutions for the complete equation of radiative transfer including polarization effects were used by Eschelbach (1973). He found that the reflection of the planet earth is increased for small and medium values of the surface albedo when the aerosols are nonabsorbent. Such aerosols show that the reflection is almost independent of the surface in cases of high surface albedo. When considering absorbent aerosols, the reflection of the planet earth is decreased for medium and large values of the surface albedo. Under these conditions the gain of energy to the earth-atmosphere system is almost exclusively taken by the atmosphere. The surface of the ground receives less energy in the case of an absorbent aerosol than in the case of a non-absorbent one. Eschelbach (1973) also concluded that the effect of the aerosol on the energy balance of the atmosphere is not to be neglected.

Plass and Kattawar (1968) calculated the reflected and transmitted radiances of the earth's atmosphere by Monte Carlo techniques. Although polarization effects were not included in the calculations, the scattering function for the aerosols used was calculated from the Mie theory. Rayleigh and aerosol scattering events were included in the calculations as well as the ozone absorption. Two different aerosol number density distributions with height were used and compared in the calculations.

The first distribution as given by Elterman (1965) has more aerosols in the lowest 2 km of the atmosphere than the second distribution developed by Kondratiev et al. (1967). However the Kondratiev distribution has more aerosols at all altitudes above 6 km than Elterman's distribution.

For 0.27 μm, the ozone absorption coefficient was found to be larger than either the Rayleigh or aerosol attenuation coefficient at all altitudes and at 0.3 μm, the ozone absorption was still important from 10 km to 50 km. The Rayleigh scattering was shown to be more important than aerosol scattering at a wavelength of 0.4 μm for altitudes greater than 2 km. At 0.7 μm the aerosol scattering showed an important contribution while at 1.67 μm Rayleigh scattering was found to be of minor importance.

Complications of the processes involved in radiative transfer when viewing distant objects are well known to pilots and aerial photogrammetrists. The visibility of distant objects is reduced by atmospheric haze by decreasing the apparent contrast. An approach to this problem was outlined by Schuster (1903) in his discussion of primary and secondary scattering in a diffusing material. The treatment is general and the source could be the sun, moon, searchlight, laser, the sky or ground objects. Schuster developed his relationships from two fluxes moving in opposite directions through the diffusing material. The upward flux is diminished as:

$$dt/dr = \mu_r t - B_r t + l_t + B_r s + F'_r I'_r \qquad [6]$$

where:

t = upward moving flux

dr = thickness of the lamina

μ_r = absorption coefficient

B_r = backscattering coefficient

l_t = space light

s = backward scattered light from the opposite flux

F'_r = proportionality forward scattering coefficient for directed flux

I'_r = spectral irradiance caused by a directed beam.

Changes in the downward flux can be shown as:

$$-ds/dr = -\mu_r s - B_r s + l_s + B_r t + B'_r I'_r \qquad [7]$$

where:

B'_r = proportionality backward scattered coefficient for directed flux.

Solutions of these differential equations for various problems were presented by Duntley (1948). Problems of upward, downward and horizontal visibility were investigated.

Mazurowski and Sink (1965) related atmospheric turbidity to atmospheric meteorological conditions and its effects on aerial photography. Flights were made at different altitudes and data were collected using photometers with filters as well as from aerial photography. They found

little spectral selection by the atmosphere below 10,000 feet but above 10,000 feet the spectral selectivity approaches that of Rayleigh scattering. The target-background contrast was shown as:

$$C = (Nt - Nb)/(Nt + Nb) \qquad [8]$$

where:

Nt = target radiance

Nb = background radiance

C = target-background contrast.

Since the beam in the target-background beam path has both light scattered into and out of the beam, the apparent contrast may differ greatly with altitude from the inherent contrast.

In this study estimates of extra-terrestrial fluxes of radiant flux density were made from the results of Plass and Kattawar (1968) and Bullrich et al. (1965) for the appropriate solar angle and ground albedo values which corresponded to the conditions under which space satellite imagery was examined. Plass and Kattawar used two aerosol distributions in their calculations and results from both are presented. Bullrich et al. (1965) calculated fluxes for a wide range of turbidity factors which enables examining the change of extra-terrestrial fluxes as turbidity changes. Estimates are shown for turbidity factors of two and six.

Comparison of satellite-obtained data to estimates of radiation emerging from the top of the atmosphere

The satellite-obtained data used for comparison with the estimates of emergent radiation were obtained by the Earth Resources Technology Satellite (ERTS) as described by Thomas (1973). The values were collected from the multi-spectral scanner (MSS) subsystem. The MSS is a four-band scanner operating in the spectral region of the reflected solar energy from 0.5 to 1.1 μm. Bands 1 through 3 use photomultiplier tubes as detectors and cover the spectral bands of 0.5 to 0.6 μm, 0.6 to 0.7 μm, and 0.7 to 0.8 μm. Band 4 uses silicon photodiodes and covers the spectral range 0.8 to 1.1 μm. Each of the four bands consists of six detectors. The MSS scans cross-track swaths 185 km wide at the nominal altitude of 918.6 km by an oscillating flat mirror.

In this study, 9.5 x 9.5 inch photographic negatives were used for obtaining the radiance values. The negatives were produced from the sensor data by the Electron Beam Recorder. The relationships between the 15 steps of gray scales on each negative and the calibrated radiances for each step were developed. Then a microdensitometer was used to obtain the radiances desired from the imagery.

The imagery examined was collected on May 11, 1974 with the nadir of the imagery located at latitude 33°17' and longitude 105°58'. The two locations examined in this study, measuring sites in the White Sands area and the lava beds, are located 19' and 17' off the flight line, respectively. At the time the imagery was collected, the solar elevation angle was 59° and the solar azimuth angle was 113°.

Figure 103 shows the results obtained from the MSS channels of the ERTS satellite as well as estimates of emergent radiation derived from the calculations of Bullrich et al. (1965) and Plass and Kattawar (1968). The MSS data presented here are in units of $cal/cm^2 min/0.1\ \mu m$. Since band 4 has a bandpass three times the width of the other three bands, the actual measured values for band 4 were divided by three so that the true dependence of irradiance *vs* wavelength could be shown. The values were plotted in the center of each MSS band; i.e. 0.55, 0.65, 0.75, and 0.95 μm.

The actual radiances sensed by the MSS were corrected for anistropy by applying the proper aniostropic correction factor of 1.035 for 59° solar angle as shown in Figure 42. Since no knowledge was available for the angular distribution of reflected radiation over the lava beds region, this feature was approximated as isotropic.

Figure 103 shows estimates of extra-terrestrial radiant flux densities derived from the calculations of Bullrich et al. (1965) by using the albedo for the White Sands and lava beds area as shown in Figure 6 for a wavelength of 0.65 μm. Interpolations were made from the calculations to obtain the values for the desired spectral albedoes and solar angle of 59°. Estimates are presented for turbidity factors of two and six and the results imply that the turbidity was very low over the lava beds region and slightly greater than two over the White Sands region.

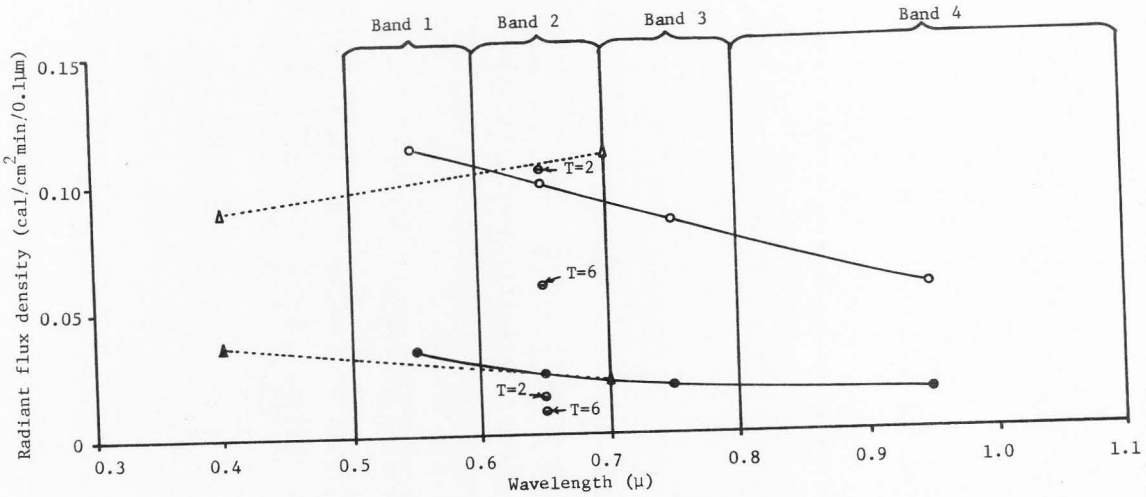

○ = MSS values for White Sands dune field and Alkali Flats
● = MSS values for lava beds region
△ = Plass and Kattawar (1965) estimates for White Sands dune field and Alkali Flats
▲ = Plass and Kattawar (1968) estimates for lava beds region
⊖ = Bullrich et al. (1965) estimates for White Sands dune field and Alkali Flats
⊖ = Bullrich et al. (1965) estimates for lava beds region

Figure 103. Radiant flux density measured by the MSS channels of the ERTS as well as estimates of emergent radiation

In order to gain some insight into the actual turbidity conditions at the time the space satellite imagery was collected over the White Sands and lava beds regions, U.S. Daily Weather Maps (1974) were examined. It was found that a new storm developed on May 8, 1974, and on the following day the winds aloft increased while a new low center formed. On May 10, 1974, the low moved across the study area in southern New Mexico. Winds of 20 knots were reported at El Paso, Texas and 10 knots at Roswell, New Mexico at 5 a.m. The 500 mb level showed winds of 40-50 knots. With the instability generally present at that time of the year, the winds during the day might temporarily have reached even greater speeds than the reported values. On May 11, 1974, the date the space satellite imagery was examined, the skies were reported clear but winds of 10 knots were still reported at El Paso, Texas. Probably some fine particles were still in suspension on May 11 over the White Sands area increasing the turbidity slightly. The lava beds region with the stable surface it possesses however probably showed little change in turbidity after the same storm.

The estimates derived from the calculations of Plass and Kattawar (1968) are shown for the wavelengths of 0.4 μm and 0.7 μm. The 0.4 μm values were derived from the Eltermann aerosol distribution while the 0.7 μm values were found using the Kondratiev aerosol distribution. The surface spectral albedoes were also found from Figure 6 for the two features examined. Interpolations were made from the calculations for the proper surface albedoes and solar angle. The estimates derived from the Plass and Kattawar (1968) estimates agree quite closely with

the MSS data for the lava beds but imply some turbidity over the White Sands region. These results for the White Sands region agree with Eschelbach (1973) who found that the reflection of the planet earth is decreased for values of high surface albedo when considering absorbent aerosols.

Estimates were also made of the actual radiant flux densities reflected from the ground surface for the same spectral ranges that were sensed by the MSS subsystem. Since the solar angle was 59° when the MSS Imagery was collected, the global radiation value for this solar angle was obtained from actual measurements on May 20, 1974. The pr - portion of the total global radiation for each spectral band was then found and each of these values were then multiplied by the integrated percent of reflection values for each spectral band obtained from Figures 5 and 6. The features examined were White Sands gypsum sand, Alkali Flats, lava, and plants.

Figure 104 shows a comparison of the spectral reflected radiation values at the ground surface compared to the ERTS-obtained values corrected for anisotropy. Since the Alkali Flats cover approximately 60 percent of the White Sands area, a weighted mean of 60 percent Alkali Flats and 40 percent White Sands gypsum sands reflection is shown. The results show that the MSS subsystem obtained values are in general lower than the radiation values leaving the ground. Only the shortest wavelength band shows close agreement with the reflected radiation emerging from the ground surface. This effect may be attributed to Rayleigh scattering.

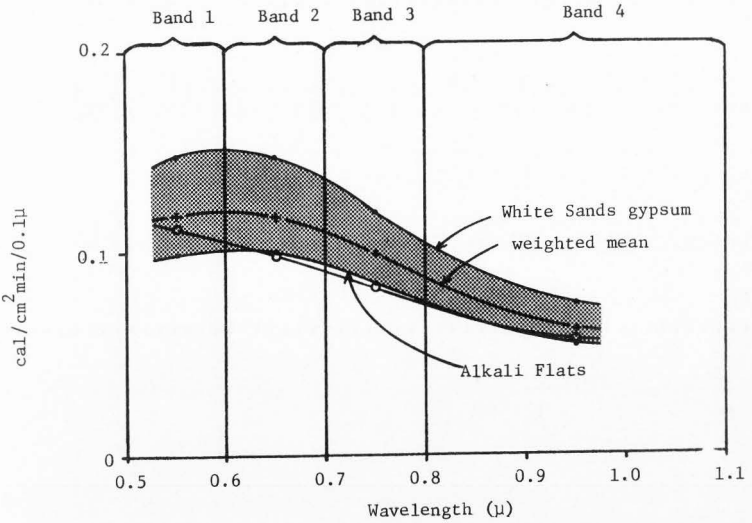

Figure 104. Comparison of MSS-obtained values (o) to radiation emerging from the earth's surface for the White Sands dune field and Alkali Flats.

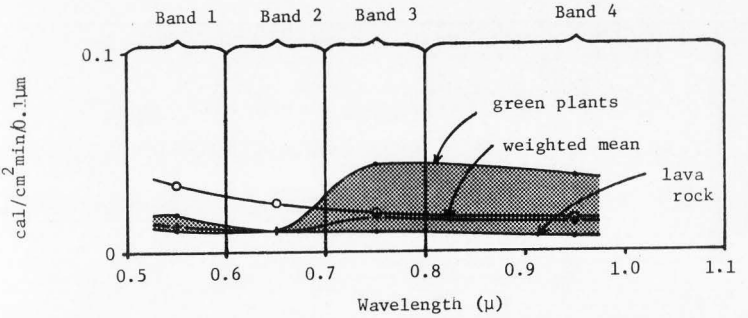

Figure 105. Comparison of MSS-obtained values (o) to radiation emerging from the earth's surface for green plants and lava rock.

Figure 105 shows estimates of the reflected radiation from the ground per spectral band for plants and lava derived in a similar manner as described for the gypsum sand and Alkali Flats. From visual observations on the lava bed site, it was estimated that the surface cover consisted of 25 percent plant cover and 75 percent lava. A weighted mean using these values for plants and lava is also shown in Figure 105. Here the satellite-obtained data show greater radiant flux density values than that emerging from the ground surface. From these two examples it can be concluded that the radiation emerging to space is less than that leaving the ground surface when high surfac albedo is present such as over the White Sands area while the opposite effect is found when the surface albedo is very low as found over the lava beds region. This effect agrees with the contrast considerations previously discussed.

The target-background contrast C as defined by Mazurowski and Sink (1965) was used as:

$$C = (Nt - Nb)/(Nt + Nb) \qquad [8]$$

where:

Nt = target radiance, and

Nb = background radiance.

Here the White Sands area was considered the target and the lava beds area was the background. The inherent contrast was calculated for the values at the ground surface using the values from Figures 104 and 105 and the apparent contrast was found from the ERTS-obtained data. Results are shown in Figure 106. There is a marked decrease in contrast when examining the space-obtained values from the inherent contrast. The curves show a convergence as wavelength increases.

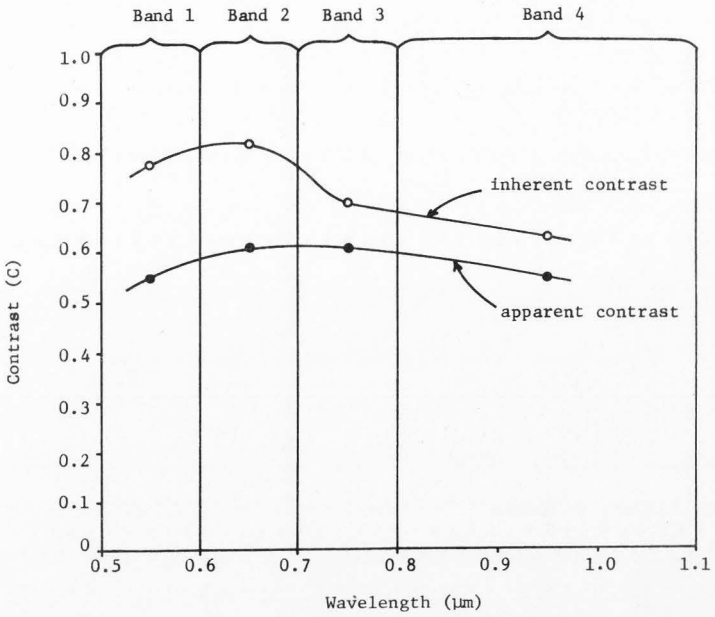

Figure 106. Inherent and apparent contrasts with the White Sands dune field and Alkali Flats as the target and the lava beds region as the background.

SUMMARY AND CONCLUSIONS

A summary of the comparisons of the reflection characteristics for the different surfaces for which the indicatrices were developed is shown in Table 6. Land, snow, agricultural crops and desert surfaces which were examined in this study show similarities as well as differences in their reflection properties. The surfaces are listed in decreasing order for the particular reflection characteristic examined.

A. Nature of the forward scatter:

Both trends, an increase or a decrease of forward scatter can be found.

B. Backscatter: Certain surfaces show a clearly defined anti-solar point characterized by a small zone of maximum reflectance and are listed in descending order of charity of the anti-solar point. Other surfaces show a broad pattern of backscatter.

The anisotropic correction factors, developed by integrating the indicatrices and representing the correction that must be applied to a normal reflectance of 100.0 percent to obtain hemispherical reflection can be summarized by grouping the factors for surfaces that exhibit similar reflectance patterns. Values for the anisotropic correction factors for mineral surfaces are shown in Figure 107. Alkali Flats and Bonneville Salt Flats show similar values which approach isotropy at the highest solar angles.

Table 6. Comparison of reflection characteristics for the land, snow, agricultural crops and desert surfaces examined

A. Nature of forward scatter

1. Increase of reflectance from nadir angle = 0° to nadir angle = 90°

   Snow
   Alfalfa
   Sugar beets
   Corn
   Crested wheatgrass $\leq$ 23° solar angle
   Sagebrush $\leq$ 20° solar angle
   White Sands Alkali Flats
   Bonneville Salt Flats

2. Decrease of reflectance from nadir angle = 0° to nadir angle = 90°

   Crested wheatgrass $\geq$ 36.2° solar angle
   Sagebrush $\geq$ 47.4° solar angle
   Plowed field

B. Nature of backscatter

1. Anti-solar point clearly defined

   Plowed field
   Sugar beets
   Alfalfa
   Corn
   Sagebrush
   Crested wheatgrass $\geq$ 36.2°

2. Broad pattern of backscatter

   Crested wheatgrass $\leq$ 23.0°
   Snow
   White Sands Alkali Flats
   Bonneville Salt Flats

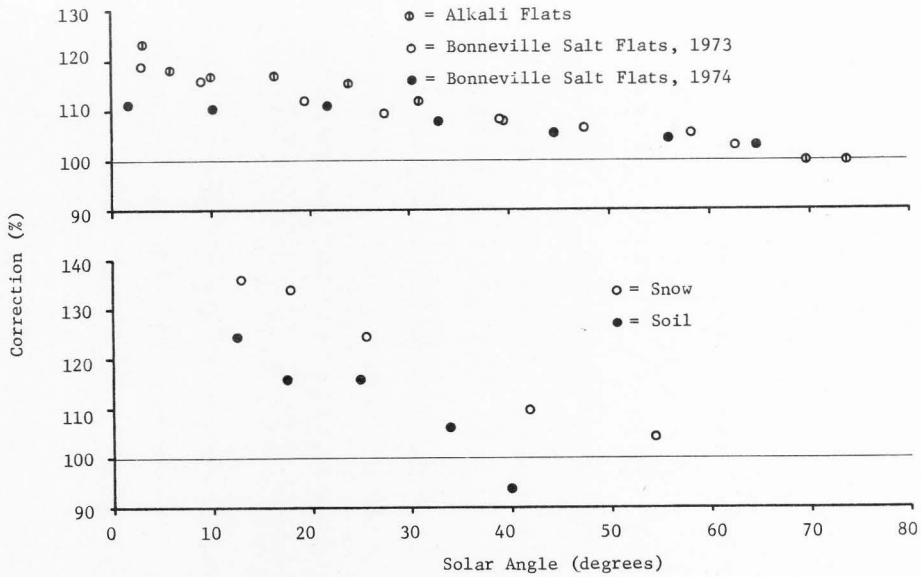

Figure 107. Percentage of correction *vs* solar angle that must be applied to reflectances for nadir angle = 0° to obtain the hemispherical reflection values for the mineral and snow surfaces examined.

Plowed fields show a steeper slope for the curve of the anisotropic factors vs solar angle than found for the curve of the other mineral surfaces and show an approach to an anisotropic correction factor of 100.0 percent for solar angle of approximately 45^{o}. Actual measurements were not obtainable for solar angles greater than 40.0^{o} due to the maximum solar angle found during the time of the year that freshly plowed fields are available.

The anisotropic correction factors for snow are included in Figure 107. The slope of the curve for snow is slightly greater than shown for plowed fields.

Figure 108 shows the anisotropic correction factors found for all plant covers under investigation; agricultrual crops and desert surfaces. All values shown for solar angles greater than 60^{o} have an anisotropic factor less than 100.0 percent. Alfalfa values were not obtained for solar angles greater than 57.3^{o}. The trend shown for alfalfa is toward isotropy at the higher solar angles. Alfalfa with its small but densely set leaves tends to reflect light more similarly to that from the crystals and particles found on the Alkali Flats and Bonneville Salt Flats than from the large leaves of the other crops.

In general, the slope of the curve for the anisotropic correction factors for plant covers vs solar angle is steeper than found for mineral and snow surfaces.

A consequence of the nature of the backscatter is shown in the anisotropic correction factors. The surfaces exhibiting a clearly defined anti-solar point for high solar angles show correction factors

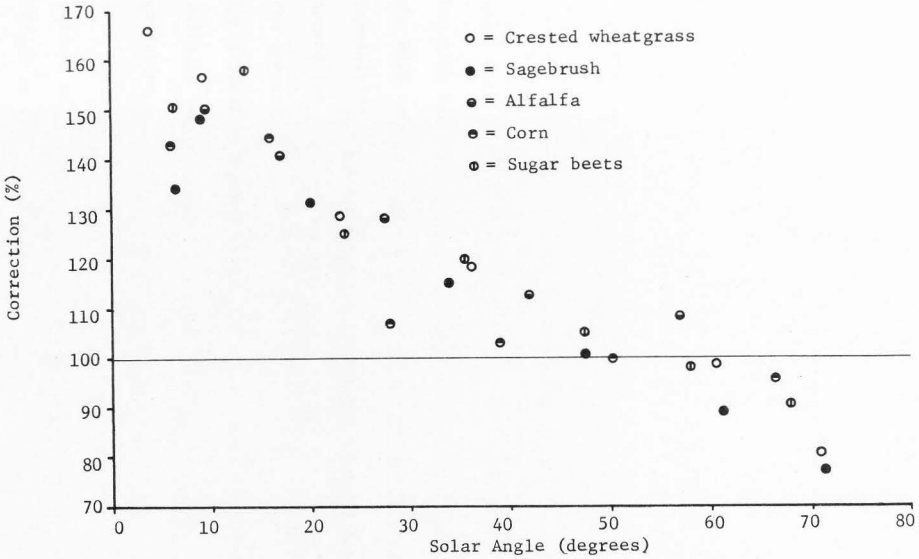

Figure 108. Percentage of correction *vs* solar angle that must be applied to reflectances for nadir angle = 0° to obtain the hemispherical reflection values for the plant and desert surfaces examined.

less than 100.0 percent. Since the Bonneville Salt Flats, Alkali Flats, and snow surfaces have a broad pattern of backscatter, the anisotropic correction factors for these surfaces are never found to be less than 100.0 percent.

In summary, 2π reflected radiation can well be determined by measuring reflectances at defined nadir angles relative to solar elevation and azimuth angles. To do so, the indicatrices have to be known and correction factors applied according to Figures 107 and 108. A grouping of surfaces that exhibit similar indicatrix patterns seems to be acceptable.

All of the indicatrices, with the exception of those over snow, were developed by taking measurements with the Nimbus MRIR. For each surface a separate calibration constant was developed for the MRIR radiometer and was found to differ for individual surfaces. Examination of possible reasons for the different calibration constants showed the interaction of the spectral sensitivity of the MRIR with the spectral characteristics of the surfaces examined to explain the largest part of the deviation between the constants. A possible shift in the MRIR spectral sensitivity was also examined due to oxidation of the three reflecting surfaces in the optical system from the time of manufacture and was found to explain up to 5.7 percent of the deviation. Other considerations such as temperature effect on the MRIR, degradation of the instrument during the time of the study period and the spectral sensitivity of the pyranometer used as a standard were found to be small or negligible in their effects.

Alkali Flats, Bonneville Salt Flats, plowed field, snow, agricultural crops, and crested wheatgrass all show a daily variation of albedo which increases as solar angle decreases. However, the values presented in Figure 93 indicate that the daily variation of albedo for a sagebrush desert may show an opposite trend. Sand dunes as measured from aircraft indicate a similar trend.

A comparison was made between estimated emerging radiation from the top of the earth's atmosphere and values of reflected radiation measured with the MSS subsystem of the ERTS program and corrected for anisotropy. Some of the estimates were derived from calculations by Bullrich et al. (1965) accounting for Rayleigh scattering, scattering on large particles, and the reflectivity of the earth's surface. Other estimates were developed from calculations of Plass and Kattawar (1968) using Monte Carlo techniques to find the radiation reflected from the earth-atmosphere system with the Kondratiev and Elterman aerosol distributions incorporated into these calculations. The results showed that the estimates derived from the Plass and Kattawar (1968) calculations as well as those derived from the Bullrich et al. (1965) values for low turbidity agreed quite closely with the MSS values obtained from the ERTS program over the lava beds, for the White Sands Region, the MSS values were found to agree with a turbidity factor in excess of two. These results imply that there were more aerosols present over the White Sands area than over the lava beds region. The antecedent meteorological conditions verify this assumption.

Comparisons were also made between estimated emerging radiation

from the surface for the same features and spectral bands to the values sensed in space. The spectral albedos for the surfaces were derived from measured global radiation assuming a standard spectral distribution and the spectral characteristics of the surfaces measured by a Beckman DK-2A spectrophotometer in the laboratory. The results show that with the high surface albedo of the White Sands region, there is a decrease in emergent radiation to space while with low surface albedo over the lava beds region, the emergent radiation to space increases. These results agree with those found concerning atmospheric contrast. Contrast was calculated considering the White Sands region the target and the lava beds the background. The inherent contrast (calculated from the values of radiation reflected from the ground surface) was found to exceed the apparent contrast (found from the space-obtained data) with a trend of increasing deviation between the two contrasts as wavelength decreases.

From these results it is concluded that it is possible to determine the true albedo of a natural surface from any reflectance measurement taken from a flying platform after accounting for both the effects of the angular distribution of reflected radiation and the effects of the intervening atmosphere. Only after these considerations are incorporated can satellite reflectance data be intelligently interpreted.

In addition the knowledge of indicatrices of reflected radiation for several solar angles as shown in this study allows the determination of the daily variation of albedo for a given surface from a single reflectance measurement. Thus these results allow both

more efficient as well as more accurate utility of space-obtained reflected radiation data.

BIBLIOGRAPHY

Bartman, F. L. 1967. The reflectance and scattering of solar radiation by the earth. Contract Report NASA-CR-83954. U.S. Government Printing Office, Washington, D. C. 13 p.

Brennan, B. 1969. Bidirectional reflectance measurements from an aircraft over natural earth surfaces. Technical Memorandum NASA-TMX-63564. U.S. Government Printing Office, Washington, D.C.

Brennan, B. and W. R. Bandeen. 1970. Anisotropic reflectance characteristics of natural earth surfaces. Journal of Applied Optics, A,2. pp. 405-412.

Bullrich, K., E. DeBary, K. Danzer, R. Eiden and K. Heger. 1965. Research on atmospheric optical radiation transmission. Scientific Report 3, Contract AF 61(052)-595. U.S. Air Force Cambridge Research Lab. 83 p.

Bullrich, K., R. Eiden, G. Eschelbach, K. Fischer, G. Hänel, K. Heger, H. Schollmayer, G. Steinhorst. 1969. Research on atmospheric optical radiation transmission. Scientific Report 7, Contract F 61052 67C 0046. U.S. Air Force Cambridge Lab. 111 p.

Burt, W. V. 1954. Albedo over wind-roughened water. Journal of Meteorology. 11(4):283-290.

Chandrasekhar, S. 1950. Radiative transfer. Dover, New York. 393 p.

Christie, A. W. 1953. The luminous directional reflectance over snow. Journal of Optical Soc. of America 43(7):621-622.

Coulson, K. L. 1959. The flux of radiation from the top of a Rayleigh atmosphere. Scientific Report 1, Contract AF 19(604)-2429. Geophysics Research Division of the Air Force Cambridge Research Center.

Coulson, K. L., G. M. Bourcius and E. L. Gray. 1965. Final report, Contract NAS5-3925. General Electric Company, Space Sciences Laboratory, Philadelphia, Pennsylvania. 73 p.

Coulson, K. L. 1966. Effects of reflection properties of natural surfaces in aerial reconnaissance. Applied Optics 5(6):905-17.

Cox, C. and W. Munk. 1954. Statistics of the sea surface derived from sun glitter. Journal of Marine Research 13(2):198-227.

Daily Weather Maps, Weather Series May 8-11. 1974. U.S. Department of Commerce NOAA. Environmental Data Service, Washington, D.C.

Dirmhirn, I. 1967. On the applicability of silicon cells in atmospheric radiation studies. Report for Contract NASA=NGR-06-002-038. U.S. Government Printing Office, Washington, D. C.

Dirmhirn, I. 1972. The radiative environment and the surface temperature on a microscale in a sagebrush desert. Research Memorandum RM72-36 Desert Biome USIBP. 13 p.

Dirmhirn, I. and F. Eaton. 1975. Some characteristics of the albedo of snow. Journal of Applied Meteorology 14(3):375-379.

Duntley, S. Q. 1948. The reduction of apparent contrast by the atmosphere. Journal of the Optical Society of America 38(2):179-190.

Elterman, L. 1965. Handbook of Geophysics and Space Environments. S. L. Valley, Ed. McGraw-Hill Book Company, Inc., New York.

Eschelbach, G. 1973. Computations of the influence of aerosols on the atmospheric radiation balance in the visible spectrum. Beiträge zur Physik der Atmosphäre, 36. Band S. 249-261.

Farb and Filter Glas. 1965. Für wissenschaft und technik Jenaer Glaswerk schott and gen, Mainz. 43 p.

Fletcher, J. E. and W. P. Martin. 1948. Some effects of algae and molds in the raincrust of desert soils. Ecology 29:95-100.

Hapke, B. and H. VanHorn. 1963. Photometric studies of complex surfaces with application to the moon. Journal of Geophysics Research 68(05):4545-4570.

Heger, K. 1971. Primary, secondary, and third order scattering of solar radiation in the turbid atmosphere. Beiträge zur Physik der Atmosphere 44. Band S 201-204.

Hubley, R. D. 1955. Measurements of diurnal variations in snow albedo on Lemon Creek, Glacier, Alaska. Journal of Glaciology 2:560-563.

Kondratiev, K. Ya., G. A. Nicolsky, I. Ya. Badinov and S. D. Andrew. 1967. Direct solar radiation up to 30 km and stratification of attenuation components in the stratosphere. Applied Optics 6(2):197-207.

Lettau, H. and K. Lettau. 1969. Shortwave radiation climatology. Tellus 21(2):208-222.

London, J. 1957. A study of the atmospheric heat balance. Final Report Contract AF 19(122)-165. Department of Meteorology and Oceanography, New York University. 99 p.

London, J. and T. Sasamori. 1971. Radiative energy budget of the atmosphere. Space Research XI, Berlin, Akad-Verlag. pp. 639-649.

Malinowski, F. R. 1966. Nimbus medium resolution infrared radiometer F-2 data book supplement for NASA Contract NAS 5-757, Goddard Space Flight Center. 111 p.

Manual of Color Aerial Photography. 1968. J. T. Smith, Ed. American Society of Photogrammetry. 1st ed. 550 p.

Mazurowski, M. J. and D. R. Sink. 1965. Attenuation of photographic contrast by the atmosphere. Journal of the Optical Society of America 44(1):26-30.

McKee, E. D. 1966. Structures of dunes at White Sands National Monument, New Mexico (and a comparison with structures of dunes fro other selected areas). Sedimentology 7(1):69.

Middleton, W. E.K. and A. G. Mungall. 1952. The luminous directional reflectance of snow. Journal of the Optical Society of America 42(8):572-579.

Plass, G. N., and G. W. Kattawar. 1968. Calculations of reflected and transmitted radiance for earth's atmosphere. Applied Optics 7(6):1129-1135.

Raschke, E., T. H. VanderHaar, W. R. Bandeen and M. Pasternak. 1973. The annual radiation balance of the earth-atmosphere system during 1969-1970 from Nimbus 3 measurements. Journal of Atmospheric Science 30(3):341-364.

Rayleigh, L. 1899. On the transmission of light through an atmosphere containing small particles, and on the origin of the blue of the sky. Phil. Mag. 47:375-384.

Ruff, I., R. Koffler, S. Fritz, J. S. Winston, and P. K. Rao. 1967. Angular distribution of solar radiation reflected from clouds as determined from TIROS IV radiometer measurements. ESSA Tech. Report NESC-38. U. S. Government Printing Office, Washington, D.C.

Salomonson, V. V. 1966. Anisotropy of reflected solar radiation from various surfaces as measured with an aircraft-mounted radiometer. Research Report to the NASA under contract NaSr-147. U.S. Government Printing Office, Washington, D.C.

Sauberer, F. and I. Dirmhirn. 1952. Der Strahlungshaushalt horizontaler Gletscherflaechen Auf dem Hohen Sonnblick. Geogra. Ann. 34:261-290.

Sekera, Z. 1956. Recent developments in the study of the polarization of sky light. Advances in Geophysics, V. 3, NY Academic Press, 378 pp.

Shields, L. M., C. Mitchell, and F. Drouet. 1957. Alga- and lichen-stabilized surface crusts as soil nitrogen sources. American Journal of Botany 44(6):489-498.

Shuster, A. 1903. The influence of radiation on the transmission of heat. Phil. Mag. 5:243-247.

Skidmore, E. L. and N. P. Woodruff. 1968. Wind erosion forces in the United States and their use in predicting soil loss. Agricultural Handbook 346 ARS, USDA. U. S. Government Printing Office, Washington, D. C.

Thomas, V. L. 1973. Generation and physical characteristics of the ERTS MSS system corrected computer compatible tapes. Report X-563-73-206, Goddard Space Flight Center.

Tooning, H. 1960. Daily and seasonal variations of albedo over some natural surfaces in the Estonian SSR. Tr Inst. Fiz.-Astron Akak. Nank Est. SSR 2:115-163.

Utah Climatological Data Bulletin. 1973-1974. Utah State University, Logan, Utah. Vol. 74, 75, 76.

Van de Hulst, H. C. 1957. Light scattering by small particles. John Wiley and Sons, Inc., New York. 470 p.

Vonder Haar, T. H. and V. E. Suomi. 1971. Merasurements of the earth's radiation budget from satellites during a 5-year period. Part 1: Extended time and space means. Journal of the Atmospheric Sciences 28(3):305-314.

VITA

Frank D. Eaton

Candidate for the Degree of

Doctor of Philosophy

Dissertation: Albedo of the Earth's Surface--A Comparison of Measurements taken on the Ground and from Flying Platforms

Major Field: Soil Science and Biometeorology (Biometeorology)

Biographical Information:

Personal Data: Born at Cambridge, New York, May 8, 1942; son of A. Clarkson Eaton and Eleanor D. Eaton.

Education: Attended elementary school in Bennington, Vermont; attended high school in Hoosick Falls, New York; graduated in 1960; received a Bachelor of Science degree in Watershed Management from the University of Arizona, Tucson, Arizona in 1965; received a Master of Science degree in Watershed Science from Utah State University in 1971; completed requirements for the Doctor of Philosophy majoring in Biometeorology, at Utah State University, Logan, Utah in 1976.

Affiliations: Alpha Zeta, Xi Sigma Pi.